

12-2022

Phosphate Mineralogy and Paragenesis of the Fletcher Pegmatite, North Groton, New Hampshire

Susanna T. Kreinik
University of New Orleans, susanna.torrey@gmail.com

Follow this and additional works at: <https://scholarworks.uno.edu/td>



Part of the [Geochemistry Commons](#), and the [Geology Commons](#)

Recommended Citation

Kreinik, Susanna T., "Phosphate Mineralogy and Paragenesis of the Fletcher Pegmatite, North Groton, New Hampshire" (2022). *University of New Orleans Theses and Dissertations*. 3039.
<https://scholarworks.uno.edu/td/3039>

This Thesis is protected by copyright and/or related rights. It has been brought to you by ScholarWorks@UNO with permission from the rights-holder(s). You are free to use this Thesis in any way that is permitted by the copyright and related rights legislation that applies to your use. For other uses you need to obtain permission from the rights-holder(s) directly, unless additional rights are indicated by a Creative Commons license in the record and/or on the work itself.

This Thesis has been accepted for inclusion in University of New Orleans Theses and Dissertations by an authorized administrator of ScholarWorks@UNO. For more information, please contact scholarworks@uno.edu.

Phosphate Mineralogy and Paragenesis of the Fletcher Pegmatite, North Groton, New
Hampshire.

A Thesis

Submitted to the Graduate Faculty of the
University of New Orleans
In partial fulfillment of the
requirements for the degree of

Master of Science
In
Earth and Environmental Science

by

Susanna T. "Sasha" Kreinik

B.S. University of New Orleans, 2013

December 2022

Acknowledgements

To appropriately recognize everyone who has been impactful on this road I have taken would require the length of a bible. I shall abbreviate.

My thesis advisors deserve the greatest thanks, without doubt. First and foremost, I owe a huge debt of gratitude to Dr. William "Skip" Simmons, whose guidance, endless experience, knowledge, and willingness to take on just one more graduate student have allowed me the chance to pursue something I love. His near superhuman patience and humor have also been remarkable in this undertaking. For all of these things, and far too many more to list, I am eternally grateful though surely undeserving. Dr. Karen Webber's knowledge, wit and critique have been invaluable. Even at the times when they are only in my head, which is often. Learning from Karen and Skip has helped me become what I set out to be: a geologist, a better scientist, and a better teacher.

Alexander Falster is a man without equal. The debt of gratitude for friendship, illumination, and time he has gifted runs deep and can never be repaid. There was rarely a day in my time at the University of New Orleans that did not include Al and the final few months without his ever-present help, encyclopedic knowledge of all things ever, and tendency to lighten any mood without lessening the importance of the research have been sorely missed. These three people have been my navigators and I am truly thankful. Skip and Al never gave up on me, even when they had every reason to. I cannot imagine why, but I am so glad they had faith where I had doubt.

R.W. "Bob" Whitmore made this thesis possible by his gift of the Fletcher samples to the MP² group. He has given me countless hours of time, stories, and advice. As the only person I know alive who actually spent any time at the Fletcher, he is an

irreplaceable resource, and his generosity has been large. I am heartily thankful to both him and his wonderful wife, Edna, for their continued support.

Ioannis Georgiou and Mark Kulp for so much support over so many years, and Kraig Derstler, who I am fortunate to call a great and dear friend, must also get some recognition.

Much support came from without the University as well. Foremost among these is the incomparable Pietro Vignola, whose work with XRD for this research was crucial and also generously given. He is most responsible for my discovery of and fascination with phosphates. Pietro has been a friend, mentor, and advisor almost since we met. His friendship is one I cherish deeply.

Also, for his words of encouragement such as “why would you want to work with phosphates?” and “are you crazy” I must thank Jim Nizamoff.

Dr. Encarnacion “Encar” Roda, too, has been a champion and has patiently helped me get through what at first seemed like a muddle of intricate and complex information. Like so many of the people I met on this road, she remains a dear friend. She also corrects my Spanish kindly, unlike my Cuban husband,

My husband, Diego Rodriguez, (see above) has been my stalwart supporter and companion through all of this. Ten years and he hasn't ever doubted I would complete this. Diego has made it possible for me to pursue this dream and for that alone he deserves my everlasting gratitude. He already has my everlasting love. This is as much his baby as mine. Well, almost.

Finally, I dedicate this work to Sandra Kreinik, Paddy Hoyt, and Betsy Brisk. They were my guides through life and every day without my mother, my cousin, and my godmother has been a fierce reminder of how much I owe them.

Table of Contents

List of Figures.....	vi
List of Tables	viii
Abstract	ix
Introduction.....	1
Previous Work	2
Geologic Setting.....	4
Geology of the Pegmatite.....	9
Descriptive Mineralogy	13
Selected Materials	13
Association I	14
Association II.....	16
Association III.....	18
Association IV	20
Group V	20
Analytical Methods	25
Sample Collection	25
Thin Sections	25
Polished Sections.....	25
Electron Microprobe.....	26
Data Recalculation	27
Scanning Electron Microscopy	27
X Ray Diffractometry.....	27
Direct Current plasma Spectrophotometry.....	28
Analytical Results	29
Chemical Composition and Structure	29
Fluorapatite	30
Triphylite	33
Ferrisicklerite	38
Heterosite.....	40

Rockbridgeite	44
Jahnsite	49
Vauxite	53
Messelite	55
Strunzite	58
Ludlamite	59
Laueite	61
Stewartite	61
Phosphosiderite	63
Beraunite	65
Huréaulite	67
Mitridatite	68
Leucophosphite	70
Trace Elements	72
Zinc	72
Lithium	75
Discussion and Conclusions	77
Overall Mineralogy	77
Phosphate Paragenesis	79
Select Associations Paragenesis	89
Unknown Aluminum Rich Phase	95
Classification	96
Conclusions	99
Works Cited	101
Vita	105

List of Figures

Figure 1 Landsat image of Fletcher pegmatite location near N. Groton, NH.....	4
Figure 2: Formations of the NHPS and Grafton Pegmatite field.....	7
Figure 3: Geologic map and sections of the Fletcher Mine, Groton,NH. USGS.....	11
Figure 4: Stewartite with leucophosphite and phosphosiderite on rockbridgeite:	15
Figure 5:Thin section showing ferrisicklerite, heterosite, rockbridgeite, and jahnsite.	15
Figure 6 Top: ABS II (FMP_B49) Bottom: Thin section of B49 under PPL.....	17
Figure 7: Top: ABS III (FMP_B74) 5cm x 4cm. Bottom: ABS IV(FMP_A11)FOV 2cm.....	19
Figure 8: Back Scatter electron image of FMP_B22	21
Figure 9: False color EDS overlay map of FMP_B22.	22
Figure 10: Back scatter electron images of FMP_A25 (top) and FMP_A15 (bottom)	23
Figure 11: Back scatter electron image of FMP_A34 with bands and rind	24
Figure 12: Back scatter electron image of fluorapatite and rockbridgeite.....	30
Figure 13 Fluorapatite anion ratio. Data confirms fluorapatite.....	31
Figure 14: Comparison differentiation in Fletcher pegmatite v. Palermo #2 triphylites..	35
Figure 15 Ternary diagram of divalent metal cations in Fletcher pegmatite triphylite ...	36
Figure 16: Thin section showing ferrisicklerite with heterosite and rockbridgeite in PPL..	38
Figure 17: 3 cm x 4 cm sample of heterosite with jahnsite and rockbridgeite.	40
Figure 18: Thin section of FMP_U7 showing characteristic red-violet heterosite.	41
Figure 19: Fe+Mn/Mn ratios for heterosite v. triphylite	42
Figure 20: Rockbridgeite with jahnsite and hureaulite.	44
Figure 21: Rockbridgeite with jahnsite and phosphosiderite..	45
Figure 22: Ternary diagram of divalent cations Fe, Mn and Mg in rockbridgeite	46
Figure 23: Jahnsite.	49

Figure 24: ternary diagram of jahnsite divalent cations Ca, Fe, Mn.....	50
Figure 25: FMP_B38 containing vauxite.....	53
Figure 26: Ternary diagram of divalent cations in messelite..	56
Figure 27 Prismatic straw yellow strunzite.....	58
Figure 28: Phosphosiderite.....	63
Figure 29: Ternary diagram for beraunite Fe, Mn, all other group 2 (divalent) cations ..	65
Figure 30: Huréaulite.....	67
Figure 31: Mitridatite. Pale olive green upper right quadrant.....	68
Figure 32: Leucophosphite spherule on stewartite.....	70
Figure 33: Zn concentration v. Temperature of select phosphate formation	74
Figure 34: Geochemistry of Fletcher pegmatite primary and secondary phosphates ..	78
Figure 35: Phosphate temperatures of formation	80
Figure 36: General phosphate paragenesis.....	81
Figure 37: Alteration of triphylite under oxidizing conditions.....	84
Figure 38: Alteration of triphylite under reducing conditions.....	86
Figure 39: Paragenesis of Fletcher pegmatite Mine Pegmatite sample B28	90
Figure 40: False color EDS overlay element map FMP_B49.....	91
Figure 41: False color EDS overlay element map of FMP_B49_field 56.....	93
Figure 42: Paragenesis of Fletcher pegmatite Mine Pegmatite sample B49	94
Figure 43: Electron microprobe data: unidentified Al phosphate.....	95
Figure 44: Černý-Ercit pegmatite classification 2005	96
Figure 45: Pegmatite classification groups. Wise, et al., 2022	97

List of Tables

Table 1: Representative electron microprobe analysis of fluorapatite	32
Table 2: Representative compositional data for triphylite.	37
Table 3: Representative electron microprobe analysis of heterosite	43
Table 4: Select representative electron microprobe data for rockbridgeite	48
Table 5: Select electron microprobe data for jahnsite.....	52
Table 6: Representative electron microprobe data for vauxite	54
Table 7: Representative electron microprobe data for messelite	57
Table 8: Representative electron microprobe data for ludlamite	60
Table 9: Representative microprobe data for phosphosiderite	64
Table 10: Representative electron microprobe analysis for beraunite	66
Table 11: Representative microprobe analysis for leucophosphite	71
Table 12: Zinc concentration in select secondary phosphates.....	73
Table 13: Trace Lithium in rockbridgeites	76

Abstract

Investigation of phosphate assemblages selectively collected at the Fletcher Mine pegmatite, North Groton, New Hampshire, yielded eighteen discrete secondary phosphate species. Secondary phases were formed via metasomatic (high temperature) and hydrothermal (low temperature) alteration of primary triphylite and fluorapatite. Mineral associations bear proximal phases known to occur under contrasting conditions, both oxidizing and reducing, suggesting the formation of microenvironments during concomitant mineral generation. Late-stage hydrothermal fluids provide ions taken up in low temperature secondary phases with calcium and magnesium most prevalent in these suites. High iron to manganese ratios in analyzed specimens establish the relative evolution of the pegmatite host. Ubiquitous presence of Huréaulite in all associations suggests trend in late-stage cooling. An unidentified aluminum rich phase requires further investigation. Updated standards of pegmatite classification allow for more precise categorization of the Fletcher Pegmatite based on mineralogy and complexity.

Introduction

The pegmatites of the Grafton pegmatite field in west central New Hampshire have long been known for the phosphate species found there. Few of the hundreds of pegmatites that make up the field exhibit the diversity and quantity of primary and secondary phosphates that the Fletcher pegmatite does. Of those well studied, the Palermo #1 hosts an extraordinary array of phosphates. The Charles Davis mine has been of note, as well (Cameron 1954). The Fletcher pegmatite mine is the location of at least 28 phosphate species to date and the type locality for Jahnsite-CaMnFe (Moore 1974). However, as with most of the hundreds of pegmatites of the Grafton field, there has been little research done on the Fletcher pegmatite outside the realm of Mica mining, which, in the case of the Fletcher pegmatite, ceased decades ago. The Fletcher pegmatite was originally opened in the late 1880s as an open-pit sheet mica mine. After nearly one hundred years of often-changing ownership, since the mid 1970s it has been privately owned and public access to the mine has not been permitted.

Although the past 50 years have seen a marked increase in the amount of research concerning pegmatite phosphate species and paragenesis in general, (Moore 1974, 1978; Fransolet 1986; Francis 1993; Roda, 2004) and the Grafton field in particular (Nizamoff, 2006), the field is still relatively unexplored. Published works regarding phosphates mainly focused on descriptive mineralogy before the 1980s. Phosphate paragenesis has been investigated in few of the major phosphate bearing pegmatites worldwide. They are by no means common. This investigation is the first known discussion of the phosphate paragenesis of the Fletcher pegmatite.

Previous Work

The Fletcher pegmatite mine lies 1.1 km east of the town of North Groton, New Hampshire on the summit of a narrow ridge of Fletcher Mountain. North Groton and surroundings lie in extreme southeast of the Rumney 15-minute Quadrangle. Sheet muscovite was discovered in 1880 and mined almost constantly until 1914. The mine was studied first by D.B. Sterret in 1914, as the ownership of the workings turned over to General Electric. Groton mines, of Franklin, NH took over operation of the mine from 1914 until 1944, at which time further studies were carried out by A.H. McNair, G.B. Burnett and J.B. Headly, Jr. The Fletcher pegmatite was mapped during that time by J.J. Paige and F.H. Main (Cameron, 1954) (Fig 3).

IN 1954, Cameron compiled his work "Pegmatite Investigations, 1942-45 New England" in which he gives detailed information for hundreds of pegmatites in the Northeastern United States. This remains, to date, the most comprehensive description of the Fletcher pegmatite on record in terms of location and historical information.

In the period after WWII Paul Brian Moore analyzed several species from the Fletcher pegmatite as well as described a new mineral of the Whiteite group, which he designated Jahnsite-CaMnFe. The Fletcher pegmatite is the type locality for this mineral. Moore mentions the Fletcher pegmatite in terms of the jahnsite mineral species found there (Moore 1974) (Moore, Ito 1978). Fletcher pegmatite samples of rockbridgeite are also mentioned in this publication and in Moore, 1970. (It is unknown, however, how many trips Moore made to the Fletcher pegmatite before publishing these papers the early to mid-70s.)

Personal communications with R.W. "Bob" Whitmore, who provided the samples for this study, have been the most illuminating as to the current (or most recently

available) state of the mine. From 1969-1974, Whitmore collected phosphate samples from the Fletcher pegmatite, specifically searching for herderites, for which the Fletcher pegmatite is well known. To date, it is the locale of the largest hydroxylherderite (> 3cm) found in New England.

No scientific work has been done at the Fletcher pegmatite since 1974. At this time, a private citizen who has not allowed renewed access to the mine bought the property. Attempts are underway, under a recent new owner, to achieve this goal and if successful will allow for continued and more in-depth work on the geochemistry and genesis of the pegmatite itself. This researcher hopes to be the one to further it.

Geologic Setting

The Grafton pegmatite field (GPF) lies in central western New Hampshire. (Fig. 1) Francis (1993) defines a pegmatite field as an area including one or more pegmatite groups occurring within a common geological environment and generated during a single tectonomagmatic event. Most of the pegmatitic bodies within the GPF exhibit a northeast-southwest trending strike, though some exceptions are seen as apophyses of the northwest trending dikes.

The Fletcher pegmatite (N 43° 45' 35'', W 71° 49' 39'') lies at the extreme north of the GPF, in the extreme southeast of the Rumney 15-minute quadrangle of Grafton County, New Hampshire, located within the New England Appalachians.

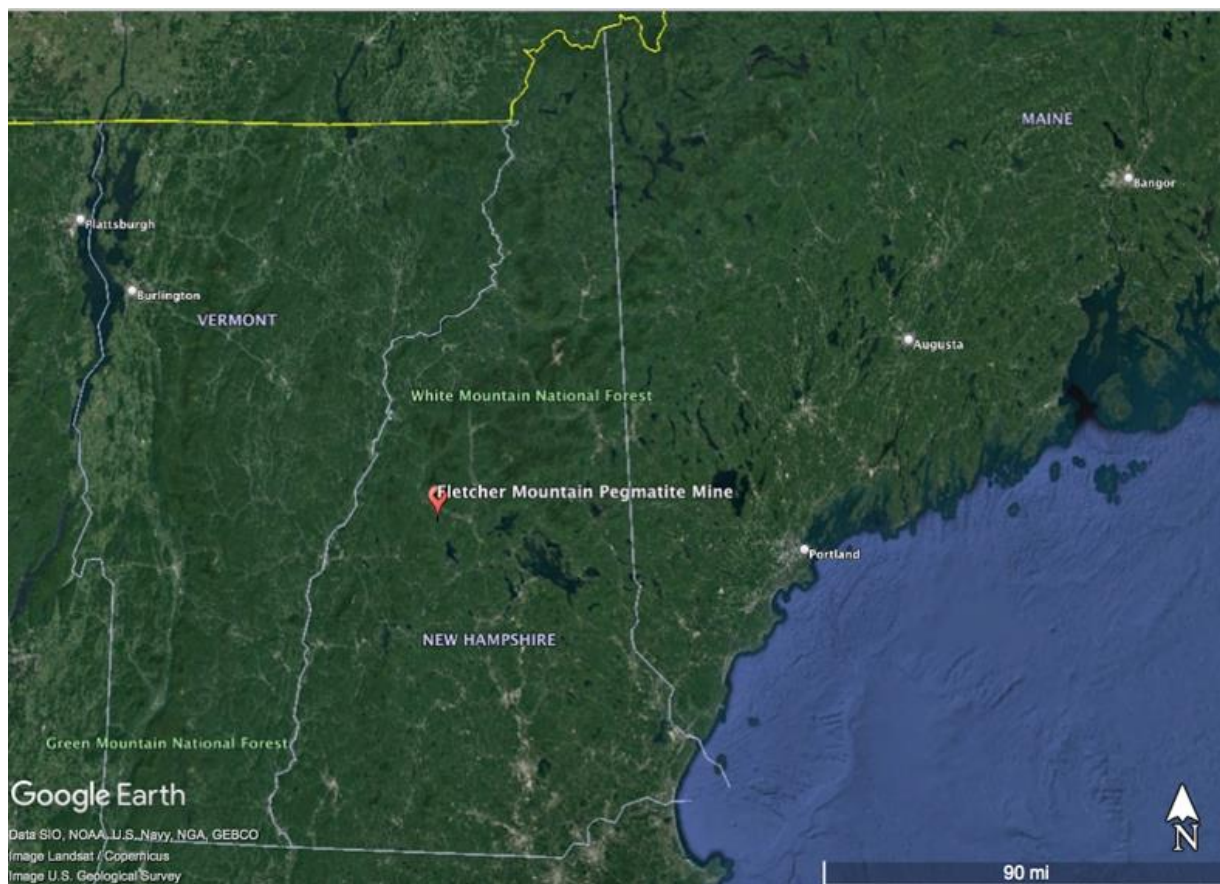


Figure 1 Landsat image of Fletcher pegmatite location near N. Groton New Hampshire

The Taconic, Acadian, and to an extent, Alleghenian orogenies of the Early- to Mid-Paleozoic formed the New Hampshire Appalachians. The first involved the collision of the Taconic (sometimes referred to as the Bronson Hill) volcanic arc with the proto-North American continent, Laurentia. In the late Ordovician, a large segment of the western (leading) edge of the continent Gondwana rifted to create the micro-continent Avalonia. This micro-continental arc is believed to have fused to the continent Baltica in the early Devonian (Torsvik, 2003). As Baltica and Gondwana moved toward collision with Laurentia, Baltica came in contact first with what is modern Greenland, Scotland, and Northeastern Canada, resulting in the Caledonian orogeny. The subsequent collision of the Avalonian arc with Laurentia began the Acadian orogeny, which formed the New England section of the Appalachian range.

Convergence of Laurentia and the micro-continent resulted in episodic volcanism and deposition of flysch and molasse successions (Eusden and Lyon, 1993). The massive dark grey metapelites that comprise the lower member of the Devonian Littleton formation are a result of this flysch deposition and deformation. Syn- to post-tectonic plutonism is thought to be responsible for the emplacement of the New Hampshire Plutonic Suite (NHPS) likely host to the parental source(s) of the Grafton field pegmatites (Spears, et al. 2003).

The Central Maine Terrain (CMT) in New Hampshire comprises metasedimentary rocks of Silurian to Devonian age intruded by sheet-like granitoids of the NHPS (Eusden and Barreiro, 1989). Eusden and Lyon (1993) recognize four major deformational phases (D₁-D₄) and corresponding or subsequent metamorphic episodes (M₁-M₂) for the Central Maine Terrane. These episodes resulted in formation of three major structures that lie partially or entirely within New Hampshire. From west to east these are the

Bronson Hill anticlinorium, the Kearsarge-Central Maine synclinorium and the Central New Hampshire anticlinorium (Fig. 2).

M_1 metamorphism generated a sillimanite-andalusite/kyanite assemblage in association with D_1 deformation, characterized by east and west verging nappes on an axis formed by the Central New Hampshire Anticlinorium (Eusden and Lyon, 1993). D_2 deformation is characterized by isoclinal inclined folds about NE trending axes verging ESE and defined by the presence of second generation of foliated mica porphyroblasts. Eusden and Lyon (1993) note that D_2 effects seem to be restricted to the area east of the CNHA. Broad, open inclined folds distinguish D_3 deformation. This episode was accompanied by peak high-grade CMT metamorphism to a sillimanite-muscovite-biotite assemblage, overprinting the early andalusite phase (Nizamoff 2006) (Eusden and Barreiro 1989). D_4 deformation exhibits evidence of greater intensity and is characterized by tight to isoclinal inclined and recumbent folds about northeast trending axes. Stage-four deformation is only visible west of the Central New Hampshire Anticlinorium, and the easternmost portion is interpreted to represent the eastern limit of backfolding. Deformational and metamorphic episodes are believed to have ended 380ma, whereas concurrent and subsequent magmatic pulses responsible for the emplacement of the New Hampshire Plutonic Suite continued until ~ 355ma.

The New Hampshire plutonic suite is host to the likely source(s) for Grafton Field pegmatites. Eusden and Barreiro (1989) identify three different categories (syn-tectonic, syn-post tectonic, and post-tectonic) of granitoid comprising the sheet-like series of plutons intruding the rocks of the Central Maine Terrane. Of greatest interest to this study are the Early Devonian Bethlehem and Kinsman granodiorites (category 1)

and Mid- to Late Devonian Concord two mica granite (category 2) (Fig. 2). Timing of emplacement of the Kinsman and Bethlehem granodiorites and the Concord granite

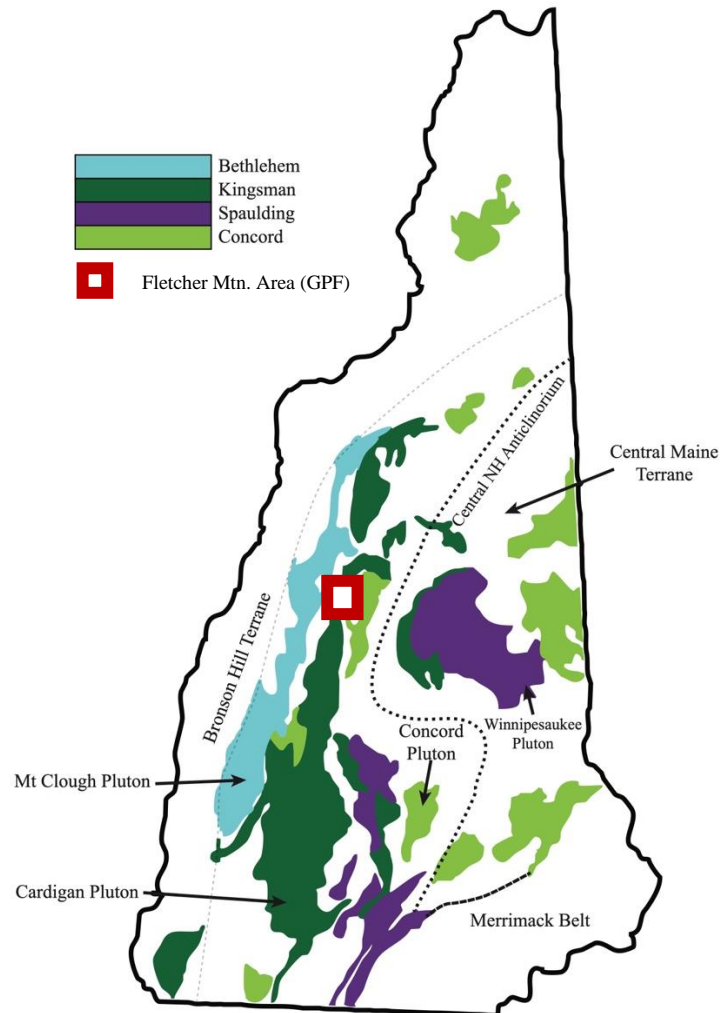


Figure 2: Formations of the NHPS and Grafton Pegmatite field. After Nizamoff 2006, from Dorais 2003.

gives a general idea of the timing of emplacement of the pegmatites according to Nizamoff (2006). Cameron (1954) suggests the Concord two-mica granite as the likeliest source for the Fletcher pegmatite, Palermo, and other pegmatites in the field based on

a lack of crosscutting relationships. However, Nizamoff (2006) reported crosscutting of the Esty mine, 4 km south of the Fletcher pegmatite, with the Concord granite. More recently, the age of the pegmatites has become a known quantity. Bradley et al; (2016) have constrained the age of the Palermo #1 pegmatite, also in the GPF and less than 2km from the Fletcher pegmatite to 326-294 Ma based on $^{206}\text{Pb}/^{238}\text{U}$ analysis of zircons from the wall zone, and $^{40}\text{Ar}/^{39}\text{Ar}$ analysis of muscovite. Proximity of the Fletcher and Palermo pegmatites allows the application of these ages to the Fletcher, which in turn makes the argument that these are likely anatectic in origin, as they are determined to be 30-55 million years younger than the latest limits for the emplacement of the NHPS.

Geology of the Pegmatite

Description of the pegmatite body comes from two main sources: Cameron's 1954 Pegmatite Investigations and from personal communications with one of the last public citizens to collect at the Fletcher pegmatite, R.W. "Bob" Whitmore, before it was privately acquired and closed to the public. The pegmatite lies on the ridge of Fletcher Mountain, 4 Km east of the village of North Groton, New Hampshire. The body is 183 meters in length striking N15°East. The dip of the pegmatite varies considerably over a range from 40-85°E; average dip is 55°E. The dip lies concordant to the foliation of the schist of the Littleton formation, into which the pegmatite intrudes. Between 1880 and 1944, three main cuts were made in the pegmatite, across strike, on the north and south ends and in the center. The south cut is the closest to the core (Cameron 1954).

The pegmatite itself exhibits an irregular zonal structure comprising border, discontinuous wall, outer and inner intermediate, core margin and discontinuous core zones.

The border zone of the Fletcher pegmatite is a fine-grained aplite consisting of quartz and plagioclase. Muscovite is present in places on the hanging wall. Border zone thickness ranges from less than 1 cm to as much as 1 m. This zone exhibits its greatest thickness in the east wall of the north cut in one of the apophyses striking N60°E and dipping 65°SE in the enclosing schist. This offshoot is described as having sharp, deeply weathered contacts (Cameron 1954).

The wall zone is thickest near the hanging wall and is as thick as 0.5 m in areas. This zone is discontinuous and is composed of plagioclase, quartz, and muscovite. At the time of description, sheet muscovite was found on the hanging wall, which is clearly

exposed for much of the length of the dike. The footwall is poorly exposed and bore little or no sheet mica.

The bulk of the pegmatite lies in the outer intermediate zone. This discontinuous zone is rich in plagioclase and quartz with minor perthite and muscovite and contains small accessory garnets. The quartz present throughout the zone is grey and is found either as small bodies or else intergrown with plagioclase. Scrap beryl and muscovite have been found contained in some of these quartz masses.

The inner intermediate zone is discontinuous, consisting almost entirely of perthite. It only exists in the thickest parts of the pegmatite. No accessory minerals are reported from this zone, which trends closer to the footwall. Small strips of biotite were found where the north cut penetrates the inner intermediate zone.

The quartz-muscovite core margin bears small, irregular books of greenish and deep ruby red-red brown mica books, described as very hard and very flat by Sterret and exhibiting edge-parallel color zoning (Cameron 1954).

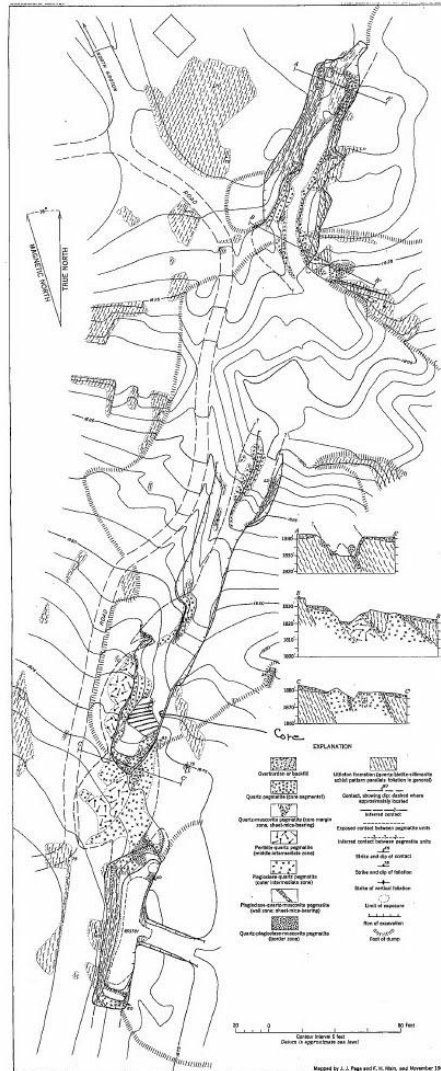


Figure 3: Geologic map and sections of the Fletcher pegmatite Mine, Groton New Hampshire. USGS

What remains of the quartz core is concentrated in the southwest section of the pegmatite, below the "south cut." The core is approximately 15 m in length, comprising several discontinuous, large, quartz pods. Anecdotal description of the pegmatite describes a change in the color of the quartz found in the core and southern section of the pegmatite from that found at the northern end of the pegmatite. The majority of the quartz found is milky grey "bull" quartz. However, at the northern in end, a sugary

white quartz “like that in the core of Palermo #1” has been identified (Pers. Comm., RW Whitmore). It is in south end of the cut, according to Cameron, 1954 that “triphyllite, purpurite, and other manganese phosphates and their alteration products also are found within the pods” (Cameron 1954). These “manganese phosphates and their alteration products” are in fact the iron rich end members of the minerals first described. It is heterosite, for example, the ferric end member in the heterosite-purpurite series, that is found in the Fletcher pegmatite. Phosphate minerals described from the Fletcher to date are autunite, beraunite, bermanite, brazilianite, eosphorite, frondelite, heterosite, hureaulite, hydroxylherderite, jahnsite, laeuite, leucophosphate, ludlamite, metaautunite, metatorbernite, phosphosiderite, rockbridgeite, stewartite, strengite, strunzite, tavorite, torbernite, triphylite, vivianite, and xanthoxenite (MinDat, 2022). The samples in the current study include 18 of these phosphate minerals as well as one aluminum-rich sample yet to be identified. The primary goal of the collector was to find hydroxylherderites, for which the Fletcher pegmatite is so well known, thus there exists a sample bias toward those minerals most often found in association with it.

Descriptive Mineralogy

Selected materials

The Fletcher pegmatite phosphate collection yielded 73 phosphate assemblages. Careful inspection in hand sample under 40x and 100x magnification led to the grouping of these specimens into general categories of mineral associations based roughly on not only the identity of minerals present in each but the apparent similarity of the suites and the complexity of each suite (degree of paragenesis). Though all phosphates examined for this study are triphylite derived, some show more advanced alteration than others. Single and two-phase specimens exist and are also worthy of description. Four distinct categories were chosen before any chemical or structural analysis was undertaken and they have served well throughout. These association base specimens (ABS) are labeled I, II, III, IV. Less complex, two-phase specimens make up Group V. Associations I and II and the most complex suites in this collection and will serve as examples for the paragenetic sequences described in the discussion portion of this work. Descriptions of each follow, along with descriptions of individual samples within those groups whose mineralogy is remarkable for the category. Through these descriptions, a pattern of paragenesis becomes apparent even before analyses are discussed. Detailed descriptions of individual mineral phases are also found in the Analytical Results section of this work.

Association I

(FMP_B28) ± Triphylite + ferrisicklerite + heterosite + rockbridgeite + jahnsite ± stewartite ± huréaulite + phosphosiderite ± beraunite ± leucophosphite

Association I specimens exhibit the Quensel Mason sequence (triphylite, ferrisicklerite, heterosite) either on its own or in association with one or both low temperature phases jahnsite and rockbridgeite and one to several very low temperature hydrothermally altered phosphate phases including phosphosiderite and leucophosphite. (The Quensel Mason sequence (Quensel 1937; Mason 1941) describes the progressive alteration of primary triphylite to ferrisicklerite and then heterosite through the leaching of lithium and the oxidation of divalent iron and manganese to trivalent and is described in detail in the analytical results and discussion sections of this work). Only triphylite, heterosite and rockbridgeite are easily discernable in hand sample without a microscope. Triphylite is not visible in thin section in FMP-B28 or any of the other specimens of type I. In thin section, characteristic orange ferrisicklerite is visible at the top center of the field almost completely replaced by the diagnostic red violet heterosite with dendritic to almost lamellar bright gold, highly pleochroic rockbridgeite extending along obvious fractures. Whitish to pale blue jahnsite replacing rockbridgeite completes the field. (Figure 4) This is the most common assemblage seen in the Fletcher pegmatite collection, with some 25 samples sharing some or all of the mineralogy.



Figure 4: Tiny euhedral Stewartite with leucophosphite (white) and phosphosiderite (blue violet) on rockbridgeite. 3mm FOV. Photo by A. Falster

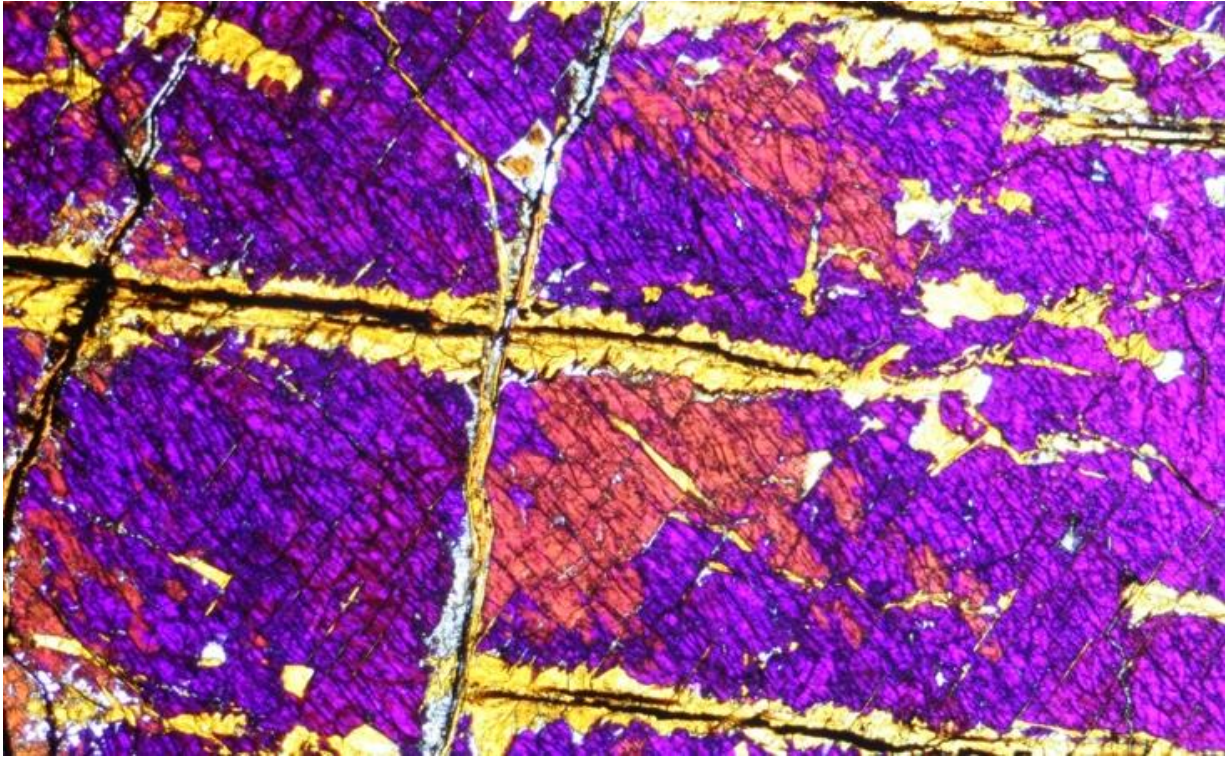


Figure 5: Thin section showing ferrisicklerite (orange) replaced by heterosite (violet), dendritic rockbridgeite (gold), and jahnsite (blue). Scale: 2cm= 500 μ m

Stewartite is found in a small vug in which masses of spherical blue-violet to lavender phosphosiderite are covered by white, earthy spherical crystals of leucophosphite. Leucophosphite grows atop euhedral yellow stewartite crystals and forms a rind on phosphosiderite (Figure 4). Other specimens in this group include FMP_U7, B29, A32, A19A, U8. Beraunite, brick red rather than the common pale green, covers botryoidal rockbridgeite in a thin rind in some of these specimens.

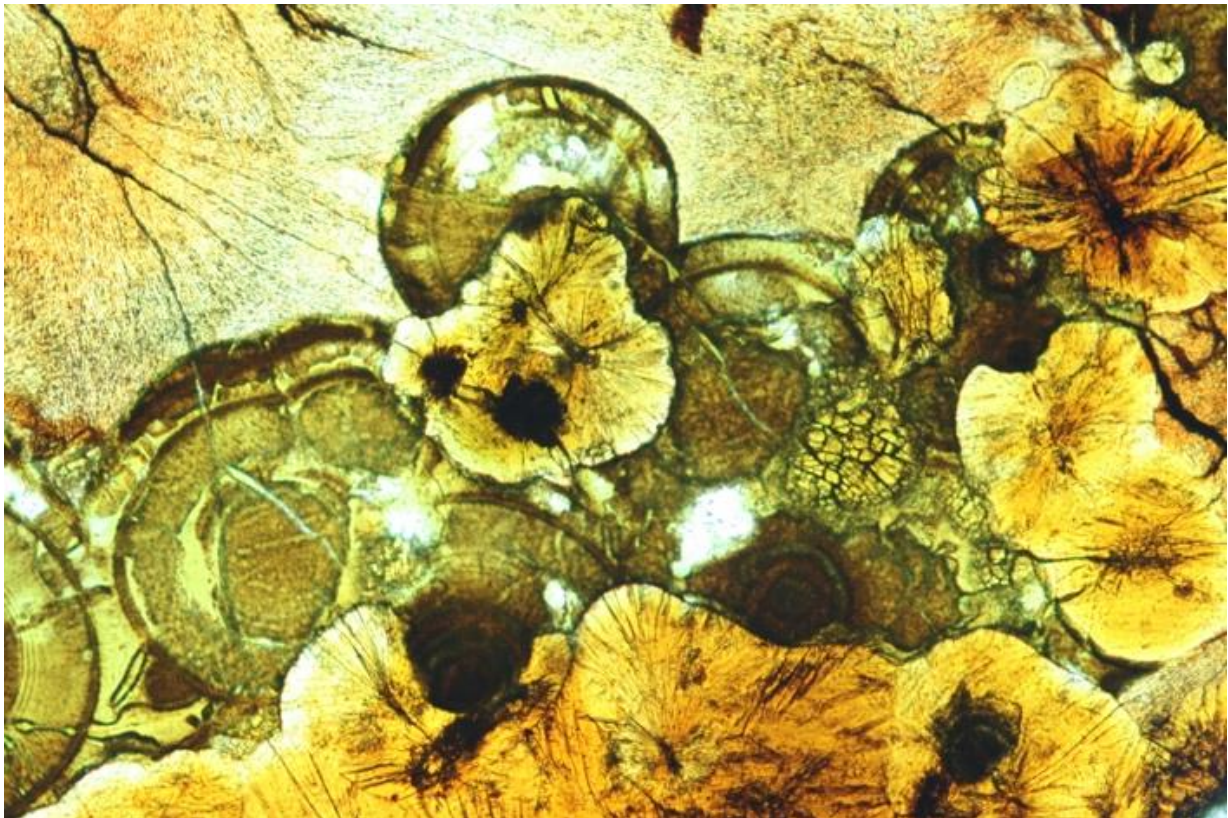
Association II

(FMP_B49) rockbridgeite + jahnsite ± fluorapatite ± messelite ± ludlamite ± strunzite ± laueite + mitridatite

The ubiquitous rockbridgeite forms much the core of this suite and all others in association II. Minor muscovite and albite can be seen in hand sample and pale green almost powdery mitridatite covers one end. The most remarkable aspect of this hand sample is the thick rind of straw-colored acicular strunzite crystal clusters covering much of the sample and partially obscuring equally remarkable pale green fluorapatite crystals. In thin section, highly pleochroic sub-spherical acicular rockbridgeite can be seen in the lower left quadrant with fluorapatite clearly identifiable by its habit. A mineral consistent with Jahnsite takes up the upper right quadrant. FMP_B49 boasts a high number of discrete calcic phases for this collection: fluorapatite, jahnsite-CaMnMn, jahnsite-CaFeMn, messelite and mitridatite. Calcium in association II is likely derived from fluorapatite, either primary or secondary.



Figure 6 **Top:** ABS II (FMP_B49) 3cmx4cm **Bottom:** Thin section of B49 under PPL. 2cm=500 μ m



Association III

(FMP_B74)

Masses of glassy, black, radially aggregated rockbridgeite and fractured quartz make up the bulk of FMP_B74 in hand sample (Fig. 7). On one face, within and surrounding vugs in the rockbridgeite, sub-millimetric clusters of butter yellow tabular blades consistent with Jahnsite or stewartite are partially replaced by spherical aggregates of pale pink needles of hureaulite and tiny white spherules consistent with leucophosphite. On another face, a thin rind of pale green powdery mitridatite covers the larger, darker, radial acicular clusters of rockbridgeite near the edge of the sample. Due to the similarities between mitridatite and beraunite in hand sample, XRD or electron microprobe analysis is required to further determine the identity of the rind however similar rinds on FMP_B49 were determined via X-ray diffraction to be mitridatite and beraunite found and analyzed in this study has been of the brick red variety, rather than the common pale green. This is one of the only specimens in which triphylite is visible in hand sample. FMP_A17 boasts similar mineralogy and was used for chemical analysis of triphylite from Fletcher pegmatite.



Figure 7: **Top:** ABS III (FMP_B74) 5cm x 4cm. **Bottom:** ABS IV(FMP_A11)FOV 2cm



Association IV

(FMP_A11) Rockbridgeite + huréaulite ± quartz

Distinctive seams of sub-millimetric, very clear quartz crystals on black botryoidal rockbridgeite characterizes this association (figure 7), which is also covered with thin, dark orange, earthy rinds of huréaulite and thicker, paler orange hureaulite masses. Not chosen for chemical or structural analysis, this remarkable specimen is nonetheless a spectacular mineral suite. Samples FMP_A7, FMP_U11, FMP_U19 all share this mineralogy.

Group V

(FMP_A15, FMP_A25, FMP_B22, FMP_B34, FMP A_34) ± Quartz ± albite ± fluorapatite ± rockbridgeite ± huréaulite ± kryzhanovskite

Less complex two- and three mineral assemblages, come including rock forming minerals albite, muscovite, and quartz, were also found in the collection. These boast one to two of the more commonly seen low temperature Fletcher pegmatite phosphate phases at most, making them unsuitable for a full picture of paragenesis but no less important to the collection. FMP B_22 is a quartz nodule capped by a thin brownish green rockbridgeite rind. In thin section, veins of rockbridgeite extend into fissures in the quartz, revealing a peculiarity of late stage (hydrothermal) phosphate minerals. (Figure 8)

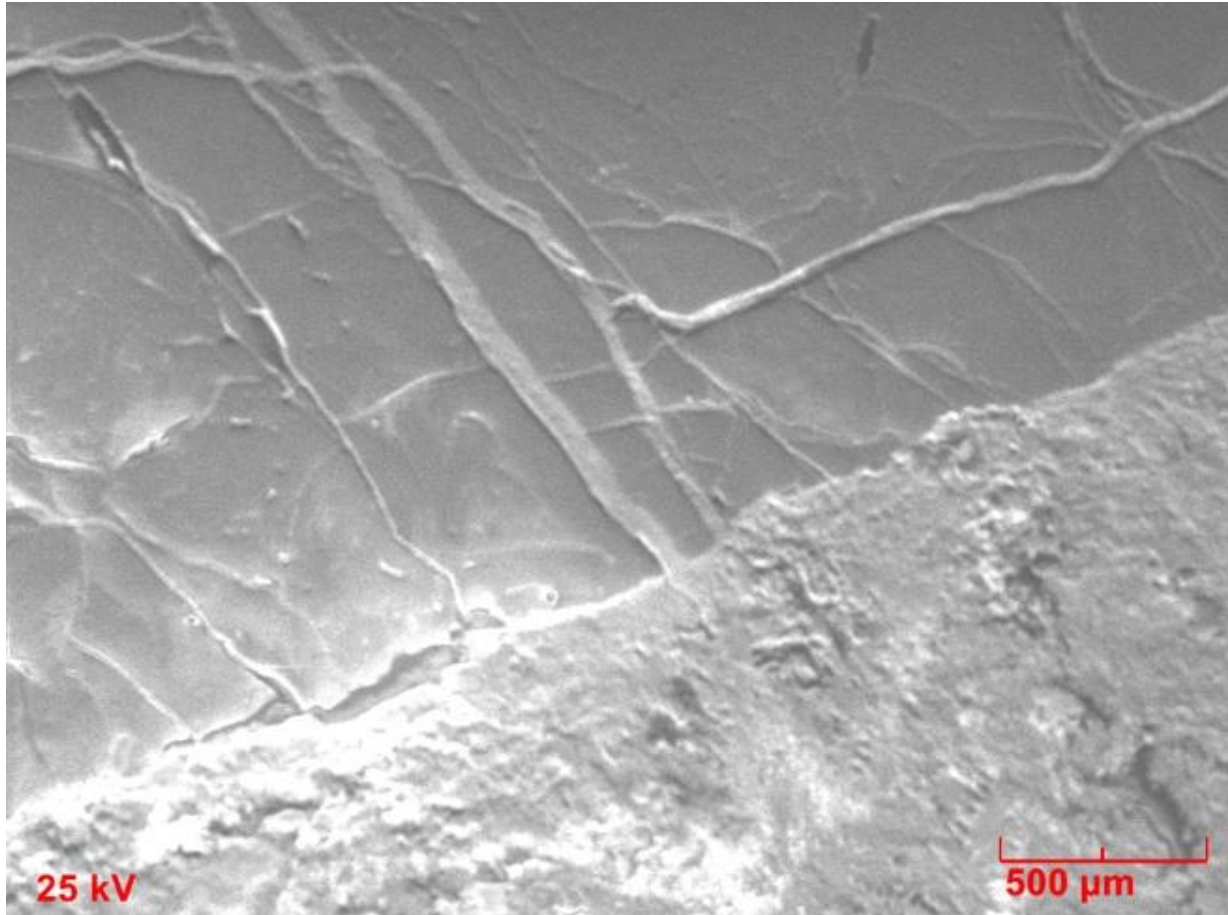


Figure 8: Back Scatter electron image of FMP_B22

The reason it is sometimes difficult to locate the source of additional cations in these stages is that no source obvious source of accessory cations can be found in proximity. Hydrothermal fluids can travel along fissures in rock or in rock forming minerals resulting in assemblages of secondary phosphates forming at some distance from the cation source (Nizamoff, 2006). FMP_B22 is a vivid example of this phenomenon. False-color energy-dispersive spectroscopy (EDS) element-distribution maps superimposed on the back-scatter electron images of this specimen can be seen in figure 9. FMB 34 is another exemplar of this mineralogy.

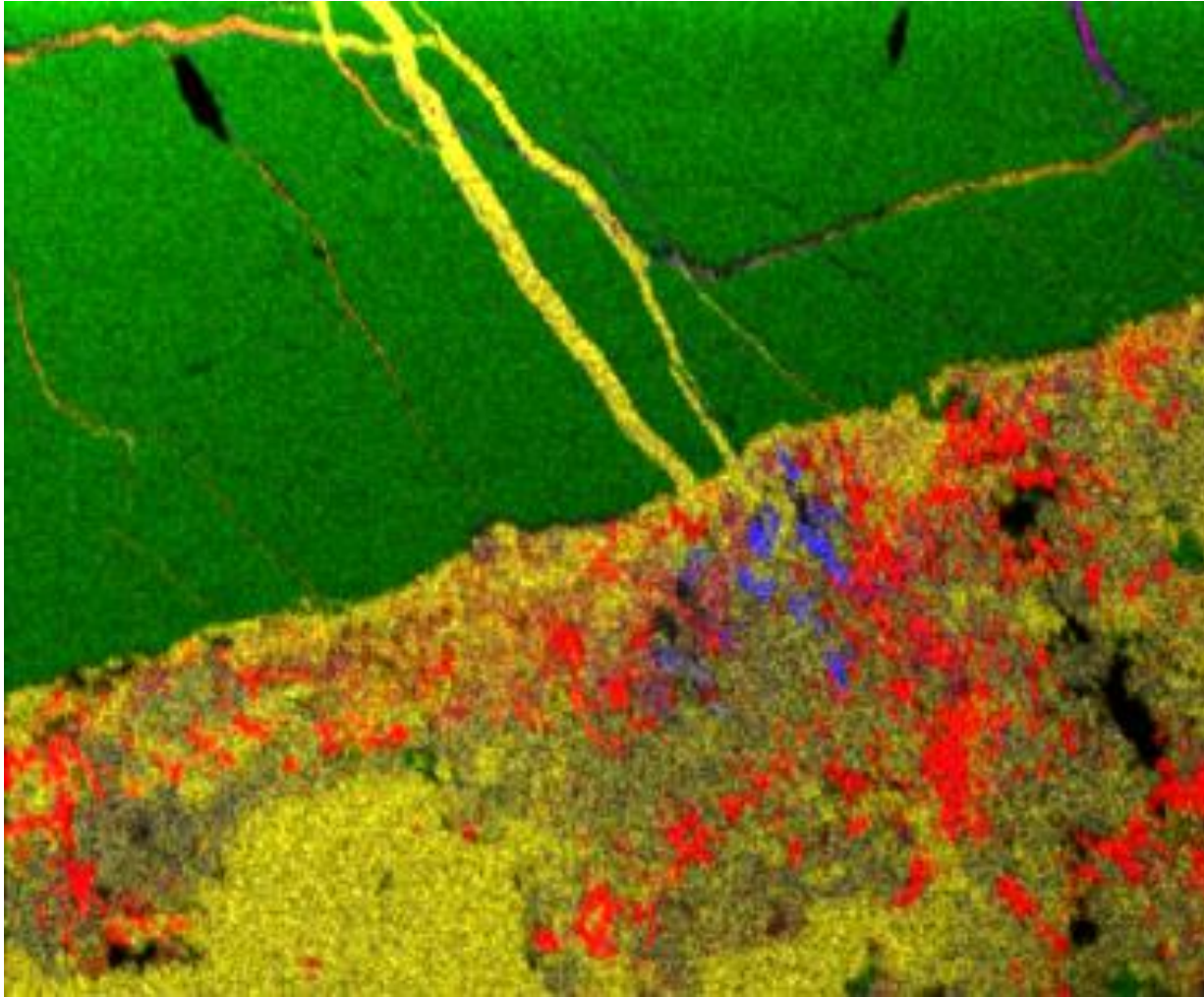


Figure 9: False color EDS overlay map of FMP_B22. Si-Green, Fe-yellow, Mn-blue, Ca-red. Scale: 2cm=500μm

FMP_A15 and FMP_A25 contain dark red hydroxylapatite. In the former, large hydroxylapatite crystals are seen intergrown within an indeterminate Fe-phosphate, in hand sample under magnification, tiny euhedral blood red hydroxylapatites are visible. In the latter, pale green material consistent with an having similar EDS spectra as hydroxylapatite is seen as inclusions in albite. Back-scattered electron images of each can be seen in figure 10.

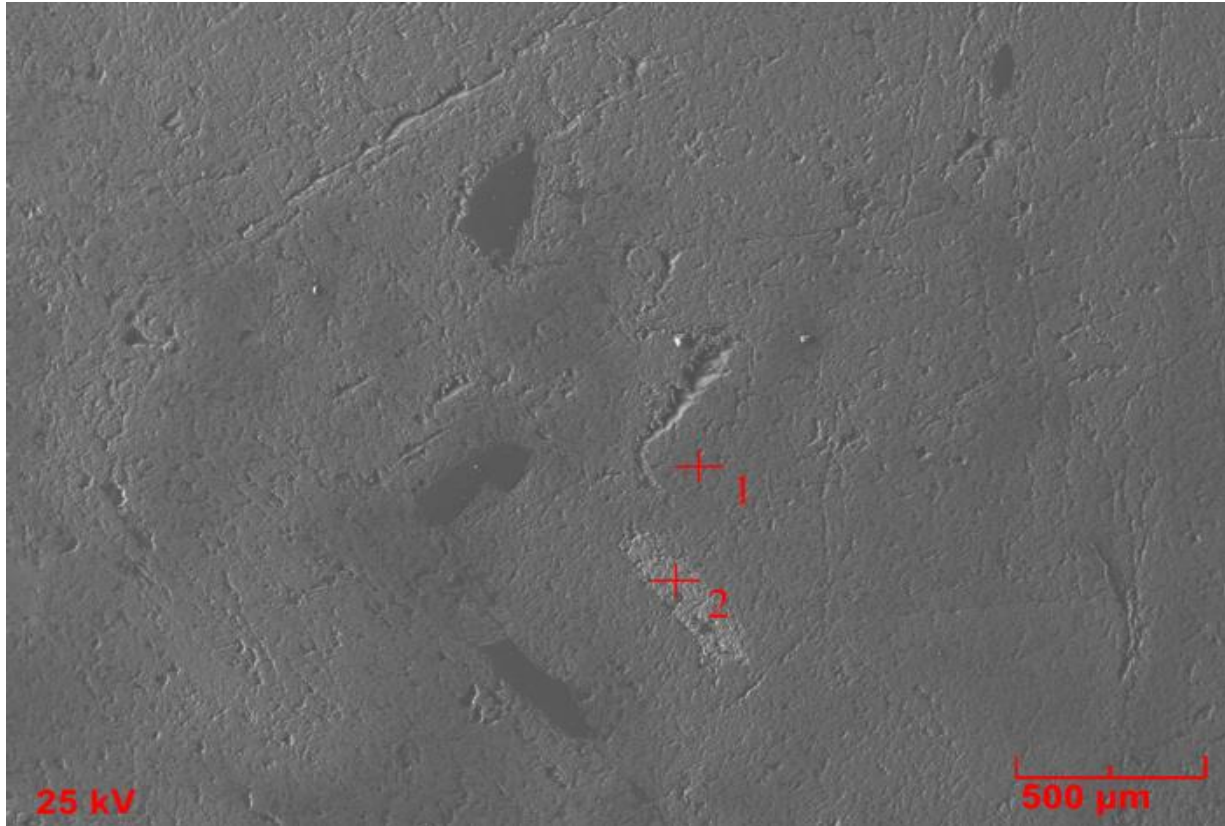
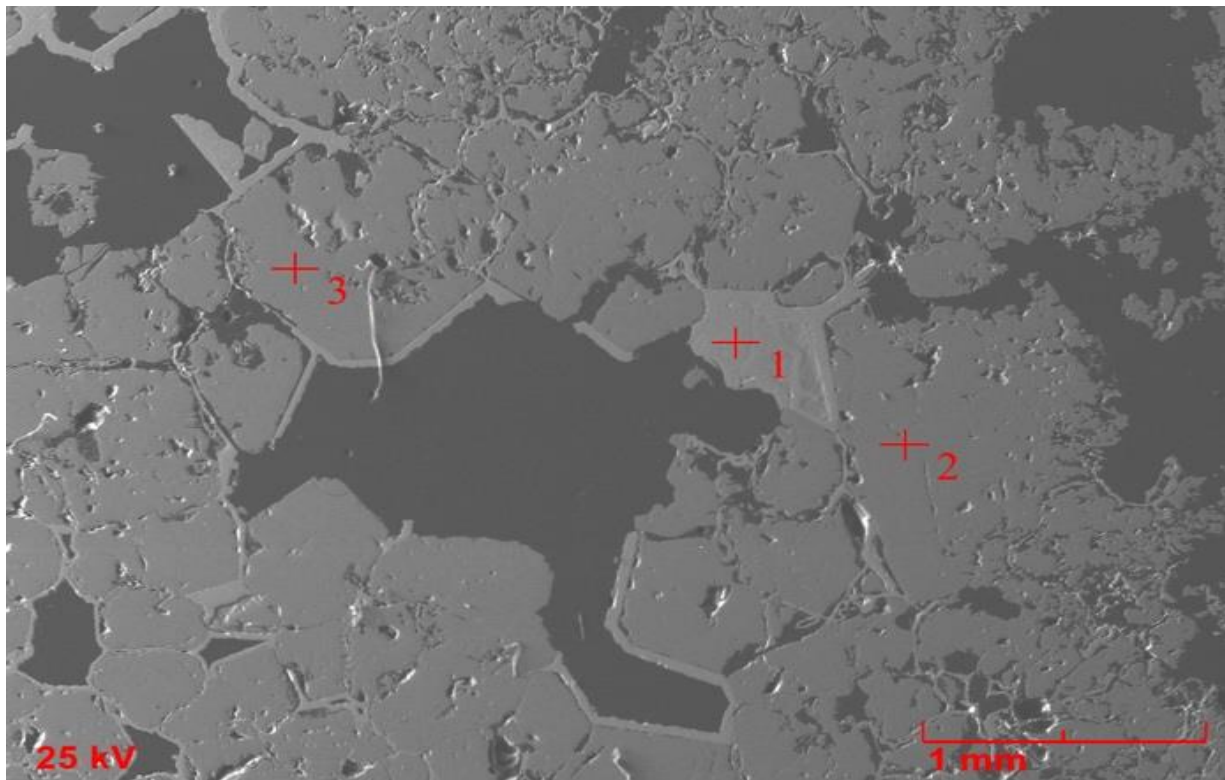


Figure 10: Back scatter electron images of FMP_A25 (**top**) and FMP_A15 (**bottom**)



Finally, FMP_A34 is a quirky member of the sample group in that it is the only one to contain a mineral morphologically consistent with kryzhanovskite (Vignola, pers. Comm. 2014). A34 in thin section shows a mass of acicular crystals chemically consistent with rockbridgeite, but unusual in habit. It is surrounded by two thick bands, one manganese rich, the next calcium rich. The calcium rich band shows the characteristic “candy ribbon” texture of apatite but contains a significant amount of Fe and thus would seem to be more consistent with jahnsite-CaFeFe. The manganese rich band is consistent with kryzhanovskite in its morphology. The crust on this sample is rockbridgeite, confirmed by electron microprobe. A back scatter electron image of this specimen with bands clearly visible can be seen in figure 11.

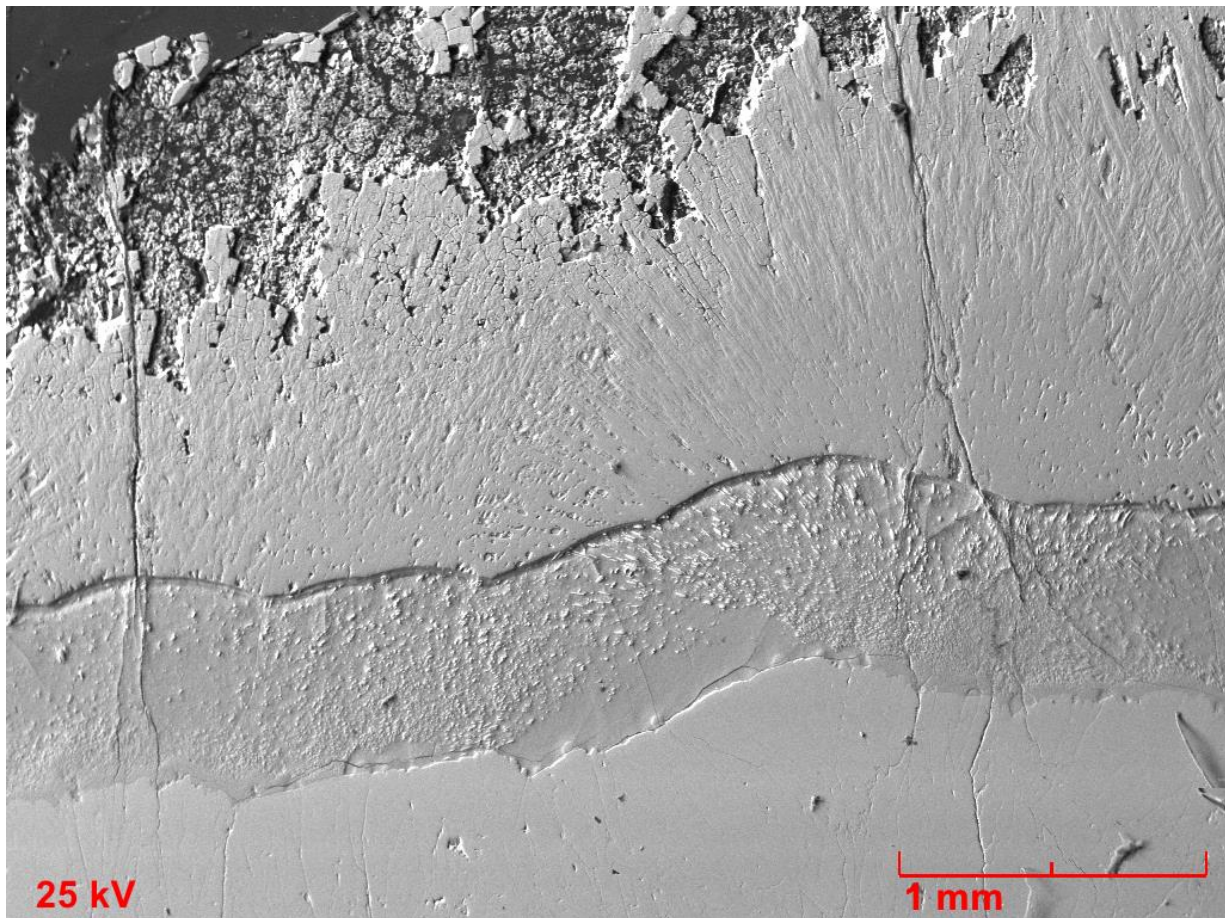


Figure 11: Back scatter electron image of FMP_A34 with bands and rind clearly delineated

Analytical Methods

Sample collection

Specimens upon which this study is based were collected over a period of several years beginning in 1969 by R.W. Whitmore and his wife, Edna. These samples were taken from the core margin of the pegmatite and from the prolific dumps. The samples were provided to the MP² research group at the University of New Orleans and through it, to this researcher, by the Whitmores.

Thin Sections

Thin sections were prepared by Applied Petrographic Services. Samples were prepared by being cut with a diamond blade saw to a size smaller than the 27x46 mm of a standard glass slide and mounting then to glass slides. Applied Petrographic then ground the samples to the standard 30 μ m thickness. Once returned, the sections were polished to a high finish on a Buehler polishing table using 0.3 μ m alumina grit.

Polished Sections

Samples were cut with a diamond blade saw. Many samples, due to the small size and relative softness and brittleness of phosphate materials, were impregnated with casting resin before cutting. These sections were then ground to a flat finish on a Buehler grinding table using a 400-grit silicon carbide powder. Sections were then polished to a high finish on a Buehler polishing table using 0.3 μ m alumina grit.

Electron Microprobe

Two groups of samples were analyzed on the electron microprobe. Raw mineral samples were mounted in epoxy and then ground and polished in the same manner as the final steps in the preparation of thin sections described above. Thin sections were also analyzed by electron microprobe. After rinsing, excess alumina grit was removed from both sample groups by placing samples in an ultrasonic cleaner for 5 minutes. After drying on a drying oven, samples were coated with 250 ± 20 angstroms carbon under a vacuum at 1×10^{-5} torr. To preserve coating, samples were placed in a desiccator until being analyzed. Analyses were performed at the University of New Orleans, by Alexander U. Falster using a fully automated ARL-SEMQ electron microprobe. Operating conditions were 15 kV acceleration potential, 15 nA beam current and 60 seconds counting time. Background determinations were done using MAN. These operating conditions were used for all analyses. A 2 micron beam diameter was used for most samples, with the exception of beam sensitive phosphates, for which a 3-4 micron beam was used. MAN standards for phosphates included hematite, vanadium (V) oxide, Zn Oxide, Quartz, and Fluorite as well as the following: Clinopyroxene (Si Ka, Fe Ka, Ti Ka, Ca Ka, Mg Ka), Albite (Si Ka, Al Ka, Na Ka), Fibbia adularia (Si Ka, Al Ka, K Ka), Plagioclase An50 (Si Ka, Al Ka, Ca Ka), Cerro de Mercado apatite (P Ka, Ca Ka, F Ka), Fayalite (Si Ka, Fe Ka), Rhodonite (Si Ka, Mn Ka), Andalusite (Si Ka, Al Ka), Fluortopaz (Al Ka, Si Ka, F Ka), Strontium sulfate (Sr La), Barium sulfate (Ba La), Pollucite (Cs La) and Rubidium Leucite (Rb La), Triphylite (P Ka, Fe Ka), Lithiophilite (P Ka, Mn Ka), Amblygonite (Al Ka, P Ka, F Ka). Data were processed via Probe for Windows by MicroBeam, Inc.

Data recalculation

Electron microprobe compositional data for minerals simultaneously bearing divalent and trivalent iron and or manganese was done stoichiometrically. Iterative normalization to the desired number of Fe³⁺, Fe²⁺, and or H₂O apfu was carried out using the goal-seek function in Microsoft excel. Use of this method is noted where employed.

Scanning Electron Microscopy

Energy dispersive spectral analyses were collected using a digital AMRAY 1820 scanning electron microscope. Thin sections were attached to an aluminum sample stub with conductive putty. Individual crystal clusters were also analyzed. They were affixed to sample stubs with conductive putty and sprayed with a conductive coating before analysis. Operating conditions included an acceleration potential of 15-25 kV, 400-micron final aperture, 18 mm working distance, 0-10 degrees sample tilt, and 3.0 spot size. Backscattered electron images were collected using a frame size of 2048x2048 pixels and X-ray maps collected at 1024x1024 pixels with a 20-50 ms dwell time per pixel. Data and images were acquired using Iridium/EDS2000 software by IXRF Systems, Inc.

X-Ray Diffractometry

X-ray diffraction patterns of powdered mineral samples were obtained by Pietro Vignola at CNR-Instituto per la Dinamica dei Processi Ambientali, Milan, Italy using a Panalytical X'Pert Pro automatic X-ray powder diffractometer working in Bragg-Brentano theta-theta geometry mounting a high speed X'Celerator strip detector

working with a window of $2.12 \text{ } 2\theta^\circ$. The radius of the goniometer was 240 mm. Fixed divergence slits of 0.5 mm were mounted on both primary and secondary beam. Patterns were collected with a Ni filtered Cu K α radiation at 40 Kv 40 mA from 5 to 120 $2\theta^\circ$ with a step size of $0.017 \text{ } 2\theta^\circ$. In order to correct zero shift of the goniometer NIST silicon 640c and lead nitrate were used as internal standards.

Direct Current Plasma Spectrophotometry

Approximately 50-100 milligrams of each given sample were drilled from matrix and dissolved in 20 ml of 51% nitric acid at room temperature. Samples were then placed in a Beckman DCP for analysis. This method was used to determine the presence of trace Zn and content in select samples For determination of Li content rockbridgeite, the process was repeated but with 50-100 milligrams of each sample drilled from matrix and dissolved in 35 ml of 51% nitric acid at room temperature.

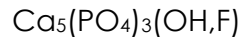
Analytical Results

In the descriptive mineralogy section of this study, the specimens for this work were organized into groups represented by association base specimens. These exemplar specimens will provide the backbone for the discussion of paragenesis in the following section. In this section the primary and secondary phosphate minerals found and analyzed via electron microprobe, Scanning-electron microscopy, X-ray powder diffraction, and study of optical properties in thin section are characterized individually, and results of trace element analysis of Zn and Li in secondary high and low temperature phosphate minerals, carried out via DCP, are also described. Representative analyses for each phase followed by analysis of the suite as a whole are also included.

Chemical Composition and Structure

Individual primary and secondary phosphates are presented in the order of their conditions of formation. The pegmatite primary phosphate triphylite forms, as other primary phosphates, between 650°C and 500°C, (Moore 1973) whereas metasomatically altered (high temperature) secondary phases form between 500° and 300° degrees (Moore 1973). Below 300°C, as molecular water can begin to be incorporated into the structure of the basic iron phosphates, hydrothermally altered, or low temperature phosphates will form. Those that form at the very lowest temperatures. (100°-50°) are also the last to form.

Fluorapatite



Apatite can appear as a primary phosphate in pegmatites or as alteration products (secondary) in the presence of ample calcium. Association II bears small (1-3mm) spherulitic inclusions of fluorapatite visible in thin section. Though appearing almost zoned in BSE imaging (figure 12) compositional data did not suggest a significant variation in chemistry. The presence of fluorapatite suggests they are the source of calcium for messelite and jahnsite, also found in this association.

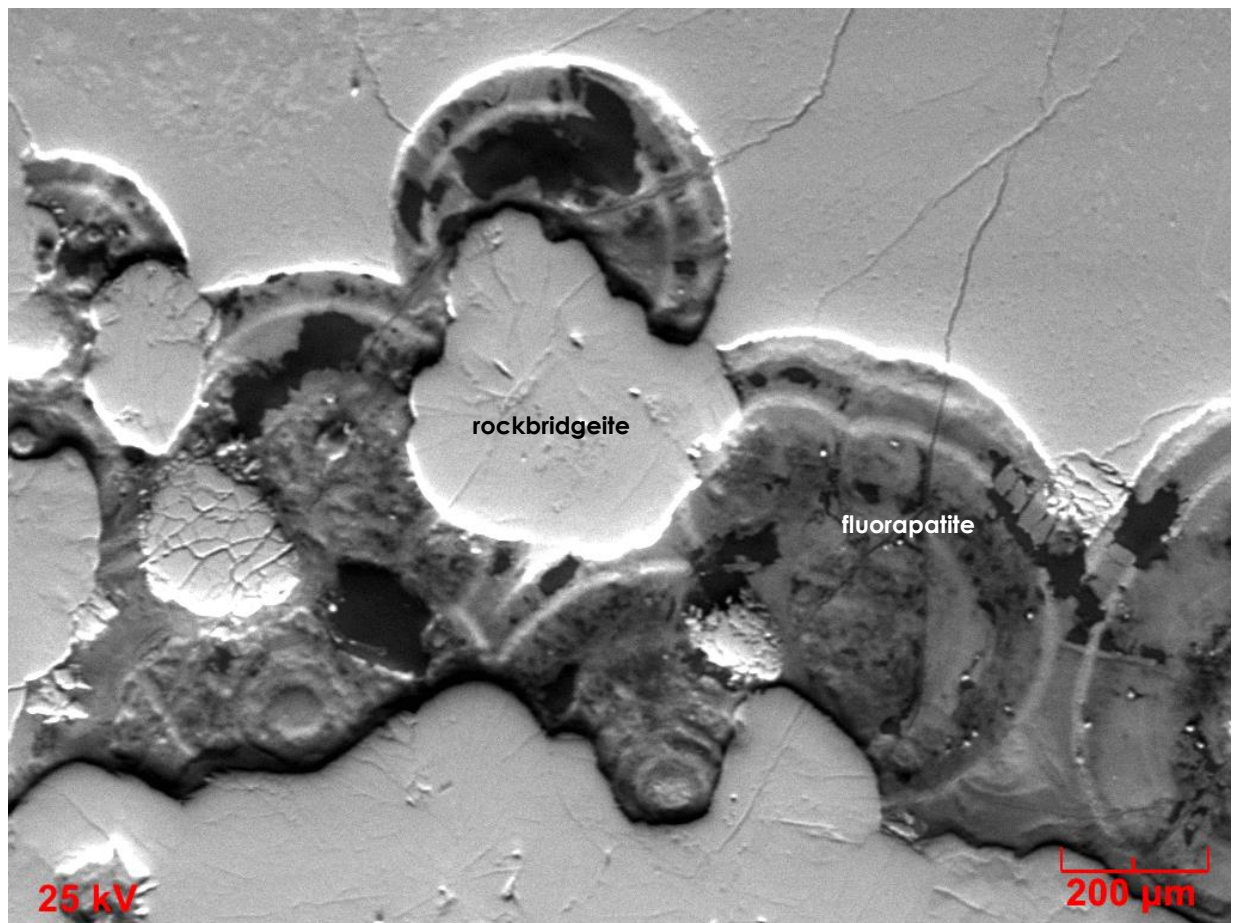


Figure 12: Back scatter electron image of fluorapatite and rockbridgeite in association base specimen II, FMP_B49

The OH/F ratio of the Fletcher pegmatite apatites in this study ranges from 0.14 to 0.17, thus identifying them as fluorapatites (see fig 13). Representative electron microprobe data of Fletcher pegmatite fluorapatite appears below in table 1.

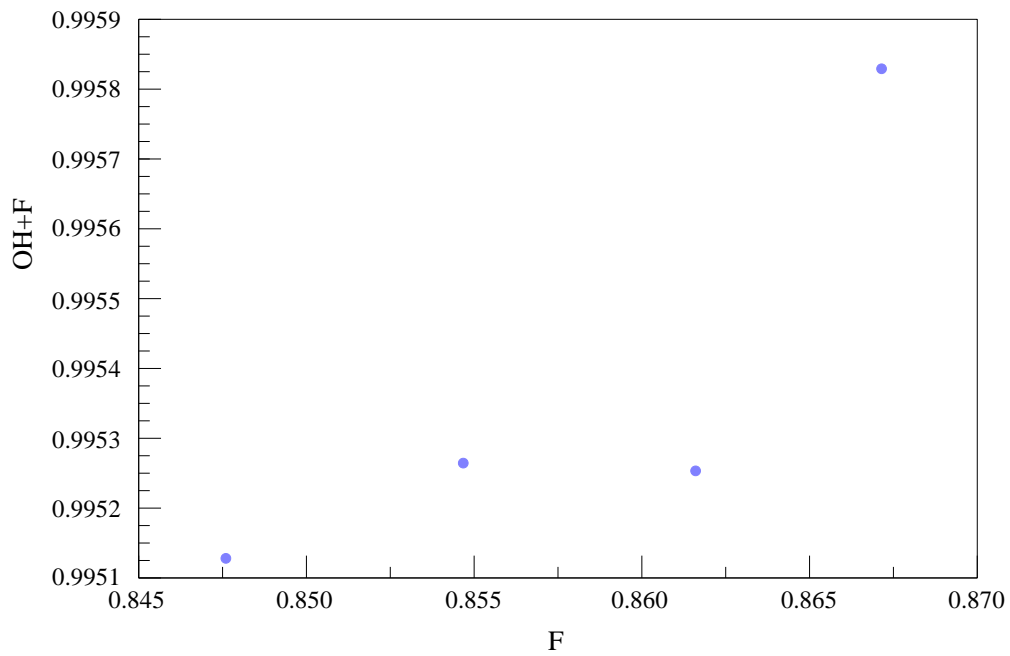


Figure 13 Fluorapatite anion ratio. Data confirms fluorapatite.

Fluorapatite

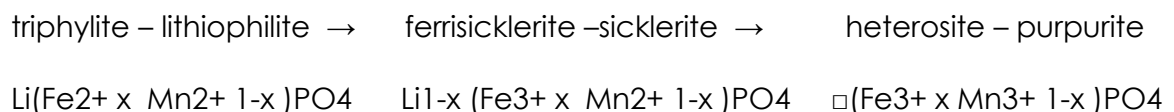
B49 Field 58-1	
Wt. %	
P2O5	42.16
SiO2	0.08
FeO	0.01
MnO	0.01
SrO	0.02
CaO	55.48
H2O calc	0.23
Cl	0.00
F	3.27
sub total	101.25
O=F+CL	1.38
<hr/>	
total	<hr/> <hr/> 99.88
<i>Normalized to 12 Oxygen atoms +1(OH, F, Cl)</i>	
P	2.998
Si	0.006
<hr/>	
	3.004
Fe	0.001
Mn	0.001
Sr	0.001
Ca	4.992
<hr/>	
Σ	4.994
H	0.129
Cl	0
F	0.867
<hr/>	
Σ	0.996

Table 1: Representative electron microprobe analysis of fluorapatite

Triphylite



Triphylite is the predominant primary phosphate at the Fletcher pegmatite. While it is physically present in 3 of the samples in most of the current sample set its presence has been inferred based on the abundance of its known alteration products where primary phases are no longer apparent. Triphylite forms the ferrous end member of the series with manganous lithiophilite. Both have been recorded at Fletcher pegmatite (Cameron, 1954), but the current sample set has yielded no obvious lithiophilite and Fe/Mn ratios of the high temperature alteration products seen in this set suggest they are triphylite derived. Triphylite crystalizes in the orthorhombic system and appears as large deep green to blue green blocky masses in association FMP_A17. The majority of the triphylite in this study has undergone some amount of metasomatic alteration, either to high temperature secondary phosphates via the Quensel-Mason sequence, resulting in ferrisicklerite and then heterosite, or else further to low temperature alteration of these phases (Quensel 1937; Mason 1941). Interestingly, there is little ferrisicklerite and heterosite found with triphylite in the set, though both phases exist elsewhere together. The Quensel-Mason series involves the leaching of lithium and the oxidation of first iron and then manganese via the substitution mechanism:



Heterosite, like ferricklerite-sicklerite, retains the original Fe/Mn ratio of the parent, triphylite (Fransolet 2007). Its presence is therefore significant to this study for the interpolation of that relationship especially in the absence of triphylite, which is not present in many of the specimens in this study. The Quensel-Mason sequence and secondary phosphate paragenesis are further addressed in the discussion section.

Triphylite is significant to the study of granitic pegmatites as the Fe/Mn ratio can indicate the degree of evolution of the pegmatite (Keller, 1991). The lower the ratio of iron to manganese, the greater the degree of evolution/fractionation. (Černý et al., 1985). FeO values range from 31.65 – 49.8 wt.%; MnO from 2.7- 10.1 wt.%. Some Fletcher pegmatite triphylite also exhibits significant amounts of MgO (1.3-3 wt.%). This is consistent with triphylite from the Palermo#2 pegmatite, but unusual for other phosphate bearing pegmatites (Nizamoff, 2006). Fletcher pegmatite triphylite has a high Fe/Mn ratio, ranging from 4.248 to 17.576. Triphylite from the Palermo #1 pegmatite, remarked upon in Nizamoff, 2006 as being high for New England pegmatites, is significantly lower than those ratios found at Fletcher pegmatite.

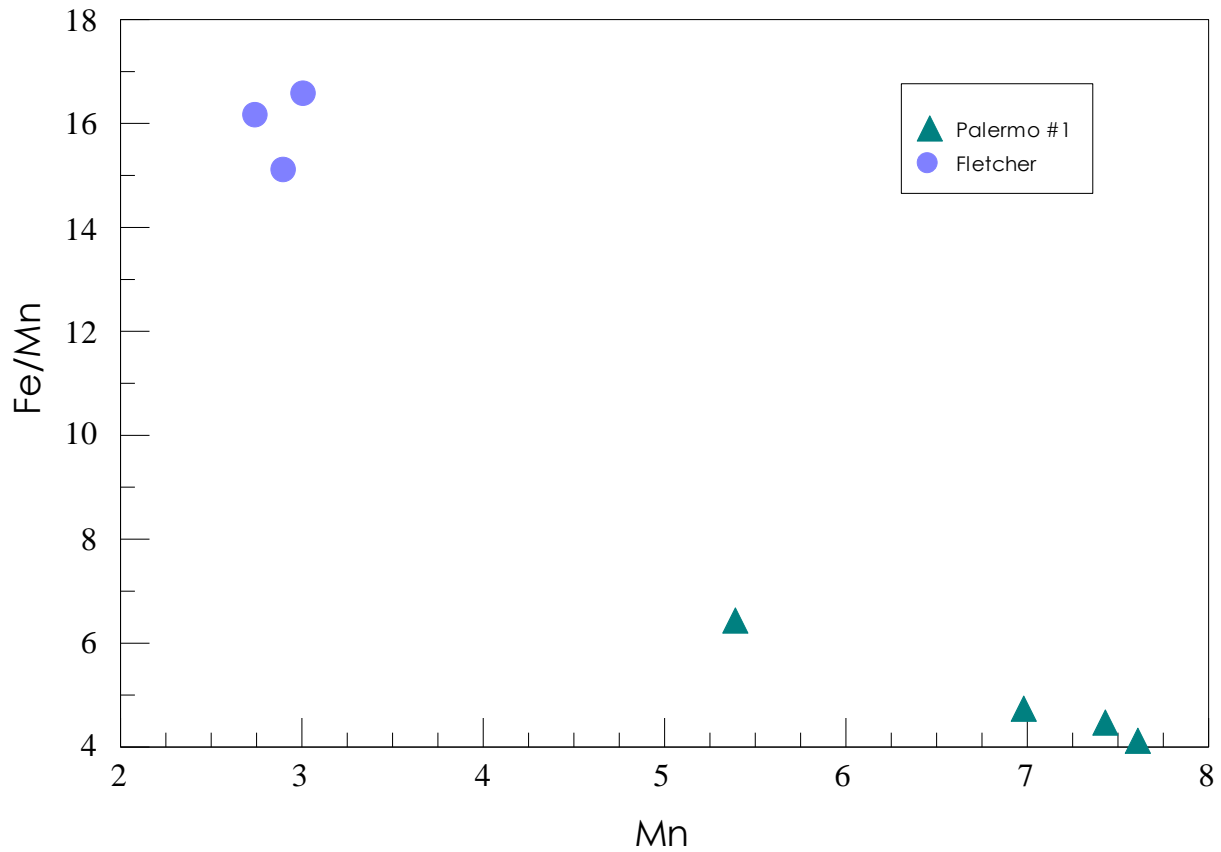


Figure 14: Comparison of degree of differentiation in Fletcher pegmatite v. Palermo #2 triphylites. Palermo data from Nizamoff 2006

A ternary diagram of Fletcher pegmatite triphylite compositional data also shows this trend. Samples including the higher-than-expected magnesium content in some of the samples are evident. Graphic analysis clearly shows the primary phosphate in FMP_A17 to be the ferrous endmember triphylite, and poorly evolved, at that.

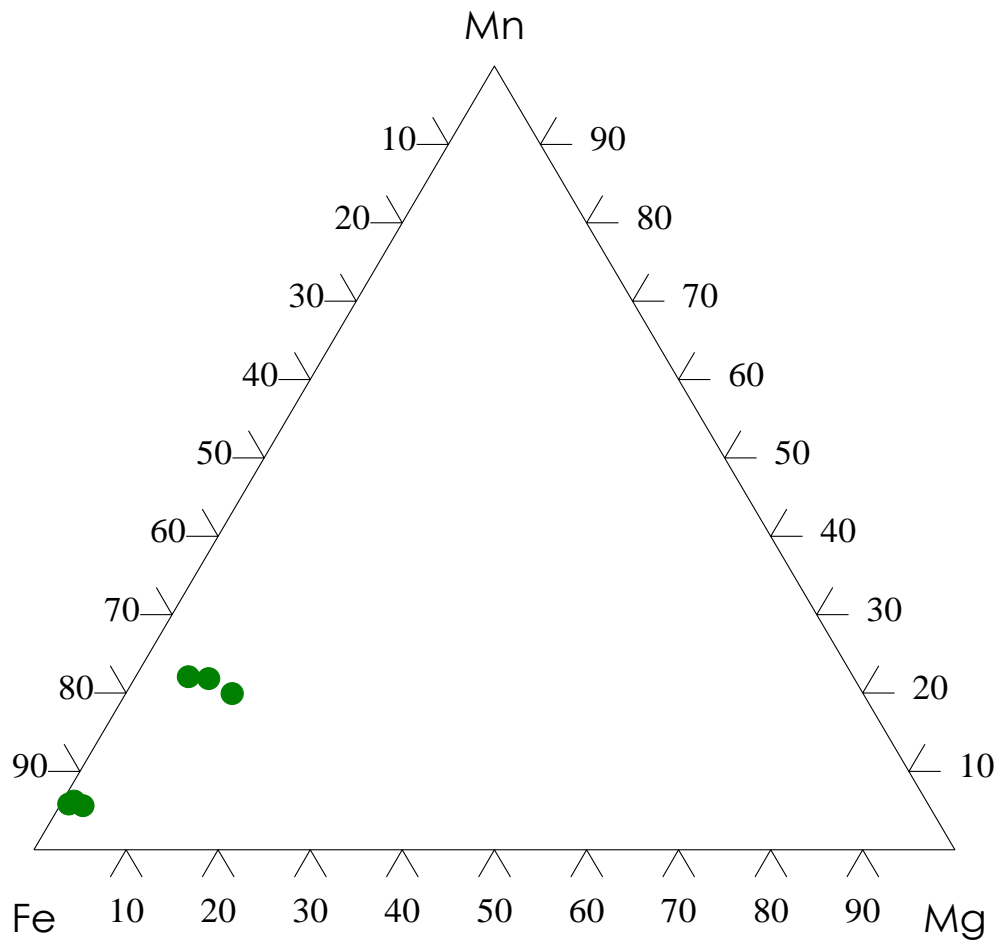


Figure 15 Ternary diagram of divalent metal cations in Fletcher pegmatite triphylite

Triphylite	
FMP_A17	
Wt%	
P2O5	51.34
FeO	31.65
MnO	9.09
MgO	3.00
Li2O calc	9.90
Totals	104.98
P	1.033
Fe	0.609
Mn	0.183
Mg	0.106
Σ	0.898
Li	1.000

Table 2: Representative compositional data for triphylite. Wt% total is high due to less precise analysis on SEM, rather than microprobe.

Ferrisicklerite

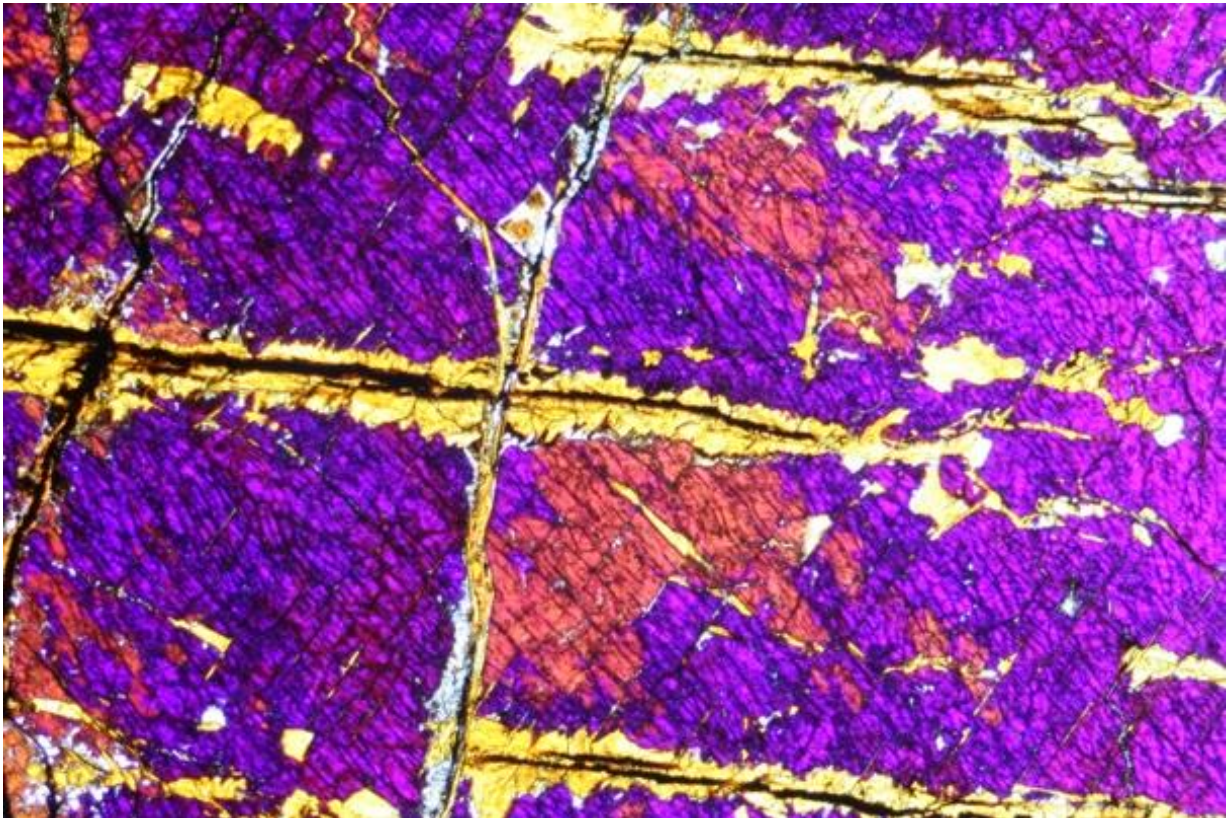


Figure 16: Thin section showing characteristic orange ferrisicklerite with heterosite and rockbridgeite in PPL. FOV 3mm

Ferrisicklerite is the iron rich end member of the series with manganese rich sicklerite and is a high temperature alteration product of triphylite-lithiophilite by way of the Quensel-Mason (Quensel 1937) (Mason 1941) sequence and thus is evidence in the absence of triphylite in many of the samples that it was, indeed, the abundant primary phosphate in the set. In the sample set Ferrisicklerite appears almost exclusively in thin section, as it has been replaced by heterosite and further altered into low temperature alteration

products of that mineral in nearly every base specimen. In thin section, ferrisicklerite exhibits (see above) a characteristic dark orange in plane polarized light and is found in association with heterosite (violet) and its alteration products rockbridgeite (bright yellow, highly pleochroic) and jahnsite (appearing above in ppl as pale blue.) Electron Microprobe analysis is needed to further determine the identity and chemical makeup of this sample.

Heterosite

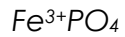


Figure 17: sample of heterosite with jahnsite and rockbridgeite. 3 cm x 4 cm.

Heterosite appears as characteristic red-violet masses in association with rockbridgeite and jahnsite-CaMnMn in association I. Heterosite is the ferric end member of the heterosite-pupurite series and is a product of high temperature alteration of triphylite under oxidizing conditions. The little ferrisicklerite that appears in the samples and heterosite are the only phases of the Quensel-Mason series present in most of the specimens. In thin section, heterosite exhibits characteristic bright violet color and is most often in association with jahnsite, rockbridgeite and ferrisicklerite as in association base specimen I, sample U7.

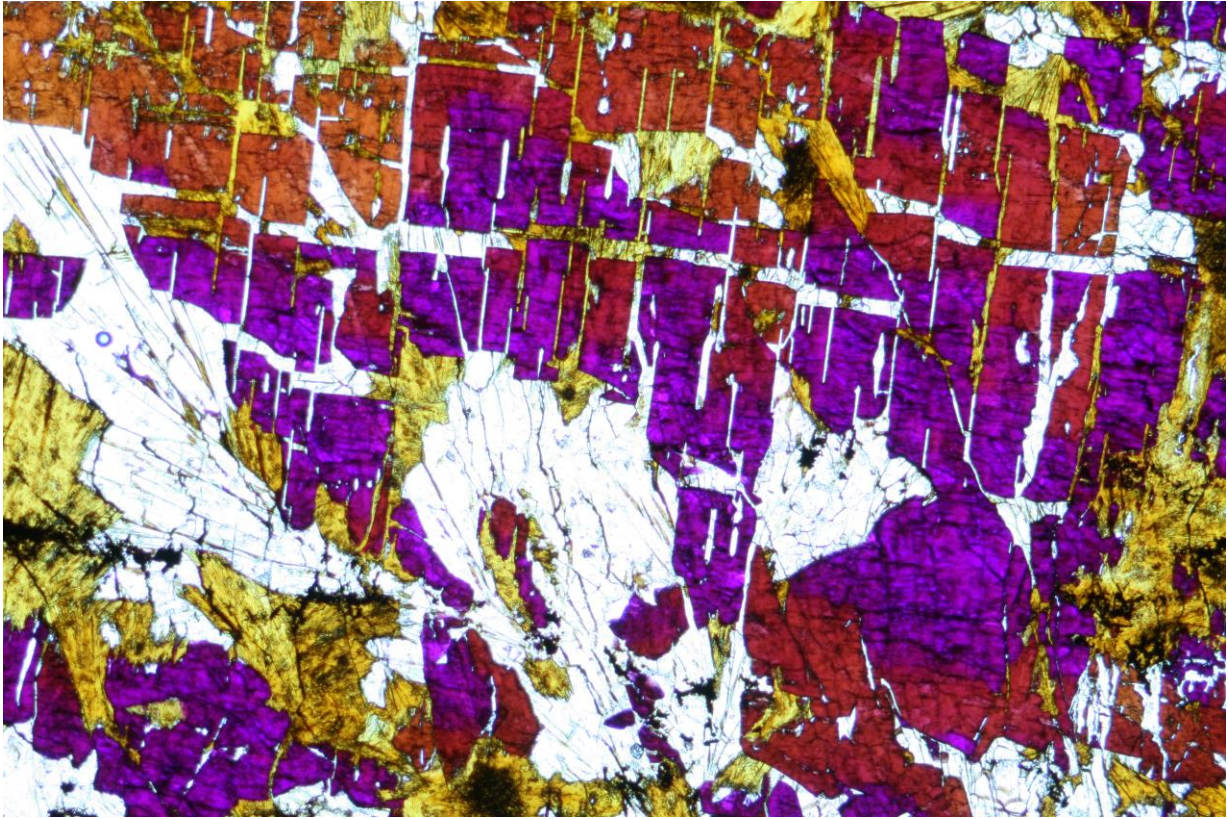


Figure 18: Thin section of FMP_U7 showing characteristic red-violet heterosite. PPL. FOV 3mm

Fe+Mn/Mn ratios for heterosite closely resemble those for triphylite, as discussed in Fransolet 2007. See figure 17 below. Heterosite, coming at the end of the Quensel-Mason sequence (described in detail on page YY) retains the Fe/Mn ratio of the parent triphylite, thus heterosite can be a useful indicator as to the degree of evolution of the pegmatite body in the absence of triphylite and/or ferrisicklerite (Černý 1985).

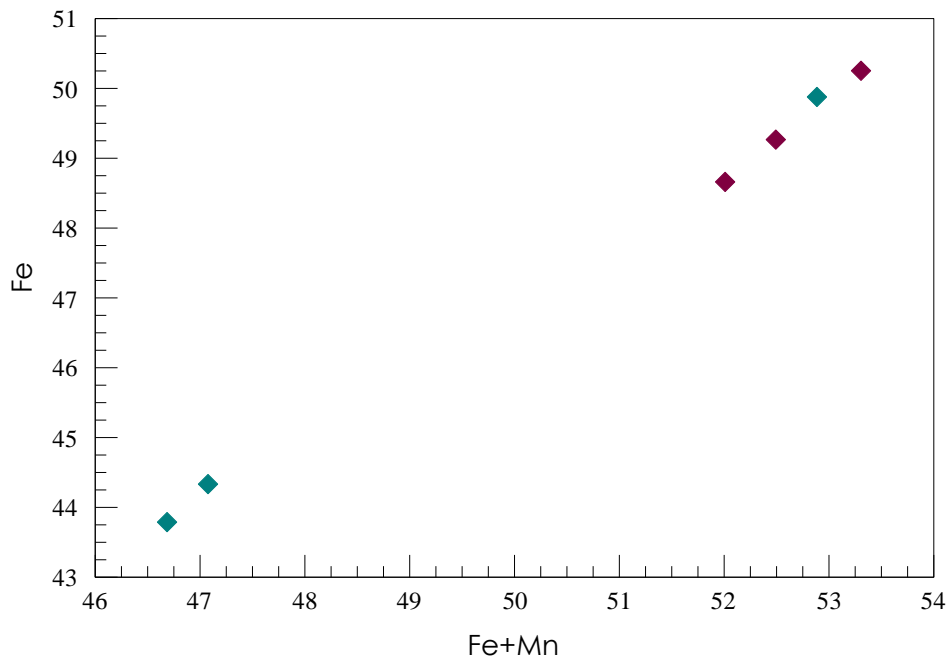


Figure 19: Fe+Mn/Mn ratios for heterosite (purple) v. triphylite (green)

Heterosite crystallizes in the orthorhombic system. X-ray diffractometry provided cell parameters a 5.827(3)Å b 9.788(5)Å c 4.763(7)Å; space group P mnb based on starting values from Eventoff, 1972. Compositional data gathered via electron microprobe analysis can be found on page 36.

Heterosite

FMP_U7-2

Wt%	
P ₂ O ₅	47.14
SiO ₂	0.04
Al ₂ O ₃	0.04
Fe ₂ O ₃	48.66
Mn ₂ O ₃	3.35
MgO	0.77
CaO	0.05
total	100.05

Cations based on 4 oxygen atoms

P	0.999
Si	0.001
Σ	1.000
Al	0.001
Fe ³⁺	0.916
Mn ³⁺	0.064
Mg	0.029
Ca	0.001
Σ	1.011

Table 3: Representative electron microprobe analysis of heterosite

Rockbridgeite

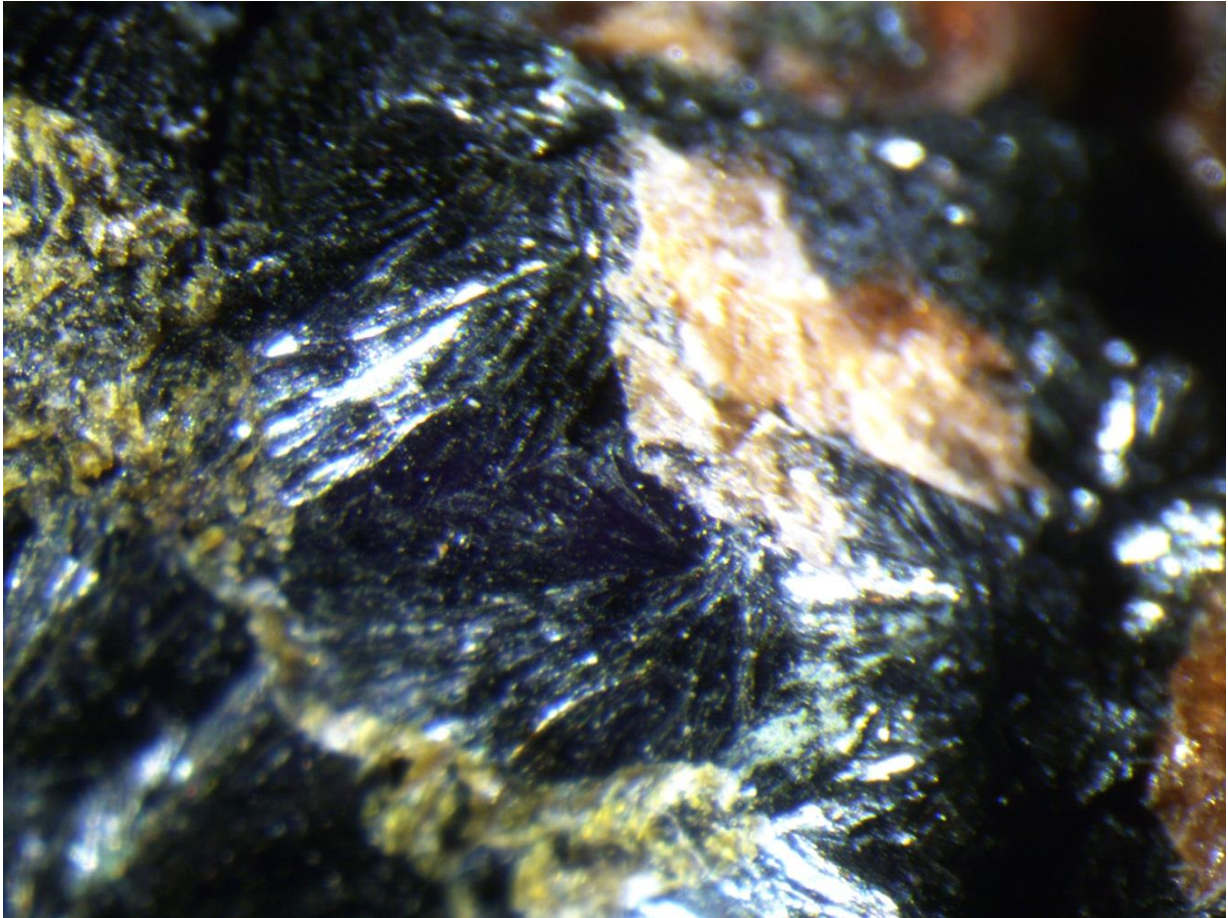
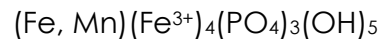


Figure 20: Rockbridgeite with jahnsite and hureaulite. Photo by A. Falster. FOV 5mm

Rockbridgeite is the ferrous end member of the rockbridgeite-frondelite series and is by far the most abundant mineral in the sample set. It appears in all but five of the samples and is present in each of the reported associations for this work.

Rockbridgeite forms due to low temperature hydrothermal alteration and hydroxylation under oxidizing conditions of the primary phosphate triphylite and its high temperature alteration products. It appears as black or dark brown to dark greenish brown radial

aggregates or else as black botryoidal masses most often in association with jahnsite, beraunite, huréaulite, mitridatite, leucophosphite, and phosphosiderite. The progressive change from brown to dark green coloration is a result of auto-oxidation of rockbridgeite, wherein some divalent iron becomes trivalent (Fransolet 2007) via the mechanism:



Rockbridgeite in thin section appears as bright yellow to bright green to brown and is strongly pleochroic. Euhedral crystals show good cleavage on {010} and excellent cleavage on {100}. It is most often in association with jahnsite and phosphosiderite, in these samples, as in sample FMP_B29 (Fig 19).

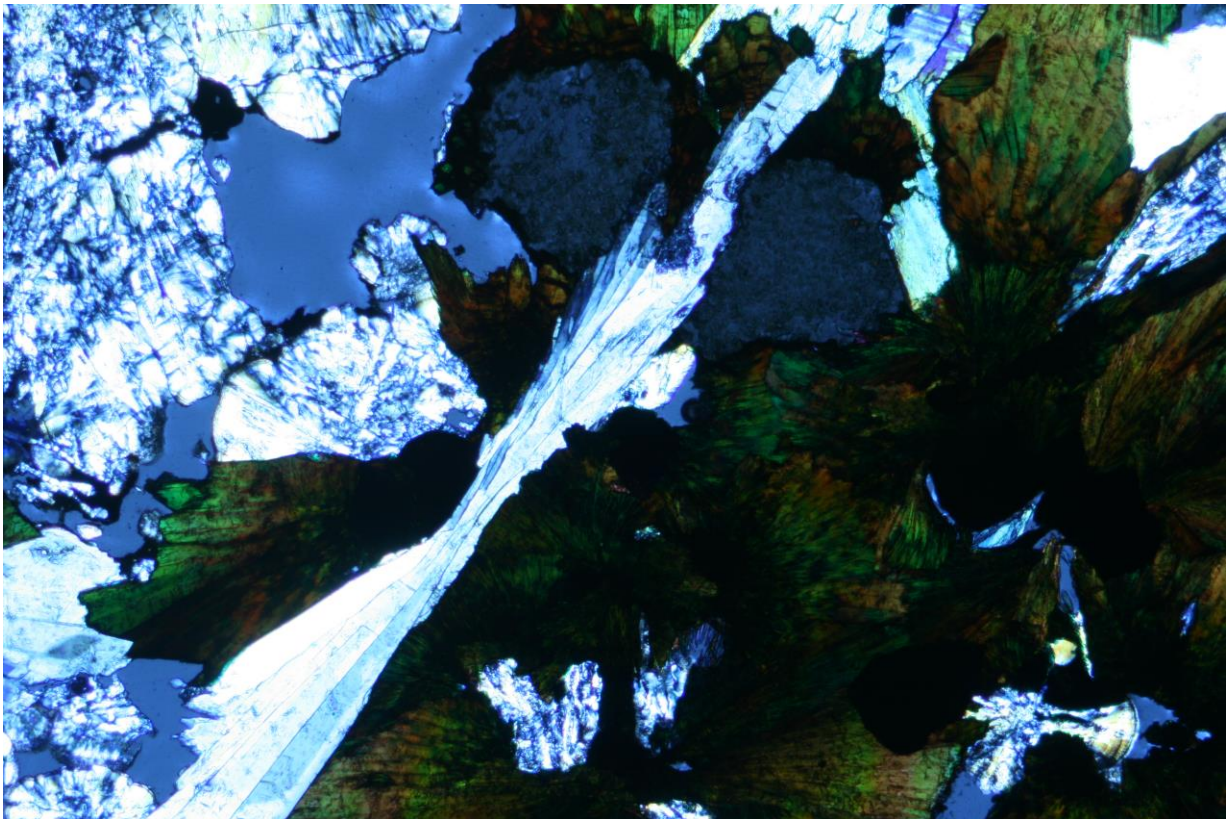


Figure 21: Rockbridgeite (highly pleochroic brownish green and green) with jahnsite and phosphosiderite. Scale: 2cm=200 μ m.

Ternary diagrams of the divalent cations place the composition of rockbridgeite at the ferrous point of the plot. See figure 20 below.

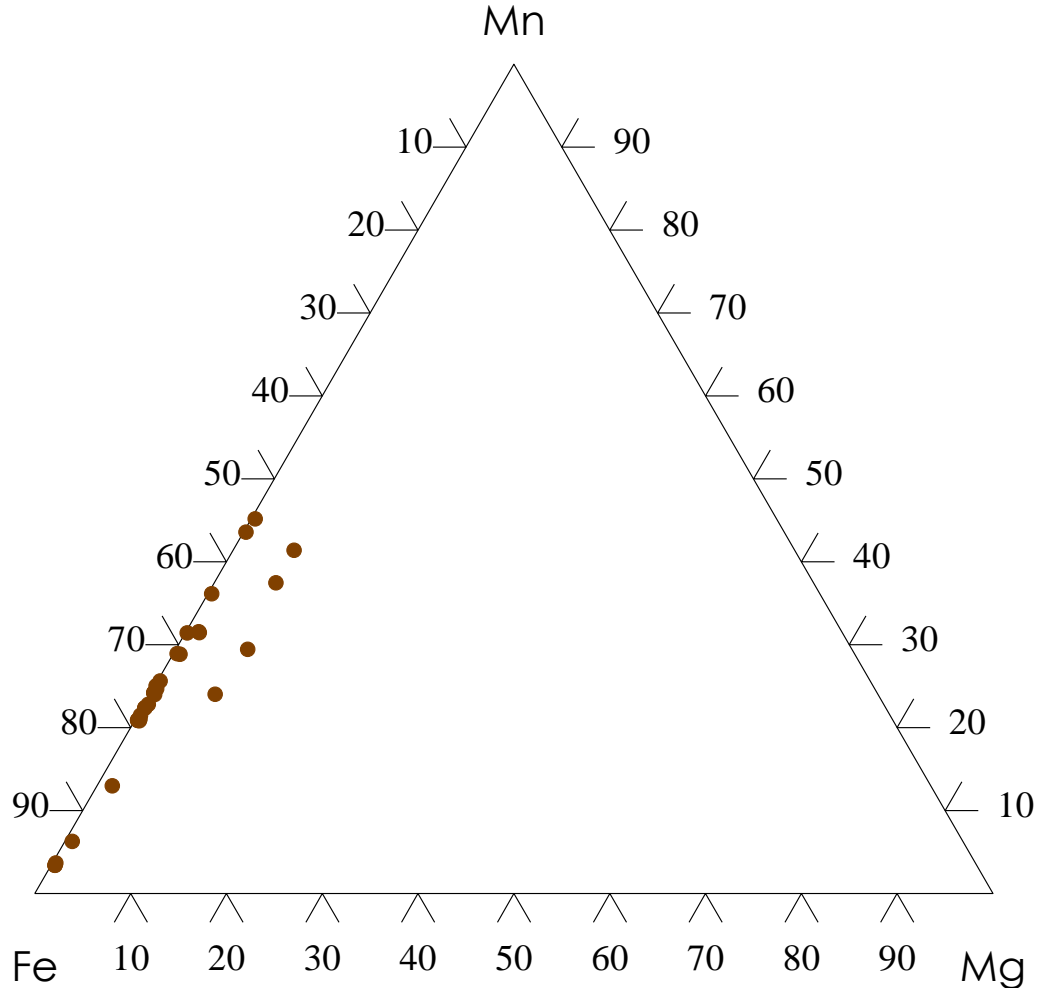


Figure 22: Ternary diagram of divalent cations Fe, Mn and Mg in rockbridgeite

Divalent Fe/Fe+Mn ratios for Fletcher pegmatite rockbridgeite vary widely from 0.52 to 0.96. The highest values were found in sample FMP_A34, which was devoid of any very low temperature hydrated and/or hydroxylated phases. Lower ratios were found in samples where rockbridgeite was in close association with such phases. Representative compositional data of rockbridgeite from several samples can be seen in table 4.

Magnesium was absent or negligible in most of the samples for which compositional

data were taken. The higher Mg values coincide with those triphylite samples which also exhibited higher than average Mg values for these Fletcher pegmatite specimens. Rockbridgeite crystallizes in the orthorhombic system. X ray diffractometry of specimen FMP_A32 provided the cell parameters a 13.780(11)Å b 16.865(26)Å c 5.193(10)Å; space group B bmm with starting values from Moore, 1970.

Rockbridgeite

	FMP_B38-2	FMP_B38-2	FMP_A34-4	FMP_A19-301	FMP_U7-101	FMP_B49-48							
Wt%													
P2O5	32.87	32.81	32.92	31.23	32.68	32.88	32.96	32.75	31.23				
SiO2	0.02	0.03	0.03	0.02	0.02	0.04	0.02	0.06	0.06				
Al2O3	0.05	0.03	0.02	0.02	0.00	0.02	0.02	0.05	0.03				
Fe2O3	49.16	49.09	49.55	47.01	48.47	49.28	49.66	49.34	46.79				
FeO	8.56	5.99	7.42	9.79	10.14	9.54	8.37	6.03	7.34				
MnO	2.44	4.91	3.44	0.66	0.36	1.43	2.72	3.98	2.96				
MgO	0.02	0.03	0.08	0.05	0.02	0.10	0.02	0.39	0.02				
CaO	0.00	0.00	0.00	0.01	0.02	0.03	0.00	0.39	0.00				
SrO	0.01	0.01	0.00	0.00	0.00	0.00	0.01	0.00	0.02				
ZnO	0.02	0.01	0.02	0.01	0.02	0.01	0.01	0.02	0.02				
H2O calc	6.94	6.94	6.97	6.62	6.86	6.97	6.99	6.95	6.61				
total	100.09	99.85	100.45	95.41	98.59	100.29	100.79	99.95	95.08				
P	3.002	3.002	2.995	2.993	3.022	2.996	2.991	2.986	3.000				
Si	0.002	0.003	0.003	0.003	0.002	0.004	0.002	0.006	0.007				
Σ	3.004	3.005	2.998	2.996	3.023	3.000	2.994	2.993	3.007				
Al	0.006	0.003	0.002	0.003	0.000	0.003	0.002	0.007	0.004				
Fe ³⁺	3.990	3.991	4.007	4.005	3.984	3.991	4.007	4.000	3.996				
Σ	3.996	3.995	4.009	4.008	3.984	3.994	4.009	4.006	3.999				
Fe	0.772	0.541	0.667	0.927	0.927	0.858	0.750	0.543	0.697				
Mn	0.223	0.450	0.313	0.063	0.033	0.130	0.247	0.363	0.285				
Mg	0.003	0.004	0.013	0.008	0.004	0.016	0.004	0.062	0.004				
Ca	0.000	0.000	0.000	0.001	0.002	0.004	0.000	0.045	0.000				
Sr	0.001	0.001	0.000	0.000	0.000	0.000	0.001	0.000	0.001				
Zn	0.001	0.001	0.002	0.001	0.002	0.001	0.001	0.001	0.002				
Σ	0.999	0.996	0.994	0.999	0.966	1.009	1.002	1.013	0.986				

Table 4: Select representative electron microprobe data for rockbridgeite

Jahnsite

Jahnsite-CaMnFe: $\text{CaMn}^{2+}\text{Fe}^{2+}_2\text{Fe}^{3+}_2(\text{PO}_4)_4(\text{OH})_2 \cdot 8\text{H}_2\text{O}$

Jahnsite-CaMnMn: $\text{CaMn}^{2+}\text{Mn}^{2+}_2\text{Fe}^{3+}_2(\text{PO}_4)_4(\text{OH})_2 \cdot 8\text{H}_2\text{O}$

Jahnsite-CaFeFe: $\text{CaFe}^{2+}\text{Fe}^{2+}_2\text{Fe}^{3+}_2(\text{PO}_4)_4(\text{OH})_2 \cdot 8\text{H}_2\text{O}$

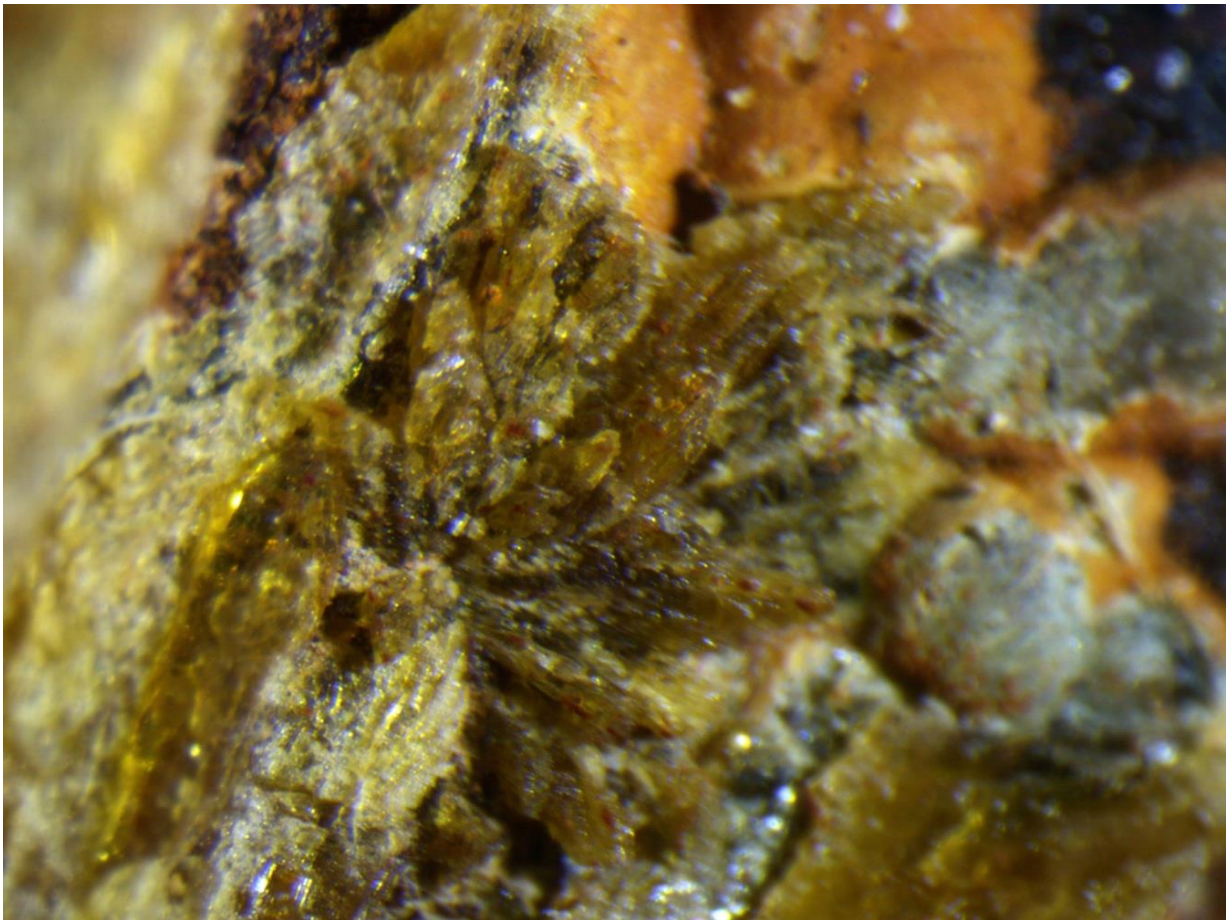


Figure 23: Jahnsite. FOV 4mm

Jahnsite is the second most abundant mineral within the sample set. A member of the whiteite group (Moore, Ito 1978), jahnsite forms as a result of low temperature alteration in oxidizing conditions. It appears in aggregates of bladed dark ochre to yellow vitreous, sub-euhedral crystals less than 2mm long in association with rockbridgeite, laueite and phosphosiderite. Euhedral crystals show good cleavage on

{001}. Three members of the group, jahnsite-CaMnMn, jahnsite-CaFeFe, and jahnsite CaMnFe, have been identified in this study. Characteristic striations on jahnsite make it difficult to differentiate from laueite. Fletcher pegmatite is the type locality for Jahnsite CaMnFe (Moore, 1970). The presence of Ca^{2+} and Mg are the result of cation exchange during low temperature alteration of triphylite and its primary alteration products. (Moore, 1973) This stage of alteration is also responsible for hydration and hydroxylation. A comparison of divalent transition metal cations of the jahnsite found in the Fletcher pegmatite sample set is shown in figure 24.

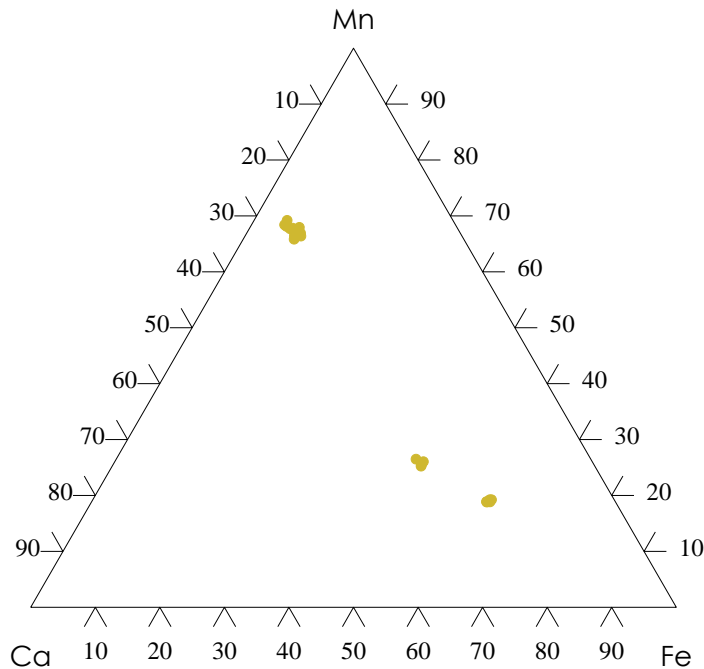


Figure 24: ternary diagram of jahnsite divalent cations Ca, Fe, Mn

Fe/Fe+Mn for jahnsite from the Fletcher pegmatite range from 0.12 in jahnsite-CaMnMn, to 0.67 in jahnsite CaFeFe, which has maximum weight percent for Fe of

19.617. Jahnsite crystallizes in the monoclinic system. X-ray powder diffractometry produces parameters a 14.942(16) Å, b 7.140(3) Å, c 9.929(9) Å, β 110.15(6)° based on starting values from Moore and Araki, 1974. Representative compositional data for Jahnsite can be found on the following page in table 5.

	Jhns-CaFeFe	Jhns-CaMnFe	Jhns-CaMnMn
	FMP_B38-2	FMP_B49-56	FMP_B49-56
Wt%			
P ₂ O ₅	32.19	32.00	31.98
SiO ₂	0.09	0.05	0.10
Al ₂ O ₃	0.19	0.21	0.05
Fe ₂ O ₃	17.64	17.78	17.92
FeO	19.88	15.29	2.55
MnO	6.00	8.04	21.05
MgO	0.02	0.27	0.02
CaO	4.89	6.68	6.64
SrO	0.02	0.01	0.02
ZnO	0.01	0.02	0.02
H ₂ O			
calc	18.21	18.32	18.28
total	99.14	98.67	98.64
<i>Cations based on 26 oxygen atoms</i>			
<i>Normalized iteratively to 18 H⁺ atoms, 2 Fe³⁺ atoms</i>			
<i>Fe²⁺ determined stoichiometrically</i>			
P	4.038	3.990	3.986
Si	0.013	0.007	0.015
Σ	4.051	3.997	4.001
Al	0.033	0.037	0.009
Fe ³⁺	1.967	1.97	1.991
Mn ³⁺	0.000	0.000	0.000
Σ	2.000	2.007	2.000
Fe	2.464	1.883	0.315
Mn	0.753	1.003	2.632
Mg	0.005	0.058	0.005
Ca	0.776	1.054	1.051
Sr	0.002	0.001	0.002
Zn	0.001	0.002	0.002
Σ	4.001	4.001	4.007

Table 5: Select electron microprobe data for jahnsite

Vauxite

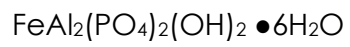


Figure 25: FMP_B38 containing vauxite. 4cm diameter

Vauxite appears in granitic pegmatites as an alteration product of fluorapatite or as a low temperature alteration product of triphylite-lithiophilite under reducing conditions in association with fluorapatite, huréaulite, and ludlamite, as in association II, seen above as pale blue nodules. Vauxite crystallizes in the triclinic system (Bauer 1968). Representative electron microprobe analysis of vauxite can be found on the next page.

Vauxite	
FMP_B38-2	
Wt%	
P ₂ O ₅	32.43
SiO ₂	0.23
Al ₂ O ₃	22.89
FeO	15.90
MnO	0.56
MgO	0.01
CaO	0.11
H ₂ O calc	28.80
total	100.93
<i>Cations based on 16 oxygen atoms normalized to 2 P atoms</i>	
P	2.001
Si	0.017
Σ	2.018
Al	1.966
Fe	0.969
Mn	0.035
Mg	0.001
Ca	0.009
Σ	1.014

Table 6: Representative electron microprobe data for vauxite

Messelite



Messelite is the ferrous member of a series with magnesium rich member collinsite and manganous fairfieldite. This series of alteration products forms at temperatures below 300°C in reducing conditions and has experienced cation exchange and hydration (Moore 1973). Messelite appears in association base specimen II in association with vauxite, ludlamite, and rockbridgeite. This is one of several unoxidized mineral phases seen in association with rockbridgeite, an oxidized alteration product, at the Fletcher pegmatite. This indicates there may be a significant change in environment of formation during paragenesis (Falster, 2020). This phenomenon is not unique to Fletcher pegmatite and will be examined in detail in the discussion portion of this study. Fletcher pegmatite messelite is appears as pale greenish white nodules or as radial aggregates of resinous acicular crystals and crystalizes in the triclinic system (Catti 1977; Flick 2003). Representative compositional data for messelite appears on the following page.

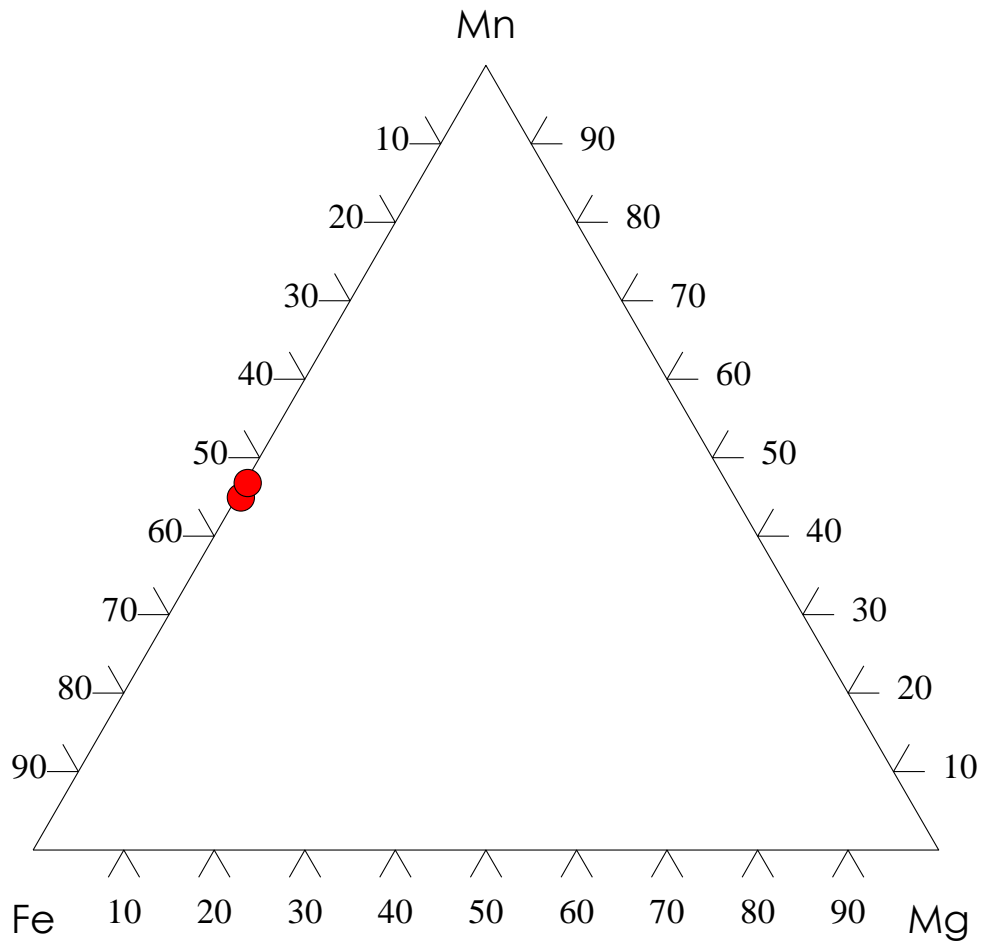


Figure 26: Ternary diagram of divalent cations in messelite. Below 50% Mn with no significant Mg identifies this member of the fairfieldite group.

Messelite

B49 field 53

Wt%	
P ₂ O ₅	38.79
SiO ₂	0.03
Al ₂ O ₃	0.09
FeO	11.09
MnO	9.01
MgO	0.06
CaO	30.89
SrO	0.01
ZnO	0.02
H ₂ O calc	9.93
Total	99.92
<i>cations based on 10 oxygen atoms</i>	
P	1.984
Si	0.002
Al	0.006
Σ	1.992
Fe	0.560
Mn	0.461
Mg	0.005
Ca	2.000
Zn	0.001
Σ	3.027

Table 7: Representative electron microprobe data for messelite

Strunzite

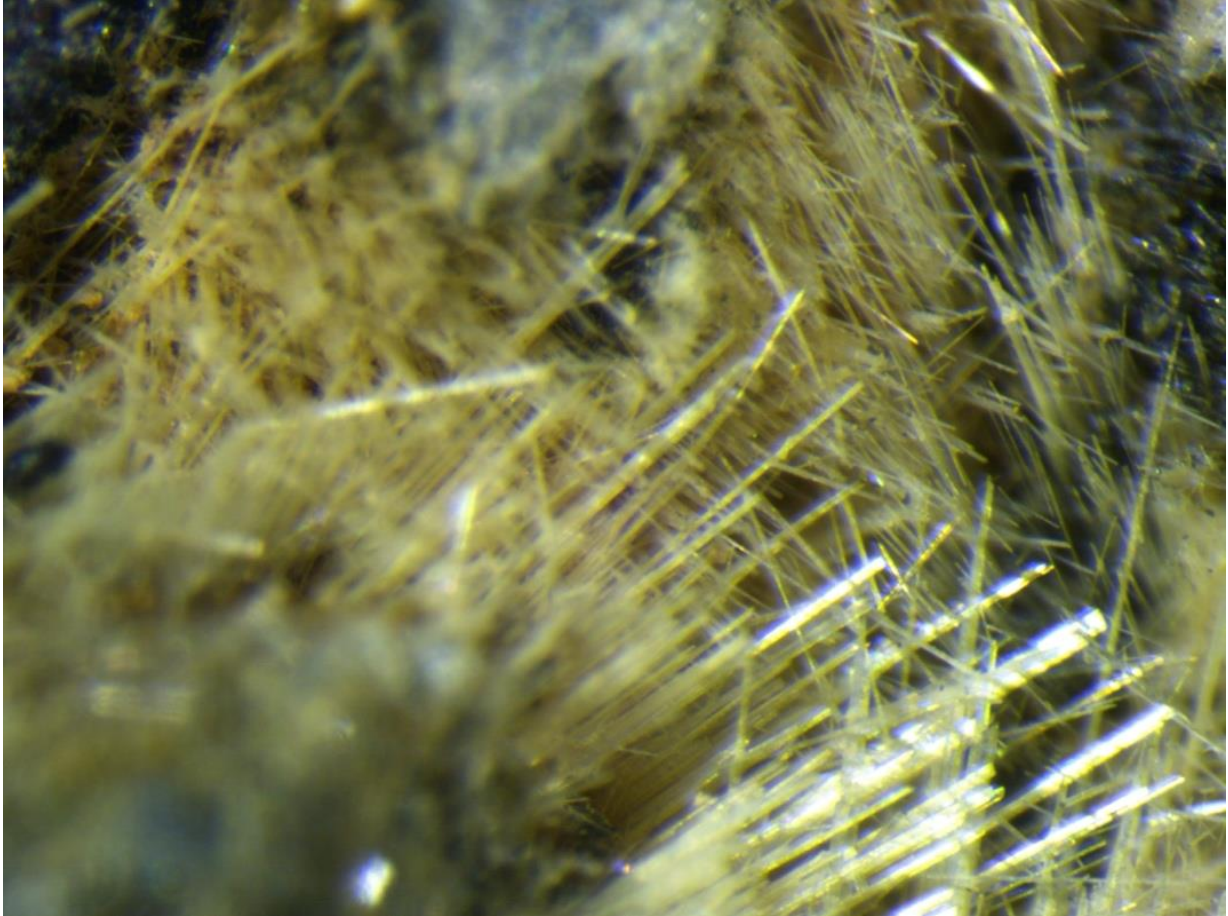
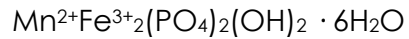
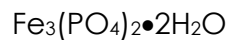


Figure 27 Prismatic straw yellow strunzite. FOV 3mm. Photo by A. Falster

Strunzite is a secondary alteration product of triphylite-lithiophilite under oxidizing conditions having undergone oxidation, hydration, and hydroxylation. It occurs at temperatures between 300 and 100°C appears as striking pale-yellow fibrous needles 1-2mm in length in association with phosphosiderite, heterosite, and rockbridgeite in association IV. Strunzite crystallizes in the triclinic system. X-Ray powder diffraction

provided the cell data a 10.225(9)Å b 9.829(8)Å c 7.293(3)Å, α 90.14(7)° β 98.46(6)° γ 117.38(6)°; space group $P-1$ based on starting values from Fanfani et al., 1978. Compositional data are required to determine Fe and Mn content and ratios.

Ludlamite



Ludlamite is a secondary phosphate species that forms as an alteration product of triphylite under reducing conditions at low temperatures (Moore, 1971). It crystallizes in the monoclinic system and appears as pale green to nearly colorless sub vitreous to resinous crystals most often in association with triphylite, messelite, and fluorapatite in the Fletcher pegmatite specimens, most notably in association II . A representative microprobe analysis of Ludlamite can be found below in table 8.

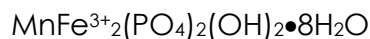
Ludlamite

FMP_A34-4

Wt%	
P2O5	32.68
SiO2	0.02
FeO	49.01
MnO	0.36
MgO	0.02
CaO	0.02
ZnO	0.02
H2O	16.57
Totals	98.70
<i>Cations based on 12 oxygen atoms</i>	
P	2.002
Si	0.001
Σ	2.003
Fe	2.966
Mn	0.022
Mg	0.002
Ca	0.002
Zn	0.001
Σ	2.993

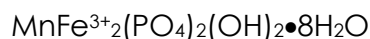
Table 8: Representative electron microprobe data for ludlamite

Laueite



Laueite appears as a late-stage hydrothermal alteration product of triphylite at temperatures at or below 200° (Hawthorne, 1998) and is pseudomorphous with stewartite and strikingly similar to jahnsite in hand sample. Both jahnsite and stewartite have also been identified in the Fletcher pegmatite specimens and a detailed discussion of their identification, difficult without unit cell data and mineral composition data, appears in the discussion of analytical results. Laueite appears in sample FMP-A16 in association with rockbridgeite, jahnsite, and beraunite. Laueite crystallizes in the triclinic system. X-ray diffractometry provides parameters a 5.283(24)Å, b 10.661(32)Å, c 7.140(29)Å, α 107.55(30)°, β 110.71(32)°, γ 71.07(29)°. Euhedral crystals will show perfect cleavage on {010}. Compositional data is required to provide more information about Fletcher pegmatite laueite.

Stewartite



Stewartite is a paravauxite group mineral, a late stage (low temperature) secondary phosphate and alteration product of triphylite that crystallizes in the triclinic system and undergoes Li-leaching, oxidation, hydroxylation, and hydration at temperature near 250 °C (Moore, Araki 1974). Laueite, another member, also appears at the Fletcher pegmatite and is described late in this section. X ray diffractometry confirmed the identity of both in the study. Fletcher pegmatite stewartite appears as yellow bladed crystals with glassy luster in association with rockbridgeite, huréaulite,

and phosphosiderite in the Fletcher pegmatite samples. Easily confused with laueite, X-Ray diffractometry and careful morphologic study is necessary to ensure proper identification. While laueite shows perfect cleavage on {010}, stewartite exhibits characteristic striations (Moore, 1974). XRD produced parameters a 5.247(18)Å , b 10.588(33)Å, c 6.967(19)Å, α 106.8(2)° β 110.7(2)° γ 72.1(2)°, space group P-1 based on starting values from Gatta et al., 2014.

Phosphosiderite

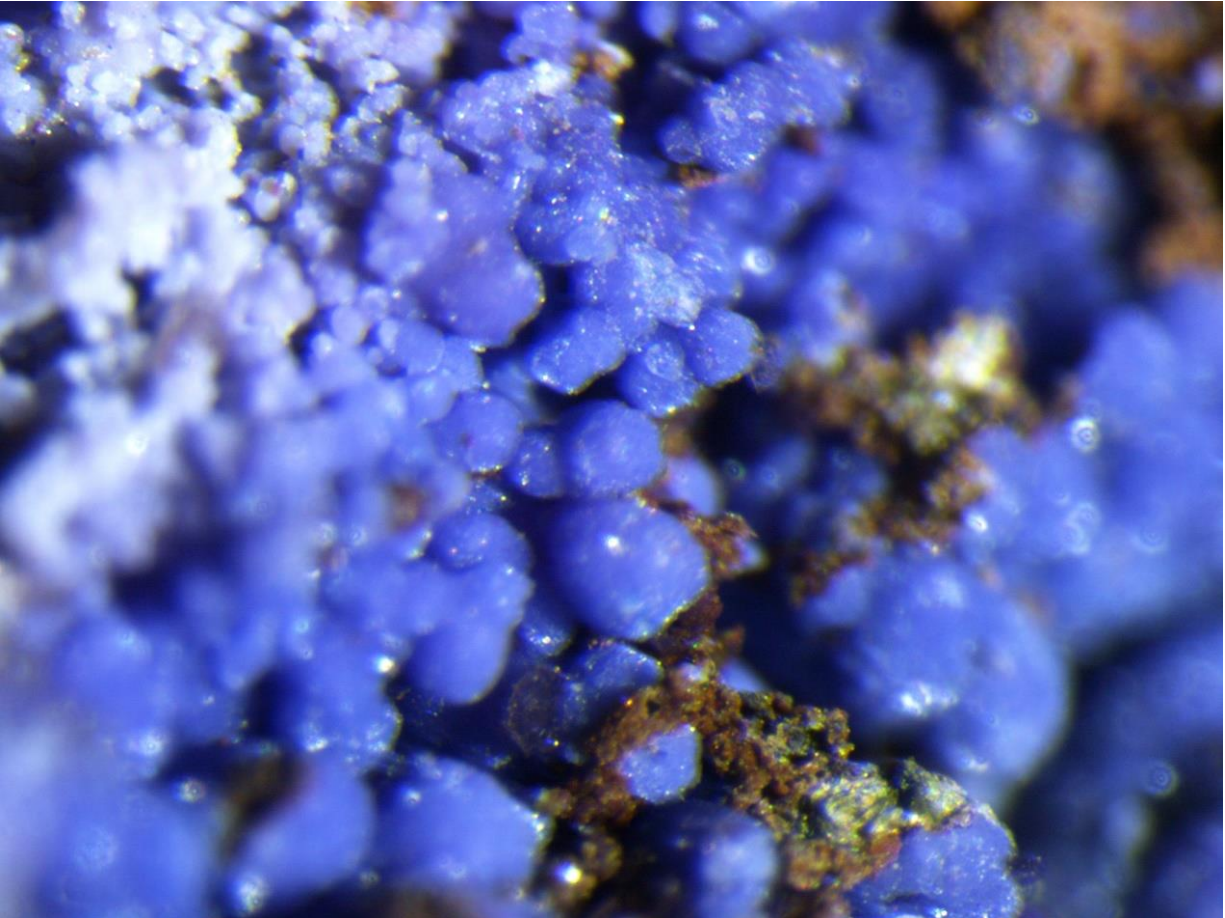


Figure 28: Phosphosiderite. FOV 4mm. Photo by A. Falster

Phosphosiderite is widespread in the phosphate assemblages at Fletcher pegmatite. It appears individually and in masses of blue violet to lavender earthy, spherical crystals in most often in crusts in association with rockbridgeite, jahnsite, and leucophosphite. Phosphosiderite is a hydrated iron phosphate that a crystalizes in the monoclinic system at low temperatures (below 200°C) as a result of late-stage hydrothermal alteration and weathering of triphylite-lithiophilite. Phosphosiderite is

dimorphic with strengite, which forms under similar conditions. X-ray powder diffraction provides cell data a 5.303(3)Å b9.788(8)Å c8.727(4)Å 90.60(6)° based on starting values from Moore, 1966. Representative electron microprobe data can be found below.

Phosphosiderite	
FMP_A19-102	
Wt%	
P2O5	37.55
SiO2	0.00
Al2O3	0.02
Fe2O3	41.35
MnO	0.33
CaO	0.09
H2O	18.97
Totals	98.31

<i>Cations based on 6 oxygen atoms</i>	
P	1.005
Σ	1.005
Al	0.001
Fe3+	0.983
Σ	0.984

Table 9: Representative microprobe data for phosphosiderite

Beraunite



Beraunite appears as clusters of dark reddish brown pearly needles of less than 1 millimeter in specimen B22 and B2, and as massive rinds in association with rockbridgeite, jahnsite, and fluorapatite in type II associations. Beraunite crystallizes in the monoclinic system at temperatures below 300°C as a hydroxylated, hydrated alteration product of triphylite-lithiophilite under oxidizing conditions. Unit cell data for beraunite from sample FMP_B32-1 reveals cell parameters space group C/2c, a 20.757(6) Å, b 5.155(1) Å, c 19.241(8) Å, $\beta = 93.54(4)^\circ$. Starting values were based on Marzoni Fecis di Cossato et al., 1989. Fe/Fe+Mn ratios for Fletcher pegmatite beraunite are in the range of 0.48 to 0.95. Representative compositional data for beraunite can be found on page 59.

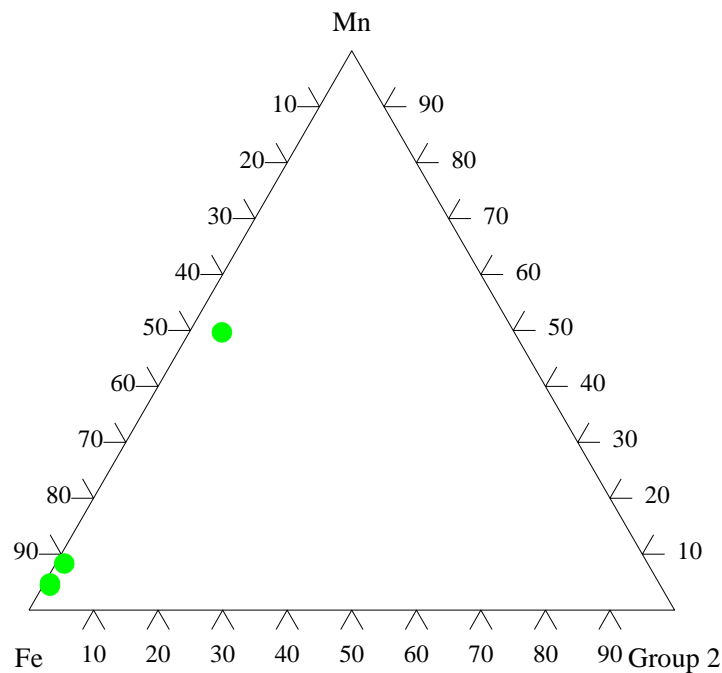


Figure 29: Ternary diagram for beraunite Fe, Mn, all other group 2 (divalent) cations

Beraunite

FMP_B49 – 48	
Wt%	
P ₂ O ₅	31.23
SiO ₂	0.02
Al ₂ O ₃	0.02
Fe ₂ O ₃	44.04
FeO	7.19
MnO	0.66
MgO	0.05
CaO	0.01
ZnO	0.01
H ₂ O calc	16.88
total	100.11

cations based on 17 oxygen atoms

normalized to 5 Fe³⁺ atoms

P	3.991
Si	0.003
<hr style="border: 0.5px solid black;"/>	
Σ	3.995
Al	0.004
Fe ³⁺	5.003
<hr style="border: 0.5px solid black;"/>	
Σ	5.007
Fe	0.908
Mn	0.084
Mg	0.010
Ca	0.002
Zn	0.001
<hr style="border: 0.5px solid black;"/>	
Σ	1.005

Table 10: Representative electron microprobe analysis for beraunite

Huréaulite

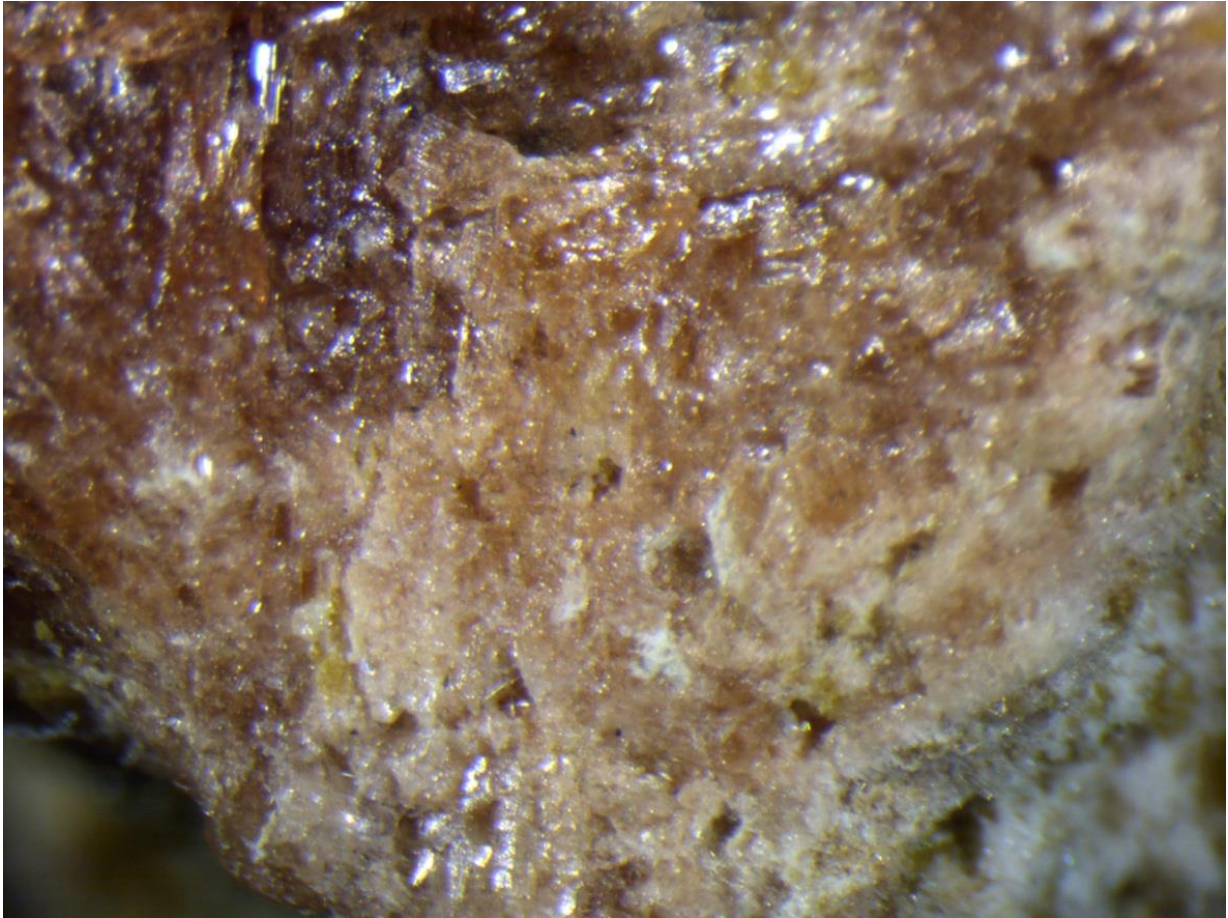


Figure 30: Huréaulite. FOV 3 cm. Photo by A. Falster.

Huréaulite appears as butter yellow crystal clusters and as masses of pale pink to reddish vitreous to sub-adamantine crystals in association with rockbridgeite, leucophosphite, jahnsite-CaMnMn, and phosphosiderite and appears in associations of the Fletcher pegmatite sample set. Huréaulite can appear either as a product of manganese rich phosphatic solutions or else, as is the case here, as a late-stage alteration product of hydrothermally attacked triphylite and as a result, is lower in

divalent iron content than the parent (Moore 1973). Hureaulite is a common alteration product of triphylite under reducing conditions (Moore & Araki, 1973). X ray diffractometry provides unit cell unit cell data a 17.614(25)Å b 9.081(5)Å c 9.391(17) Å, β 96.5(4)° consistent with cell data from Moore and Araki, 1973 from which starting values were derived. Compositional data will be necessary to describe Fletcher pegmatite hureaulite in greater detail.

Mitridatite



Figure 31: Mitridatite. Pale olive green upper right quadrant. FOV 5 mm

Mitridatite is a low temperature metasomatic alteration product of triphylite under oxidizing conditions that has undergone Li leaching, cation exchange, and

hydration. (Moore 1973, 1977) It appears as pale olive-green powdery masses on rockbridgeite and jahnsite in Association II and with quartz in sample B2. Mitridatite crystallizes in the monoclinic system. In thin section mitridatite is seen as spherulitic, replacing radial aggregates of rockbridgeite in association II. X-ray diffractometry provides parameters $a 17.0536(23)\text{\AA}$ $b 19.346(22)\text{\AA}$ $c 11.229(16)\text{\AA}$, $\beta 95.9(3)^\circ$ based on starting values from Moore and Araki 1977. Electron microprobe analysis will be necessary to describe these samples in greater detail.

Leucophosphite

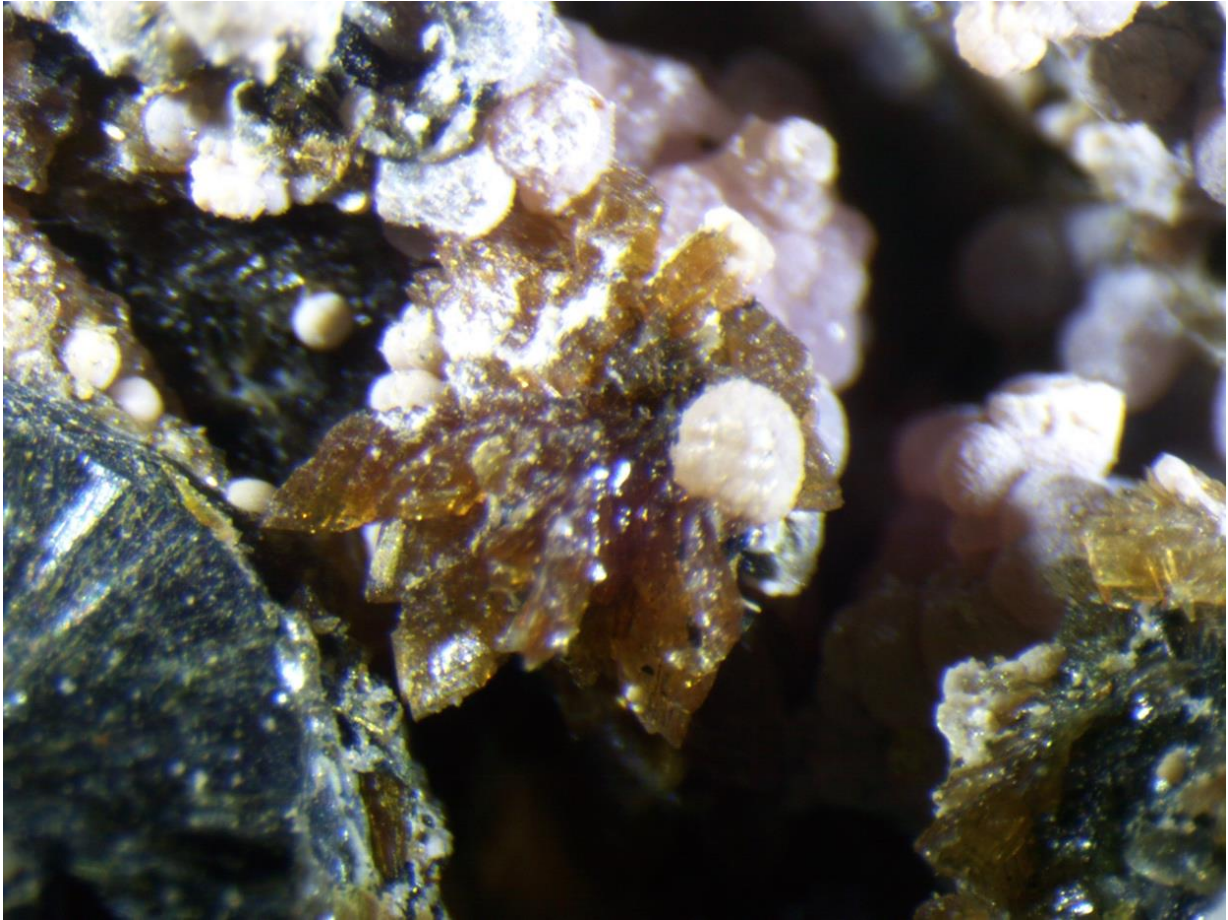
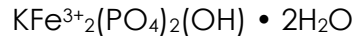


Figure 32: Leucophosphite spherule on stewartite. FOV 3mm. Photo by A. Falster.

Leucophosphite appears as white, earthy, spherules less than 1 millimeter in diameter in association with phosphosiderite, rockbridgeite, jahnsite, stewartite, and huréaulite in the Fletcher pegmatite specimens. The presence of muscovite in association I, and in the specimen pictured is the potential source of the potassium for this mineral. It is the only K-bearing phosphate mineral so far identified in this sample set. Leucophosphite forms as a late-stage very low temperature (200-50°C) alteration product of triphylite that has undergone Li leaching, hydration, hydroxylation, and cation exchange/addition under oxidizing conditions (Hawthorne 1998). It crystallizes in

the monoclinic system (Moore 1972). A representative microprobe analysis of Leucophosphite is included in table 11.

Leucophosphite	
FMP_B28-301	
Wt%	
P ₂ O ₅	35.89
SiO ₂	0.10
Al ₂ O ₃	0.23
Fe ₂ O ₃	34.45
Mn ₂ O ₃	1.98
MgO	0.11
CaO	0.21
Na ₂ O	0.34
K ₂ O	11.68
H ₂ O calc	11.10
Total	96.09
<i>Cations based on 11 Oxygen atoms</i>	
<i>Normalized to 2 P atoms</i>	
P	2.052
Si	0.007
Σ	2.058
Al	0.018
Fe ³⁺	1.750
Mn ³⁺	0.102
Σ	1.870
Mg	0.011
Ca	0.015
Σ	0.026
Na	0.045
K	1.006
Σ	1.051

Table 11: Representative microprobe analysis for leucophosphite

Trace Elements

Zinc

Direct current plasma spectrophotometry (DCP) was conducted to discern concentrations of trace zinc and lithium in primary, metasomatic secondary, and hydrothermal secondary phosphates. Samples were chosen for clean fields of these minerals, thus randomly from the collection. Roda (2014) undertook an exhaustive study of trace elements in primary phosphates and that work was the impetus for this investigation.

Primary phosphate triphylite yielded a concentration of 611 ppm. Zn concentrations in high temperature metasomatic secondary heterosite ranged from 125 ppm in FMP_A46 to 1795 ppm in FMP_A20a. Zn concentrations in low temperature hydrothermally altered phosphate rockbridgeite ranged from 329 ppm in FMP_B29 to 912 ppm in FMP_A29. No corresponding trend between phosphate phases in the Fletcher pegmatite samples or of temperature of formation and concentration of Zn was found (Fig. 31). Further investigation would benefit from chemical analyses from all heterosite and rockbridgeite in the trace element testing array in order to perform a closer comparison to other primary and secondary phosphate zinc concentrations from the GPF.

Table 12: Zinc concentration in select high and low temperature secondary phosphates

Zn in Primary and Secondary Phosphates		
	spec.	ppm
Triphylite	FMP_A17	611
Heterosite	FMP_A1	809
	FMP_A10	440
	FMP_A20a	1795
	FMP_A20b	830
	FMP_A46	125
	FMP_B2b	942
	FMP_B22	173
	FMP_B32.b	866
Rockbridgeite	FMP_B49	442
	FMP_A21.a	730
	FMP_A21b	783
	FMP_A29	912
	FMP_B2.a	650
	FMP_B29	329
	FMP_B32A	701
FMP_B49	411	
	FMP_B74	664

Zn Concentration by Temperature of Secondary Phosphate formation

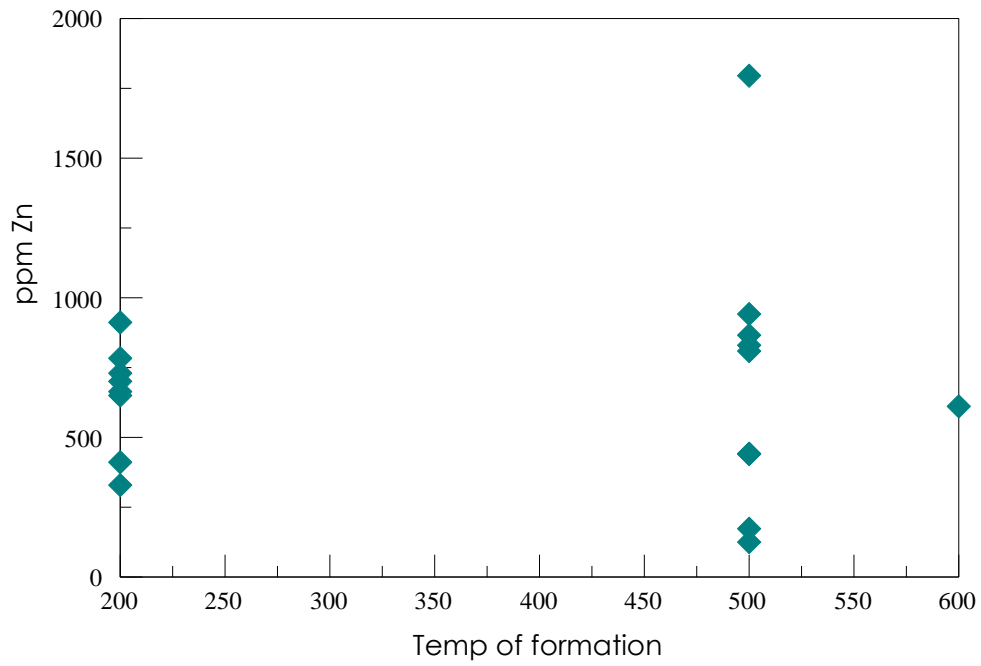


Figure 33: Zn concentration v. Temperature of select phosphate formation

Lithium

One of the hallmarks of phosphate paragenesis of triphylite is the leaching of Lithium during the high temperature metasomatic phase of alteration (Quensel 1937) (Mason 1941). Five 30-40mg samples of rockbridgeite were drilled from matrix from specimens FMP_A19A, FMP_A34, FMP_B22, FMP_B28 and FMP_B38. These samples represent a good cross section of the association types in the Fletcher pegmatite collection and were also rockbridgeite rich making clean samples easier to collect. Results of DCP analysis can be seen in table 13. Concentrations of Li⁺ in rockbridgeites from the Fletcher pegmatite samples differed a great deal, ranging from barely detectable (13 ppm) in sample FMP_B38 to strongly present in sample FMP_A34 (3180 ppm). Rockbridgeite in sample FMP_B28 (126 ppm Li) is in direct contact with heterosite, whereas in sample FMP_A34, (3180 ppm) no heterosite was found in proximity or seen in the sample at all. Sample FMP_B38 with the lowest detectable concentration of lithium, is host to the greatest number of very low temperature species and no high temperature secondary phosphates were found in the sample in thin section or via chemical analyses, suggesting a very high degree of alteration. There is some correlation between Fe²⁺/Fe²⁺+Mn²⁺ ratios in the three samples for which electron microprobe was carried out, and the trace Li concentrations (Table 13). Sample B38 had the lowest average ratio of divalent Fe to divalent Mn (0.664) and the lowest concentration of Li (13 ppm). FMP_A34 had the highest ratio of Fe to Mn in rockbridgeites in the tested array (0.824) and hosts the highest concentration of Li at 3180 ppm. Fe to Mn ratios, or degree of differentiation has long been used to define the degree of evolution of granitic pegmatites. Decreased Fe/Fe+Mn ratios denote a higher degree of evolution (Fransolet et al. 1986, Keller et al. 1984, Roda et al. 2005).

These data, then, may suggest that the greater the differentiation of the pegmatite, the lesser the concentration of Li. The apparent inconsistency of FMP_A34 could also indicate that prior to being mined or broken up, this sample was in close proximity to a Quensel Mason sequence mineral such as heterosite or ferrisicklerite while it was undergoing Li leaching during high temperature metasomatism. A more thorough chemical analysis of all the rockbridgeites and other secondary phosphates at Fletcher pegmatite and within the GPF for trace Li would prove a fruitful investigation and build upon the trace element investigation of primary phosphates conducted by Roda (2014).

Li in Rockbridgeite		
sample	Fe/Fe+Mn (avg)	ppm Li
FMP_A19A	0.752	583
FMP_A34	0.824	3180
FMP_B22	n/a	894
FMP_B28	n/a	126
FMP_B38	0.664	13

Table 13: Trace Li in rockbridgeites

Discussion and Conclusions

Overall Mineralogy

The degree of evolution of granitic pegmatites can be determined by the Fe/Fe+Mn ratio (differentiation) in the whole rock chemistry (Fransolet et al. 1986, Keller et al. 1984, Roda et al. 2005) There is a caveat that this collection is not necessarily representative of the whole Fletcher pegmatite mineralogy. Manganese in Jahnsite-CaMnFe is the sole manganese rich phase for which there is compositional data for Fletcher pegmatite. The existence of huréaulite, confirmed by XRD, is the only other manganous phase known. In the absence of rock forming mineral for electron probe analysis and the iron rich character exhibited not only by primary but secondary phosphates in the Fletcher pegmatite, the determination must be that the Fletcher pegmatite is a poorly to moderately evolved granitic pegmatite. Classification is discussed in greater depth in the discussion in section of this study.

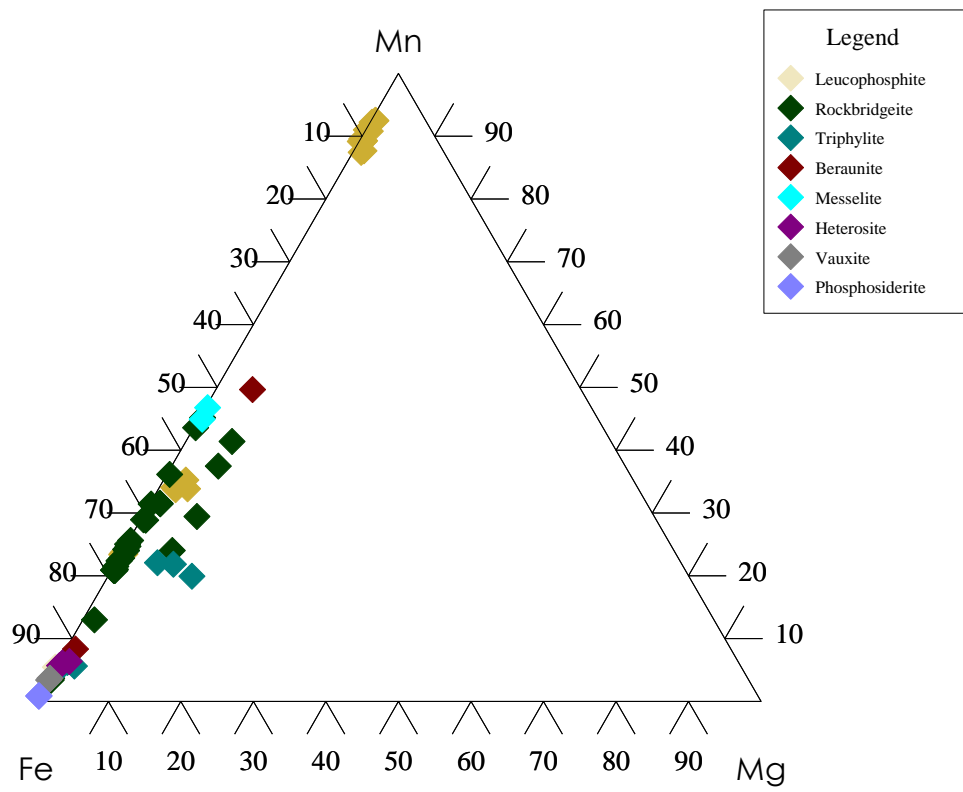


Figure 34: Geochemistry of Fletcher pegmatite primary and secondary phosphates

Phosphate Paragenesis

The past seven decades have seen investigations of pegmatite phosphate minerals unravel the paragenetic sequences that result in complex pegmatite phosphate assemblages and then determine the significance of those paths to the understanding of the evolution of pegmatitic melts. Early investigations have been crucial to deciphering the formation of pegmatite phosphates. Work by Quensel (1937) and Mason (1941), Fisher (1958) Moore (1965, 1969, 1970, 1973), Fransolet (1980, 1986, 2004), Keller (1989, 1991, 1994), Hawthorne (1998) and later paragenetic studies by Roda (2011, 2014), Vignola (2014, 2018) and Nizamoff (2006) and others has resulted in 'maps' for paragenesis under different conditions of temperature, oxidation, pH, and oxygen fugacity. The work of Fisher (1958) illuminated the alternative paths of primary phosphates (see fig. 33) and that work was later updated by Moore (1973) to include temperature regimes for the different stages of paragenesis (high temperature or metasomatic alteration and low temperature or hydrothermal alteration). Figure 33 illustrates the progressive sequence of minerals formed as residual fluids cool to ~50°C. Fransolet (1985) suggests that paragenesis can even continue at lower temperature (25°C) in near surface environments at the Angarf-Sud pegmatite, Morocco.

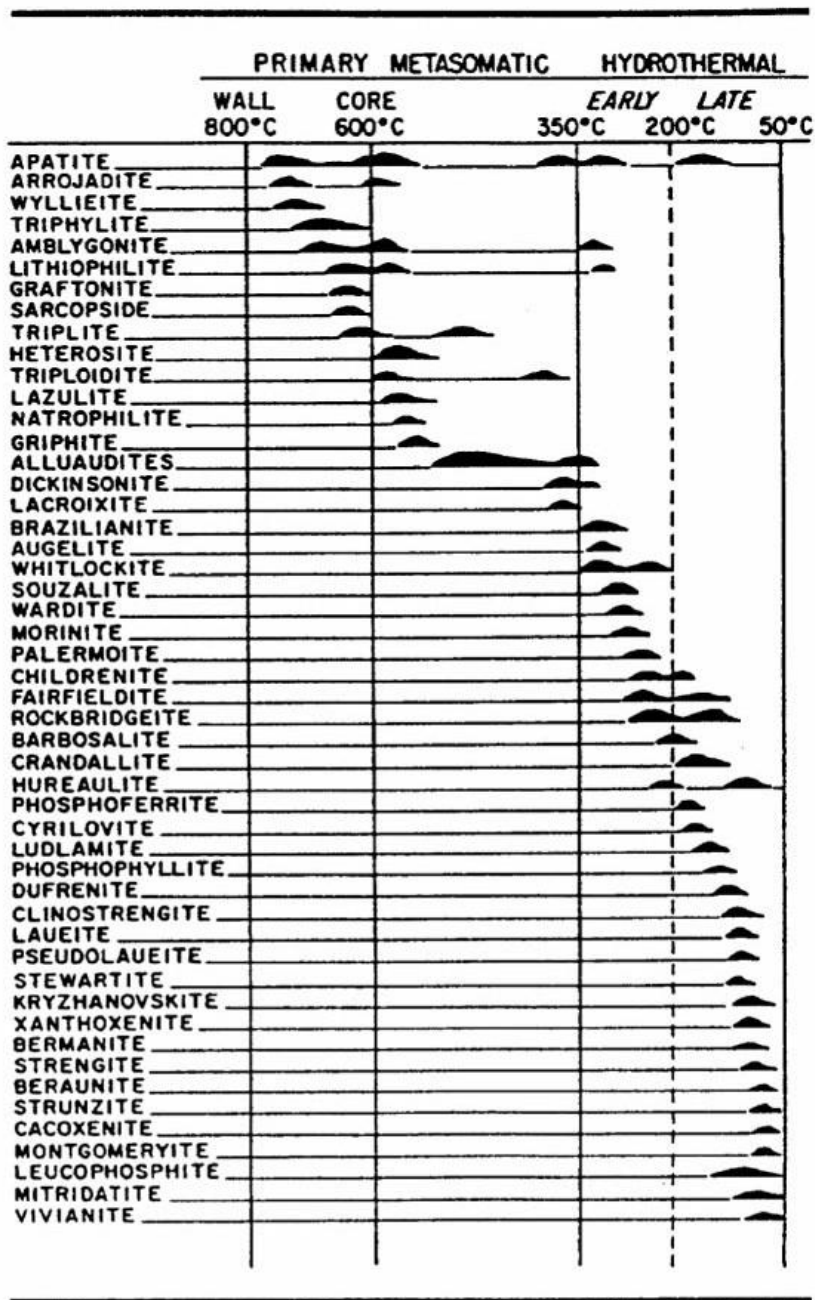


Figure 35: phosphate temperatures of formation. From Hawthorne 1998 after Moore 1973, Fisher 1958

Metasomatic alteration of phosphate minerals is caused by aqueous, post magmatic fluids (Hawthorne 1998). Alteration takes place under variable conditions of

temperature, oxidation, pH, and oxygen fugacity (Moore 1973) (Hawthorne 1998).

Figure 36 breaks the process into two general stages.

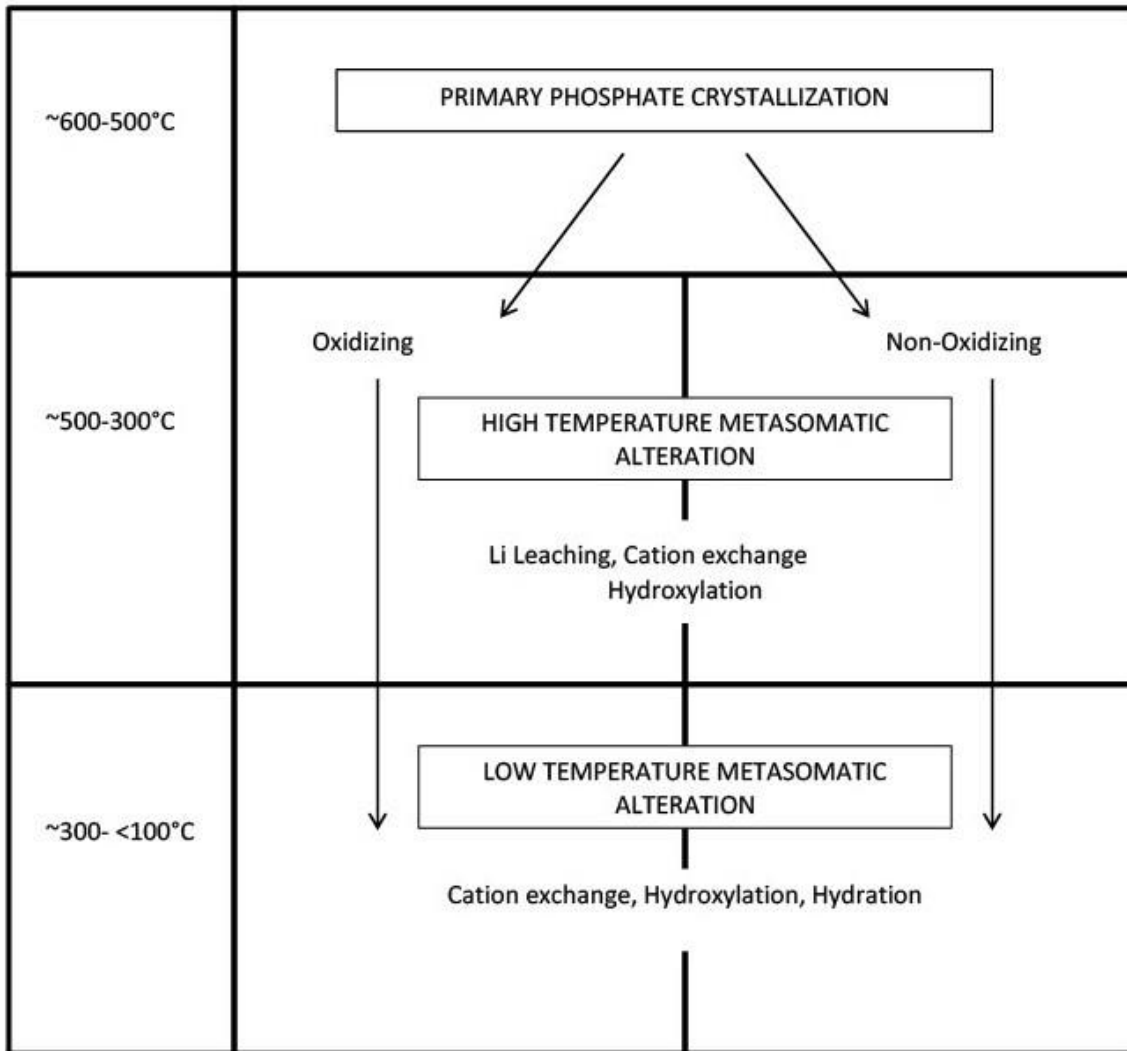


Figure 36: General phosphate paragenesis. Mod. From Nizamoff 2006 after Moore 1974

The first stage is high temperature metasomatism. This alteration takes place between ~500°C-300°C under either oxidizing or reducing conditions. Alteration includes hydroxylation and the leaching of Li⁺, and the addition and/or exchange of cations,

especially Na^+ , K^+ , Mg^{2+} , Ca^{2+} , Be^{2+} , Zn^{2+} , and Al^{3+} . The next step in the alterative process is low temperature or hydrothermal alteration. At temperatures under $\sim 300^\circ\text{C}$, hydroxylation and cation exchange continue. It is at this stage that molecular water can be incorporated into the crystal structure at temperatures below $\sim 250^\circ\text{C}$ (hydration) (Moore 1973). Secondary phosphates containing Fe^{3+} and Mn^{3+} can, therefore, illuminate the conditions of formation as can the presence or absence of incorporated molecular water into the structure of low temperature phases. Proximity of other minerals provides the cations for exchange in the low temperature stage. (Moore, 1973) Figures 35 and 36 summarize the alterative process for the triphylite series minerals at high and low temperature, under both oxidizing and non-oxidizing conditions. (Hawthorne 1998). Fletcher pegmatite phosphates in this collection appear to be entirely triphylite-derived, though little triphylite or its alteration product, ferrisicklerite, is visible in the hand samples of this collection. There are two likely reasons for this. The first is that almost all triphylite and ferrisicklerite was altered entirely to heterosite or low temperature phases. It is also important to note the sample group was collected selectively as the collector was searching for herderites (Pers. Comm. RW Whitmore). A sample bias makes it impossible to claim anything absolute regarding the one-time existence of certain phases at the Fletcher pegmatite beyond what is in the literature and in this collection. It is also of note that academic studies on the Fletcher pegmatite minerals (and therefore the confirmed species described from there) ceased long ago and have not been taken up again until the time of this writing. Several species of secondary phosphates had not yet been described or, in some cases, were to discovered to have been described incorrectly or duplicated contemporaneous mineral descriptions from other locations, at the time of original

research. Lack of access to the pegmatite makes it likely that a number of species that had yet to be described before the closing of the works to the public, will never be described for the Fletcher pegmatite unless they have already been collected.

The Quensel-Mason sequence (Quensel 1937) (Mason, 1941) is the first stage of primary phosphate alteration under oxidizing conditions (Figure 37). Along this alteration path, the divalent Fe in triphylite is oxidized to trivalent, forming ferrisicklerite. Leaching of Li^+ from ferrisicklerite and oxidation of divalent iron and manganese to trivalent yields the distinctive violet heterosite.

ALTERATION OF TRIPHYLITE-LITHIOPHILITE
(OXIDIZING CONDITIONS)

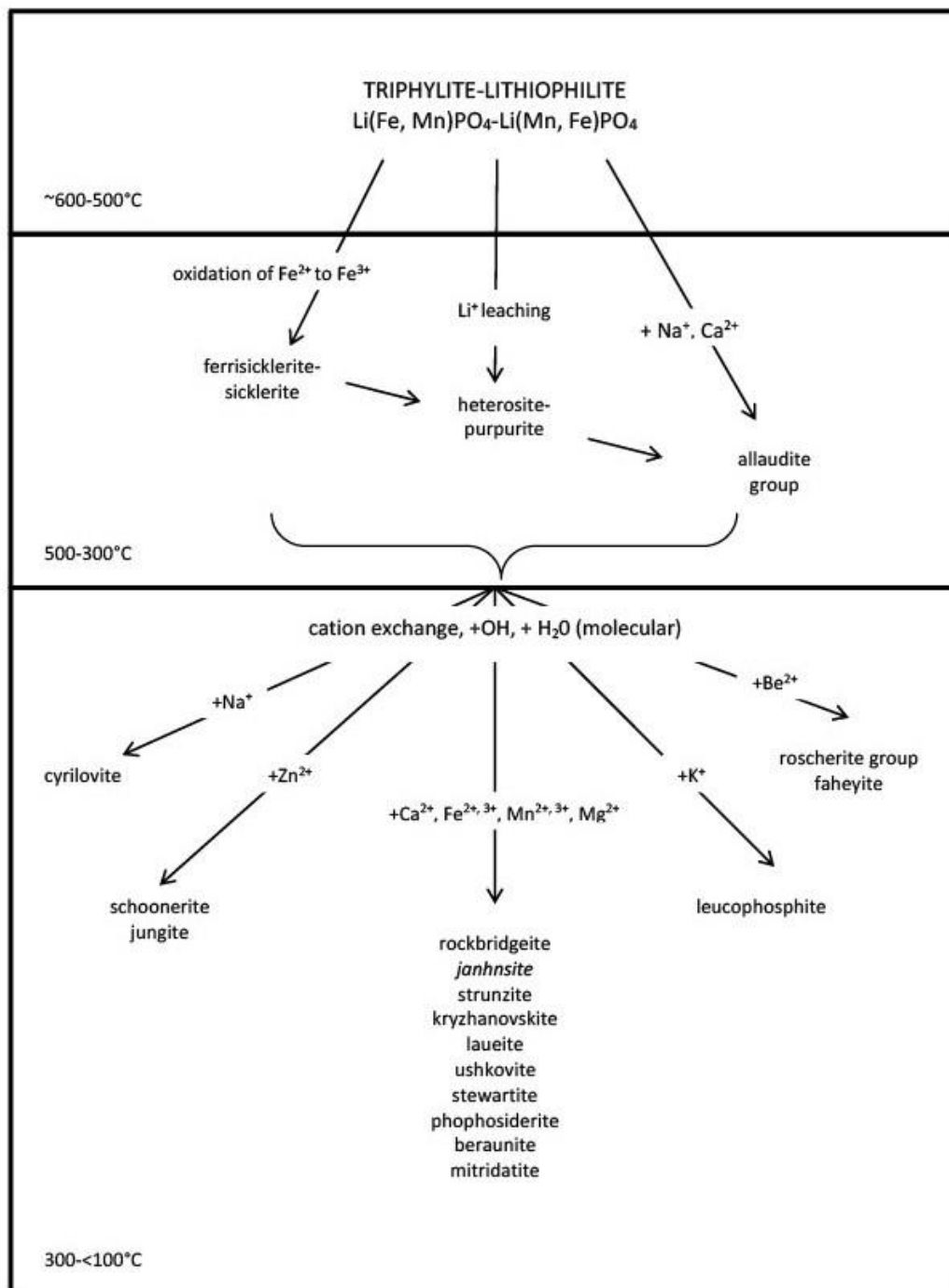


Figure 37: Alteration of triphylite under oxidizing conditions. Mod from Nizamoff 2006 after Moore 1974

Fletcher pegmatite assemblages boast abundant heterosite, which serves as a reliable determinant of the parent material in the absence of much triphylite among the samples. Heterosite is then altered to a host of low temperature secondary species depending on the availability of H₂O and metal cations. Low temperature secondary phosphate species generated under oxidizing conditions are numerous in this collection. They include apatite, rockbridgeite, jahnsite, laueite, stewartite, strunzite, leucophosphite, beraunite, mitridatite, and phosphosiderite. The likely proximal sources of the exchanged cations are the muscovite found within many of the samples, donating K⁺ to leucophosphite, and fluorapatite, found in so many of the Fletcher pegmatite samples, donating Ca⁺ to jahnsite, mitridatite, and messelite. Ca²⁺, minor Mg²⁺ and K⁺ are particularly active ions in the Fletcher pegmatite collection. Hydration and hydroxylation are still at work in at these low temperatures and the complexity of the crystal structures increases as temperatures decrease (Hawthorne 1998). The ability of these structures to integrate new cations is based on the fact that the cations in the progressively hydrated and hydroxylated iron phosphates are interstitial, allowing for more movement in and out of the framework (Moore 1974).

ALTERATION OF TRIPHYLITE-LITHIOPHILITE
(REDUCING CONDITIONS)

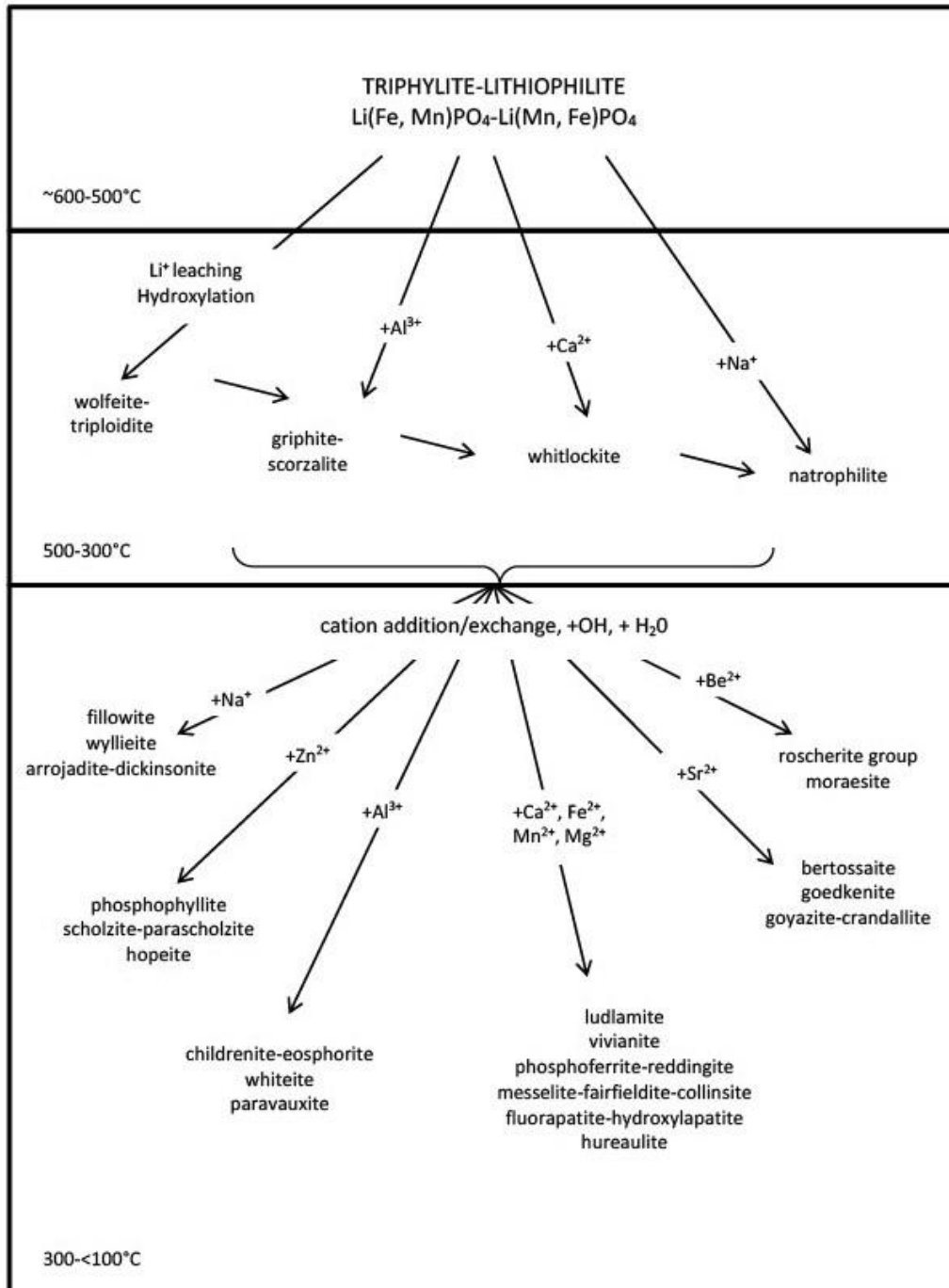


Figure 38: Alteration of triphylite under reducing conditions mod. From Nizamoff 2006 after Moore 1974

Deciphering paragenesis is tricky in that there are secondary phosphate species that can form from more than one primary phase series. In the absence of an alteration product unique to the parent, the alternative path the mineral has taken can be determined by analysis of similar associations. This has been the common mode of determining the paragenesis for Fletcher pegmatite. Under reducing conditions, triphylite can yield wolfeite-triploidite, whitlockite, natrophilite and scorzalite. For scorzalite, $(\text{Fe}^{2+}, \text{Mg}^{2+})\text{Al}_2(\text{PO}_4)_2(\text{OH})_2$, to form there must be available Al^{3+} . Although scorzalite has not yet been described at Fletcher pegmatite eosphorite has. The childrenite-eosphorite series is a good example of a secondary phase that overlaps for two common primary phosphate mineral series, triphylite-lithiophilite and montebrasite-amblygonite. The high temperature metasomatism of montebrasite-amblygonite ideally will yield scorzalite or its magnesium rich end member, lazulite under oxidizing-to-reducing conditions and with the leaching of Li, F, hydroxylation, and cation addition (Moore 1974). Figure 38 shows that scorzalite, by the addition of Al^{3+} can be formed under non-oxidizing conditions from triphylite. At the Fletcher pegmatite, only triphylite and eosphorite, of the series described above are present or have been described in the literature over the last 80 years. The predominance of triphylite derived secondary minerals; absence of any minerals unique to the montebrasite series, and the fact that many of the Al bearing phosphates in the Fletcher pegmatite samples are in association with muscovite suggests that any eosphorite was triphylite derived. Several secondary phases known to form under reducing conditions have been found at in the Fletcher pegmatite samples. Ludlamite, huréaulite, secondary fluorapatite, and vauxite are all seen in association II. Here again we might look to muscovite, this time for

providing the Al^{3+} cations necessary to form vauxite in the absence of any known montebrasite.

Of several primary phosphates found throughout the Grafton Pegmatite Field, triphylite is reportedly the most common at the Fletcher pegmatite. Triphylite, $\text{Li}(\text{Fe}, \text{Mn})\text{PO}_4$, forms a series with the manganous end member lithiophilite. Triphylite and several of its alteration products have been described (Moore 1969, 1970, 1974). In this study, four common alterative sequences are found, referred herein as association base specimens type I, II, III, and IV. Primary fluorapatite has also been found, deep blood red, in Fletcher pegmatite group V minerals in association with albite and with milky quartz.

Descriptive mineralogy for each and the rare single or two-phase specimen of the Fletcher pegmatite collection are given in the first section of this work. While each association is certainly triphylite derived, there are significant differences in the degree of alteration undergone by each as well as in the conditions of formation suggested by the presence of specific mineral phases. Most of the phases encountered have been those known to occur under oxidizing conditions, however huréaulite, known for forming under reducing conditions, is found in association with jahnsite and rockbridgeite in association I. Falster (2019) suggests the existence of micro-environments which alter the conditions of formation even in adjoining phases. Falster further suggests the presence of sulfur bearing minerals can protect Fe^{2+} and Mn^{2+} from oxidation, and that the presence of such minerals might prove the mechanism for the hureaulite phenomenon. Further investigation is needed to determine if any sulfur bearing minerals are present.

Selected Association Paragenesis

Association base specimen I (FMP_B28)

The mineral suite ABS I was selected for its complexity and the clear sequence of alteration it provides. In thin section, ferrisicklerite is visible as sub-millimetric width patches of bright orange being replaced almost entirely by the characteristic red-violet heterosite. Growth of low temperature hydroxylated rockbridgeite along fissures in heterosite are being replaced by jahnsite-CaFeFe. The dendritic to near lamellar textures attest to the movement of hydrothermal fluids through the existing high temperature metasomatic phases. The existence of two of three Quensel Mason minerals confirms this suite is triphylite derived. High temperature metasomatic alteration of triphylite in oxidizing conditions provided the environment for ferrisicklerite and heterosite. Low temperature hydrothermal alteration under oxidizing conditions with hydroxylation (rck) and hydroxylation, hydration, and Ca cation exchange (jhns) is responsible for the crystallization of rockbridgeite and jahnsite in in those fissures. Rockbridgeite forms the bulk of the rind of the ABS I, as well. A suite of low temperature secondary phosphates exists in vugs and as rinds in the rockbridgeite mass. Jahnsite, stewartite, phosphosiderite, and leucophosphite formed under oxidizing conditions. Hydration and hydroxylation are responsible for jahnsite and stewartite. Leucophosphite underwent both as well as cation exchange, with the addition of K⁺. Phosphosiderite is a hydrated iron phosphate. A diagram of the alteration sequence can be found in figure 39.

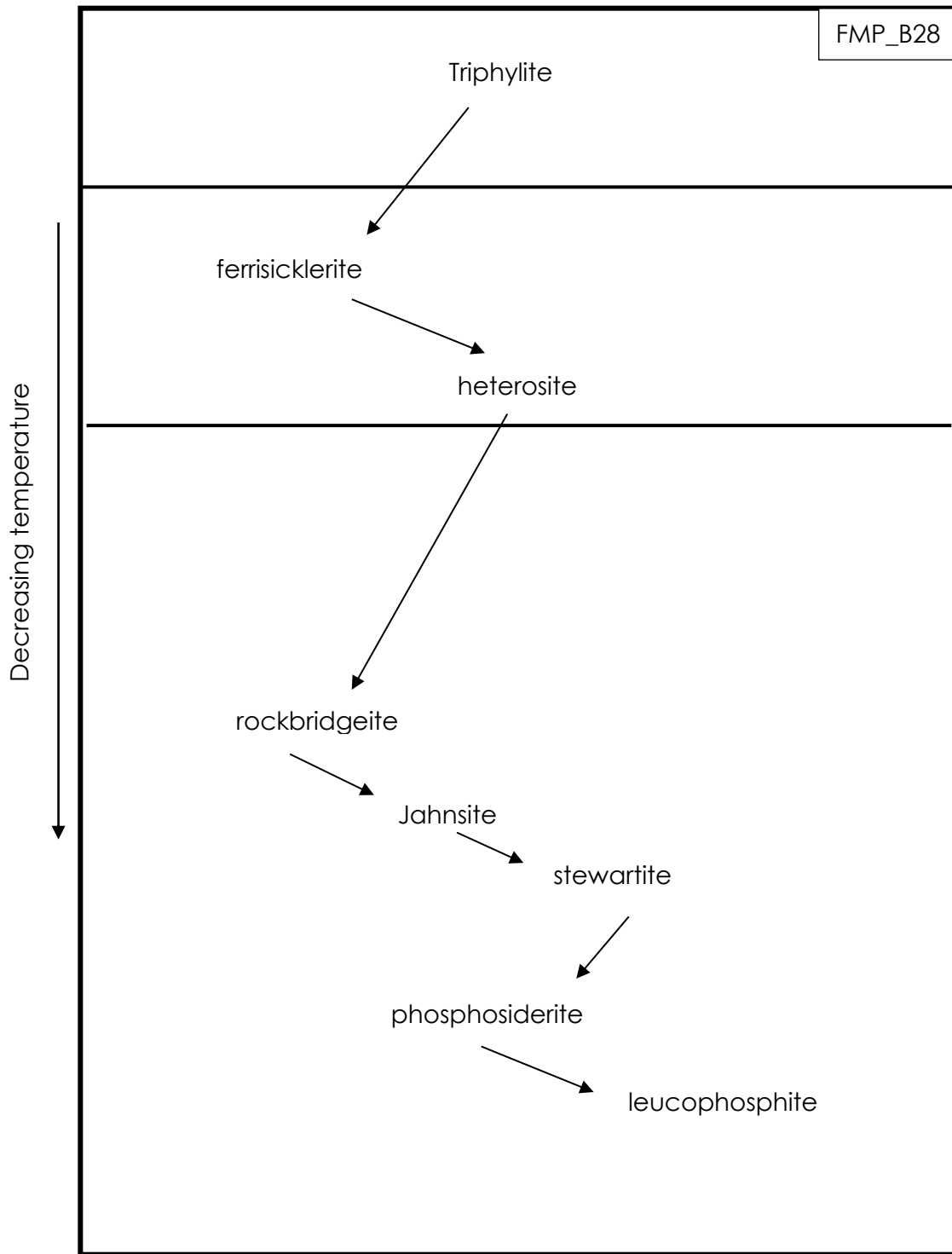


Figure 39: Paragenesis of Fletcher pegmatite Mine Pegmatite sample B28

Association Base Specimen II (FMP_B49)

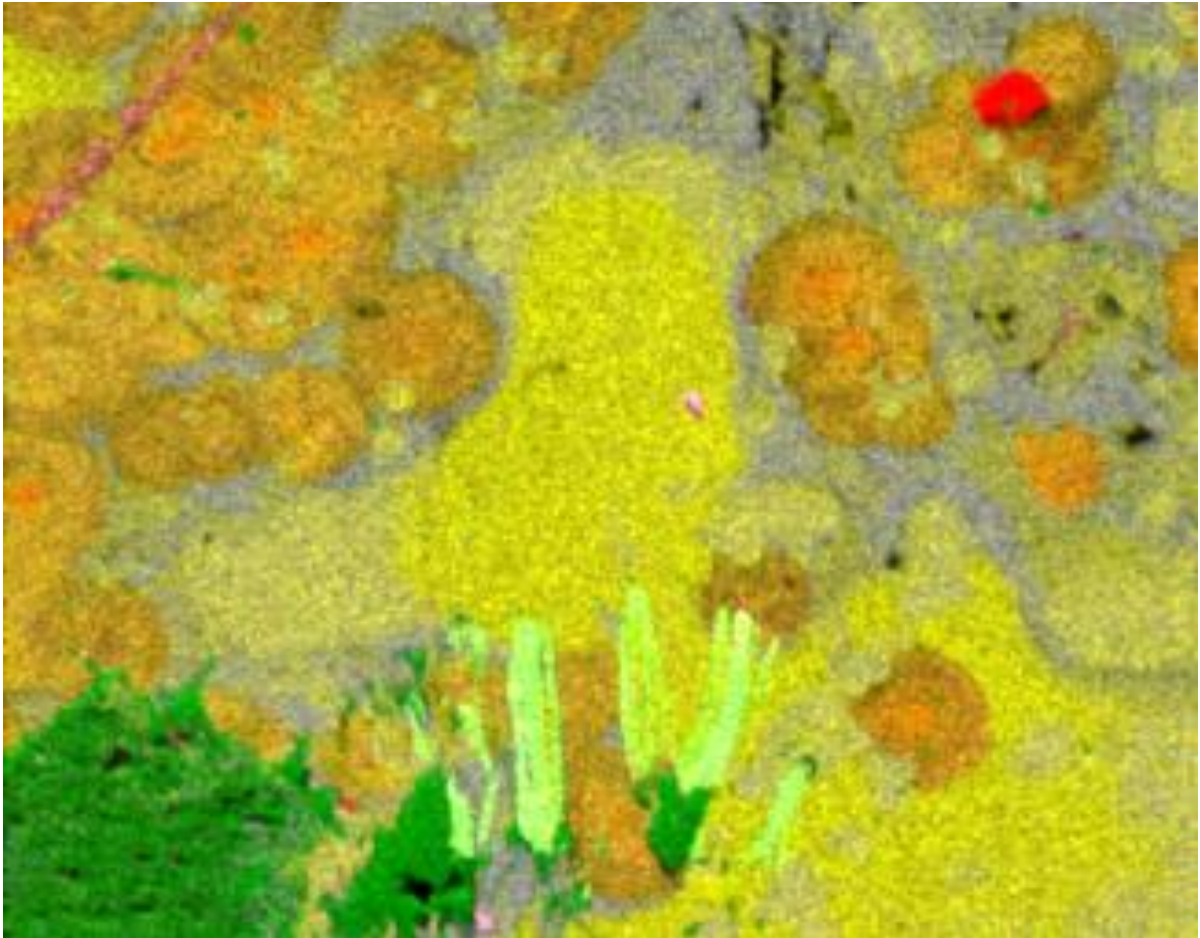


Figure 40: False color EDS overlay element map FMP_B49. Mn blue, Fe yellow, Si dk. green, Ca red, K lt. green, Al pink, P purple Scale: 2cm=500 μ m

Specimen FMP_B49 was chosen for its complexity and the divergent conditions of formation necessary to yield the minerals of this remarkable suite. Significant muscovite covers the exterior of this sample in which a crust of strunzite is seen on one side with pale green secondary fluorapatite protruding through it. Rockbridgeite forms the core of the specimen, which is seen clearly in thin section, as is jahnsite. Radial fluorapatite rims are clearly visible in thin section as well. The rind is host to several low

temperature alteration phases of triphylite, both formed in oxidizing (rockbridgeite, strunzite, mitridatite, laueite) and reducing (ludlamite, messelite, huréaulite, and vauxite) conditions which makes this specimen an interesting puzzle to solve. Falster (2019) suggests the existence of microclimates with differing conditions of pH, Eh and availability of given ions can explain this paradox as all minerals present, both products of oxidizing and reducing conditions, are forming at comparable temperatures (Simmons, et al. 2003) (Moore 1974). A diagram of the alteration sequence can be seen in figure 42. Fluorapatite is depicted as secondary but with as primary in shaded font as, if primary, it may play the role of cation donor in this case. However, there is there is evidence that the fluorapatite in sample FMP_B49 is secondary, which begs the question of where the calcium come from. Primary apatites in the Fletcher pegmatite sample group have all been dark brownish to blood red. Secondary apatites have been pale green. These in B49 are pale green. Martin (2014) suggests that there is a late-stage calcium mini-flood that can explain the seemingly sudden availability of calcium ions for hydrothermal alteration products in granitic pegmatites. This would not preclude secondary apatite, which forms at all temperatures (Moore 1974) (Hawthorne 1998) from also being a cation donor as a secondary phase.

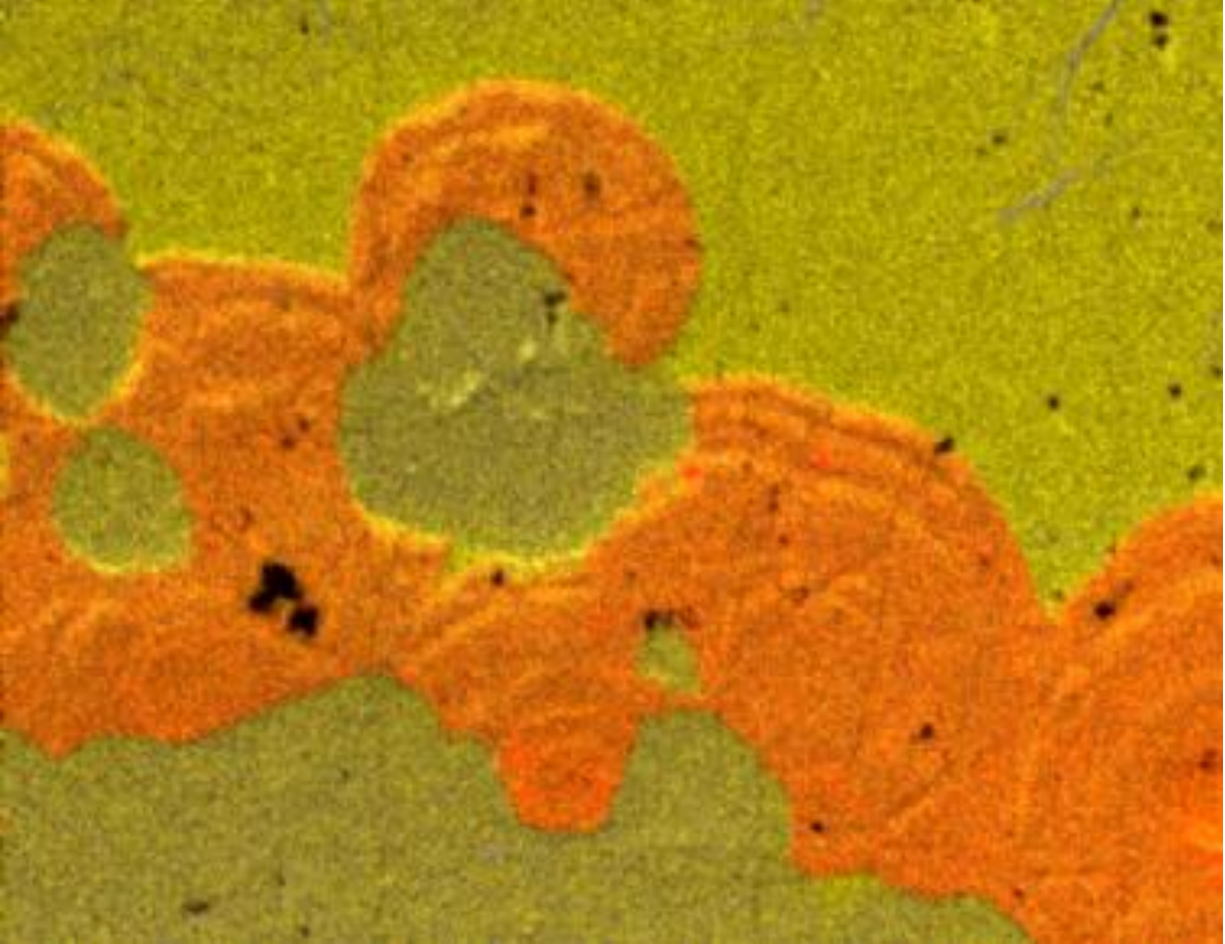


Figure 41: False color EDS overlay element map of FMP_B49_field 56. Mn-Blue, Fe Yellow, Ca red.
Scale 2cm=200 μ m

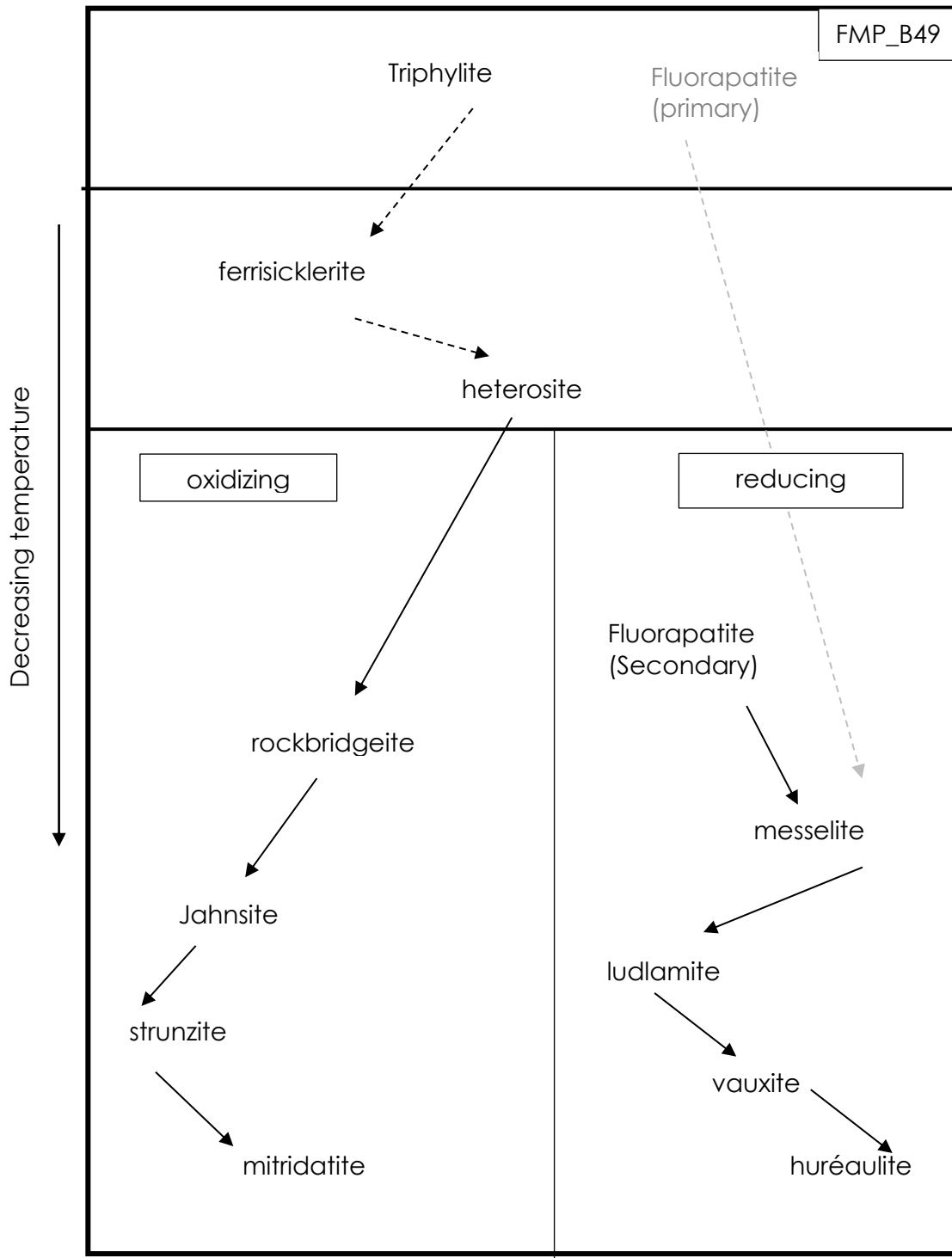


Figure 42: Paragenesis of Fletcher pegmatite Mine Pegmatite sample B49

Unknown Al-rich Phase

Electron microprobe data for sample FMP_B38 rendered two instances of analyses for which this researcher could not find analogous compositional data in Dana's or in any of the phosphate literature consulted. The initial reaction was to consider these two outliers to be error, however the presence of the similar aluminum rich phase in two completely different samples makes it less likely that this is the case. The anomalous phase in FMP_B38 is found in association with rockbridgeite and jahnsite-CaMnFe. Compositional data of the phase indicate more significant wt. % aluminum than is seen in minerals in the rest of the sample, except for vauxite, with an Wt. % Aluminum of ~22.

B38 field 2-7		
Wt. %		
P2O5	32.41	32.45
MgO	0.022	0.03
Al2O3	12.54	12.33
SiO2	0.2	0.18
TiO2	0	0
FeO	24.589	24.38
CaO	5.776	5.79
K2O	0	0
MnO	0.476	0.49
Na2O	0	0
SrO	0.009	0
BaO	0	0
ZnO	0.014	0.01
F		
Tot Wt%	76.04	75.66

Figure 43: Electron microprobe data: unidentified Al phosphate

This author believes it could be an unidentified new phase, or simply an aluminum rich version of a known mineral. It is still entirely possible that this is an error. Further study is needed to confirm the identity of the mineral phase in FMP_B38 and rule out human or technical error or contamination.

Classification

Classification of pegmatites has been a long contested and, at times, byzantine process. Several schemes were suggested beginning in the 1940s and in the years following, the penultimate of which, the Černý-Ercit classification system, has been in use since 2005 and especially and is based on depth and manner of emplacement, prevalence of Lithium, Cesium and Tantalum (LCT-Type) or else Niobium, Yttrium and Fluorine (NYF-Type), or both (Mixed-Type) as well as metamorphic grade and rare-element content. In the language of the Černý -Ercit scheme, therefore, the Fletcher pegmatite Mine Pegmatite is a rare element LCT pegmatite, beryl-phosphate subtype. This is an adequate but not altogether satisfying categorization. Rather, it is this because that is the closest fitting subtype available that resembles, to an extent, the Fletcher pegmatite body.

Class	Family	Subclass	Type	Subtype	
Abyssal	NYF	HREE			
	NYF	LREE			
	NYF	U			
	LCT	BBe			
Muscovite					
Muscovite-rare element	NYF	REE			
	LCT	Li			
Rare element	NYF	REE	allanite-monazite		
			euxenite		
				gadolinite	
	LCT	Li	beryl	beryl-columbite	
		complex	beryl-columbite-phosphate		
			spodumene		
			petalite		
			lepidolite		
			elbaite		
			amblygonite		
			albite-spodumene		
			albite		
Miarolitic	NYF	REE	topaz-beryl		
			gadolinite-fergusonite		
	LCT	Li	beryl-topaz		
			spodumene		
			petalite		
			lepidolite		

Figure 44: Černý-Ercit pegmatite classification 2005

A newer, more comprehensive system of classification has been suggested by Wise, et al. (2022). Recognizing that the Černý-Ercit has limitations, including confusion caused by the designation of “mixed type” and other imperfect categorizations of single pegmatites, this scheme was conceived with more detailed constraints. The difficulty of determining with certainty the depth of emplacement of pegmatite bodies, and the fact that degree of zonation and reliance on pegmatite fabrics and other textural considerations, such as presence or absence of miarolitic cavities, is not sufficient to draw a distinction between all the various and diverse pegmatites (Wise et al., 2022), the newly proposed system provides a greater breadth of criteria for distinguishing individual pegmatite bodies. This is essential as the previous standard was not intended to be applied to individual pegmatites (Ercit 2005). The Wise, et al. classification begins with three groups 1, 2, and 3, based upon the associations of “primary accessory rock forming minerals and rare element minerals” (Wise, 2022) (Figure 45).

Group 1	Group 2	Group 3
Beryl ± columbite ± triphylite ± graftonite	Magnetite ± epidote ± titanite	Andalusite ± sillimanite ± corundum
Beryl + amblygonite + columbite	Uraninite ± magnetite	Kyanite ± rutile
Amblygonite + spodumene	Fayalite ± magnetite	Cordierite ± beryl
Spodumene ± petalite	Arfvedsonite-riebeckite ± fayalite	Sapphirine + sillimanite
Spodumene ± elbaite	Arfvedsonite-riebeckite ± aegirine ± fluorite	Chrysoberyl ± beryl ± schorl
Spodumene + lepidolite + elbaite	Allanite ± gadolinite	Dumortierite ± grandidierite ± borasilite
Spodumene + albite	Allanite ± monazite ± euxenite	Dumortierite ± schorl
Lepidolite + elbaite	Allanite ± beryl ± columbite	
Elbaite ± danburite ± hambergite ± zeolites	Gadolinite ± euxenite ± fergusonite	
	Beryl ± topaz ± fluorite	
	Beryl ± phenakite	
	Microcline (var. amazonite) ± fluorite	
	Microcline (var. amazonite) ± topaz ± fluorite	

Figure 45: Pegmatite classification groups. Wise, et al., 2022

Group 1 pegmatites are generally enriched in lithium, rubidium, cesium, beryl, gallium, tin, and tantalum and three sub types are described. The first (i) consists of the beryl ±

phosphate bearing type. The presence of Be in hydroxylhercynites the Fletcher pegmatite is famous for, as well as the multitude of secondary phosphate species known to derive from alteration of triphylite, also present in the samples for this study, allow us to comfortably place the Fletcher pegmatite in Group 1, subtype (i). From this point, two further constraints can be placed on the classification by considering pegmatite genesis, and the complexity of the pegmatite body. Two types of geneses, or manners of emplacement are recognized here: residual melts of granite magmatism (RMG) and direct products of anatexis (DPA). This researcher looks to the descriptions of Fletcher pegmatite from Cameron's pegmatite investigations of 1954, regional geology studies especially those of Dorais (2003), Eusden and Barreiro (1989), Eusden and Lyons (1993), and Malconico (1982) Spear (2002) and Nizamoff (2006) and the character of the NHPS, and age data provided by Bradley (2016) to best decipher possible manner of emplacement for the Fletcher pegmatite body. Taking into consideration the timing of emplacement, deciphered to be post Acadian orogeny 326-294 mya (Bradley 2016), the suite of minerals found at Fletcher pegmatite (Cameron, 1954), evidence of crosscutting of the Concord two mica granite by a pegmatite with similar mineral assemblages to the nearby Palermo pegmatites (Nizamoff 2006), the concordance of the Fletcher pegmatite body with the foliation of the upper member of the Littleton Schist (Cameron, 1954), and the zonation (or complexity) of the pegmatite dyke, this researcher classifies the Fletcher pegmatite as a complexly zoned DPA Group 1 (subgroup i) type phosphate bearing pegmatite.

Conclusions

In summary, identification of secondary mineral phases is complex, as is determining the parent from which they derived. Pseudomorphs jahnsite, stewartite, and laueite of the Fletcher pegmatite group are examples of this. Compositional and unit cell data as well as close observation in thin section, and of euhedral crystals is the only way to be certain of the phase encountered. Phases that can form from different parent primary phosphates are also of note, and eosphorite described at the Fletcher (Moore 1974) but not found in the samples for this study makes the case for derivation from triphylite rather than the expected montebrazite, never described from the Fletcher pegmatite.

Fluorapatite appears as both primary and secondary phases at Fletcher. This determination was made based on chemistry and morphology as well as association to other secondary phases. A close investigation of Fletcher pegmatites fluorapatites would allow for clearer understanding of these two phases and of the paragenesis of secondary calcium bearing phosphates there.

Triphylite and, to a lesser extent, fluorapatite appear to be the dominant primary phases at the Fletcher pegmatite, responsible for the suite of secondary minerals found in the core margin and collected from the tailings dumps.

Trace lithium in select secondary phosphates shows a direct correlation to degree of differentiation in secondary high and low temperature phosphates. Increased lithium leaching of primary triphylite predicts this phenomenon. High amounts of lithium in sample FMP_A34, devoid of any Quensel Mason sequence minerals indicate a proximity to them or to another Li rich phase before being removed for collection.

Huréaulite is ubiquitous in association with all other late-stage alteration products of triphylite under both conditions of formation, suggesting a trend in the final cooling stages at the Fletcher pegmatite from oxidizing to reducing, possibly related to sulfur phases once present.

An as of yet unidentified aluminum rich phase at the Fletcher pegmatite bears further investigation.

The Fletcher pegmatite is a poorly to moderately evolved group 1 complexly zoned phosphate bearing DPA pegmatite (Wise, et al., 2022) based on Fe/Fe+Mn ratios in secondary phosphates found in this study, zonation of the pegmatite body, timing and likely manner of emplacement, and related pegmatites of the Grafton Pegmatite Field. A caveat that the samples were collected selectively cannot be ignored when discussing any apparent trend for the pegmatite as a whole.

WORKS CITED

- Bradley, D., Shea, E., Buchwaldt, R., Bowring, S., Benowitz, J., O'Sullivan, P., & McCauley, A. (2016). Geochronology and tectonic context of lithium-cesium-tantalum pegmatites in the Appalachians. *The Canadian Mineralogist*, 54(4), 945-969.
- Cameron, E.N., Larrabee, D.M., McNair, A.H., Page, J.J, Stewart, G.W. and Shainin, V.E. (1954) Pegmatite investigations 1942-45 New England. *U.S.G.S. Professional Paper* 255, 352 pp.
- Campbell, T.J. and Roberts, W.L. (1986) Phosphate minerals from the Tip Top mine, Black Hills, South Dakota. *Mineralogical Record*, 17, 237-254.
- Catti, M., Ferraris, G., & Ivaldi, G. (1977). Hydrogen bonding in the crystalline state. Structure of talmessite, $\text{Ca}_2(\text{Mg, Co})(\text{AsO}_4)_2 \cdot 2.2 \text{H}_2\text{O}$, and crystal chemistry of related minerals. *Bulletin de Mineralogie*, 100(3), 230-236.
- Černý, P. (1991a) Rare-element granitic pegmatites. Part 1: Anatomy and internal evolution of pegmatite deposits. *Geoscience Canada*, 18, 49-67.
- Černý, P. (1991b) Rare-element granitic pegmatites. Part 2: Regional to global environments and petrogenesis. *Geoscience Canada*, 18, 68-81.
- Černý, P. and Ercit, T.S. (2005) The classification of granitic pegmatites revisited. *Canadian Mineralogist*, 43, 2005-2026.
- Černý, P., Meintzer, R.E., and Anderson, A.J. (1985) Extreme fractionation in rare-element granitic pegmatites: selected examples of data and mechanisms. *Canadian Mineralogist*, 23, 381-421.
- Clark, R.G., Jr. and Lyons, J.B. (1986) Petrogenesis of the Kinsman Intrusive Suite: Peraluminous granitoids of western New Hampshire. *Journal of Petrology*, 27, 1365-1393.
- Dorais, M.J. (2003) The petrogenesis and emplacement of the New Hampshire plutonic suite. *American Journal of Science*, 303, 447-487.
- Eusden, Jr., J. D. and Barreiro, B. (1989) The timing of high-grade metamorphism in central-eastern New England. *Maritime Sediments and Atlantic Geology*, 24, 241-255.
- Eusden, Jr., J. D. and Lyons, J. B. (1993) The sequence of Acadian deformations in central New Hampshire. *Geological Society of America Special Paper* 275, 55-66. Q3
- Eventoff, W., Martin, R., & Peacor, D. R. (1972). The crystal structure of heterosite. *American Mineralogist: Journal of Earth and Planetary Materials*, 57(1-2), 45-51.

- Falster, A.U., and Simmons, W.B (2020) Juxtaposed oxidizing and reducing late stage environments in the Emmons pegmatite, Uncle Tom Mountain, Greenwood, Oxford County, Maine. *Maine Mineral and Gem Museum*
- Fisher, D. J. (1958). Pegmatite phosphates and their problems. *American Mineralogist: Journal of Earth and Planetary Materials*, 43(3-4), 181-207.
- Francis, C.A., Wise, M.A., Kampf, A.R., Brown, C.D., and Whitmore, R.W. (1993) Granitic pegmatites in northern New England, E1-E24. In: *Field Trip Guidebook for the Northeastern United States: 1993 Boston GSA, Volume 1*, Eds. Cheney, J.T. and Hepburn, J.C., Contribution No. 67, Department of Geology and Geography, University of Massachusetts, Amherst, Massachusetts.
- Fransolet, A. M., Abraham, K., & Speetjens, J. M. (1985). Genetic evolution and significance of the phosphate mineral assemblages in the Angarf-Sud pegmatite, Tazenakht Plain, Anti-Atlas, Morocco. *Bulletin de Mineralogie*, 108(3-4), 551-574.
- Fransolet, A.M., Keller, P. and Fontan, F. (1986) The phosphate mineral associations of the Tsaobismund pegmatite, Namibia. *Contributions to Mineralogy and Petrology*, 92, 502-517.
- Hawthorne, F.C. (1998) Structure and chemistry of phosphate minerals. *Mineralogical Magazine*, 62, 2, 141-164.
- Keller, P. (1991) The occurrence of Li-Fe-Mn phosphate minerals in granitic pegmatites of Namibia. *Communications of the Geological Survey of Namibia*, 7, 21-34.
- London, D., Černý, P., Loomis, J.L., and Pan, J.Y. (1990) Phosphorus in alkali feldspars of rare-element granitic pegmatites. *Canadian Mineralogist*, 28, 771-786.
- London, D. and Burt, D.M. (1982) Alteration of spodumene, montebrasite and lithiophilite in pegmatites of the White Picacho District, Arizona. *American Mineralogist*, 67, 87-113.
- Malinconico, M. (1982) *Stratigraphy and structure of the Southeastern Rumney 15-minute Quadrangle, New Hampshire*. M.S. Thesis. Dartmouth College, Hanover, New Hampshire, 234 pp
- Mason, B. (1941) Minerals of the Varuträsk pegmatite. XXIII. Some iron-manganese phosphate minerals and their alteration products, with special reference to material from Varuträsk. *Geologiska Föreningens Förhandlingar*, 63, 2, 117-175.
- Moore, P. B. (1966). The crystal structure of metastrengite and its relationship to strengite and phosphophyllite. *American Mineralogist: Journal of Earth and Planetary Materials*, 51(1-2), 168-176.

- Moore, P. B. (1970). Crystal chemistry of the basic iron phosphates. *American Mineralogist: Journal of Earth and Planetary Materials*, 55(1-2), 135-169.
- Moore, P.B. (1971) The $\text{Fe}^{2+}_3(\text{H}_2\text{O})_n(\text{PO}_4)_2$ homologous series: crystal-chemical relationships and oxidized equivalents. *American Mineralogist*, 56, 1-17.
- Moore, P.B. (1973) Pegmatite phosphates: descriptive mineralogy and crystal chemistry. *Mineralogical Record*, 4, 103-130.
- Moore, P.B. (1982) Pegmatite minerals of P (V) and B (III). In *Granitic Pegmatites in Science and Industry* (P. Černý ed.). *Mineralogical Association of Canada, Short Course Handbook 8*, 267-291.
- Moore, P.B. (2000) Analyses of Primary Phosphates from Pegmatites in Maine and Other Localities, in King, V.T., Tucker, R.D. and Marvinney, R.G. (editors), *Mineralogy of Maine: Volume 2 – mining history, gems and geology*: Maine Geological Survey, p. 333-336.
- Moore, P. B., & Araki, T. (1974). Jahnsite, $\text{CaMn}_{2+}\text{Mg}_2(\text{H}_2\text{O})_8\text{Fe}^{8+}_2(\text{OH})_2[\text{PO}_4]_4$: A novel stereoisomerism of ligands about octahedral corner-chains. *American Mineralogist: Journal of Earth and Planetary Materials*, 59(9-10), 964-973
- Moore, P. B., & Araki, T. (1977). Mitridatite, $\text{Ca}_6(\text{H}_2\text{O})_6[\text{Fe}^{3+}_9\text{O}_6(\text{PO}_4)_9] \cdot 3\text{H}_2\text{O}$. A noteworthy octahedral sheet structure. *Inorganic Chemistry*, 16(5), 1096-1106.
- Moore, P.B., Irving, A.J. and Kampf, A.R. (1975) Foggite, goedkenite, and samuelsonite: three new species from the Palermo #1 pegmatite, North Groton, New Hampshire. *American Mineralogist*, 60, 957-964.
- Moore, P. B., & Ito, J. (1978). I. Whiteite, a new species, and a proposed nomenclature for the jahnsite-whiteite complex series. II. New data on xanthoxenite. III. Salmonsite discredited. *Mineralogical Magazine*, 42(323), 309-323.
- Moore, P.B., Araki, T., and Kampf, A.R. (1980) Nomenclature of the phosphoferrite structure type: refinements of landesite and kryzhanovskite. *Mineralogical Magazine*, 43, 789-795.
- Nizamoff, J. (2006). The mineralogy, geochemistry and phosphate paragenesis of the Palermo# 2 pegmatite, North Groton, New Hampshire.
- Quensel, P. (1937) Minerals of the Varuträsk pegmatite. I. The lithium-manganese phosphates. *Geologiska Föreningens Förhandlingar*, 59, 1, 77-96.
- Roda, E., Pesquera, A., Fontan, F. and Keller, P. (2004) Phosphate mineral associations in the Cañada pegmatite (Salamanca, Spain): paragenetic relationships,

- chemical compositions and implications for pegmatite evolution. *American Mineralogist*, 89, 110-125.
- Roda-Robles, E., Pesquera, A., De Madinabeitia, S. G., Ibarguchi, J. I. G., Nizamoff, J., Simmons, W., ... & Galliski, M. A. (2014). On the geochemical character of primary Fe-Mn phosphates belonging to the triphylite-lithiophilite, grafftonite-beusite, and triplite-zwieselite series: first results and implications for pegmatite petrogenesis. *The Canadian Mineralogist*, 52(2), 321-335.
- Shigley, J.E. and Brown, G.E., Jr. (1985) Occurrence and alteration of phosphate minerals at the Stewart pegmatite, Pala district, San Diego County, California. *American Mineralogist*, 70, 395-408.
- Shigley, J.E. and Brown, G.E., Jr. (1986) Lithiophilite formation in granitic pegmatites: a reconnaissance experimental study of phosphate crystallization from hydrous aluminosilicate melts. *American Mineralogist*, 71, 356-366.
- Spear, F.S., Kohn, M.J., Cheney, J.T., and Florence, F. (2002) Metamorphic, thermal, and tectonic evolution of Central New England. *Journal of Petrology*, 43, 2097- 2120.
- Torsvik Trond H., and Rehnström, Emma F. The Tornquist Sea and Baltica–Avalonia docking, *Tectonophysics*, 362, Issues 1–4,2003, Pages 67-82,
- Vieira, R., Roda-Robles, E., Pesquera, A., & Lima, A. (2011). Chemical variation and significance of micas from the Fregeneda-Almendra pegmatitic field (Central-Iberian Zone, Spain and Portugal). *American Mineralogist*, 96(4), 637-645.
- Vignola, P., Diella, V., Ferrari, E. S., & Fransolet, A. M. (2011). Complex mechanisms of alteration in a grafftonite+ sarcopside+ triphylite association from the Luna pegmatite, Piona, Lecco province, Italy. *The Canadian Mineralogist*, 49(3), 765-776.
- Vignola, P. (2018). New evidence of alteration of grafftonite-(Mn) from the Malpensata pegmatite, Colico municipality, Lecco province, Italy. *The Canadian Mineralogist*, 56(4), 645-656.
- Vignola, P. (2013-2022) Personal communication.
- Whitmore, R.W. (2013) Personal communication.
- Whitmore, R.W. and Lawrence, R.C., Jr. (2004) *The Pegmatite Mines Known as Palermo*. Friends of Palermo mines, 213 pp.
- Wise, M. A., Müller, A., & Simmons, W. B. (2022). A proposed new mineralogical classification system for granitic pegmatites. *The Canadian Mineralogist*, 60(2), 229-248.

Vita

Susanna "Sasha" Kreinik was born in New Orleans and raised in New York city. At summer camp as a child, she would mail rocks home to her parents in letter envelopes. She attended the Chapin School and graduated in 1991, then Barnard College and NYU, majoring in nothing even remotely related to geology. Sasha moved home to New Orleans on August 25th, 2005, and promptly had to leave again. After Katrina, she volunteered at a local high school with Dr Ivan Gill, a geologist who convinced her to go back to school and become one, too. Sasha enrolled at UNO, completing a BS in 2013, and entering the graduate program in Earth and Environmental Sciences under William "Skip" Simmons and Alexander U. Falster and as part of the MP² Research Group. There she met her first pegmatite, and, at the Maine Pegmatite Workshop in 2012, her first phosphate, thanks to Pietro Vignola. Since 2015 Sasha has been a teacher of sciences and logic at the Holy Cross School, New Orleans, where she teaches a UNO dual enrollment geology class to stay happy and spend time with rocks. In December of 2022, nine years and 5 months after beginning the graduate program, she will obtain her M.S. from UNO.